

EVALUATION OF A WIND FARM PARAMETERIZATION IN AN  
OPERATIONAL MESOSCALE MODEL

POOJA RAMAKRISHNAN



Environmental Engineering  
Faculty of Civil Engineering  
TU Delft

November 2019 – Master Thesis

Pooja Ramakrishnan: *Evaluation of a wind farm parameterization in an operational mesoscale model*, © November 2019

**SUPERVISORS:**

Prof.dr. A.P. Siebesma

Dr. Sukanta Basu

Prof. Dr.ir. C.J. Simão Ferreira

Dr. ir. Bart van Stratum

Dr. ir. Remco Verzijlbergh

**LOCATION:**

Delft

**THESIS DEFENSE:**

26th November 2019

Dedicated to the loving memory of my mother and the first  
environmental scientist in my family, Shanthi Ramakrishnan.

1965–2011



---

## ABSTRACT

---

In the coming decade, the Dutch government plans to broadly expand its wind farm real estate over the North Sea region. This is a significant undertaking because, from literature, it is understood that wind turbines can affect the local environment. These impacts include, but are not limited to, changes in variables such as wind speed and turbulent kinetic energy. To accurately capture these effects and improve power forecast accuracy, weather prediction models numerically represent the physical effects of a wind farm (i.e., a wind farm's behaviour as a momentum sink and a source of turbulent kinetic energy) by incorporating a wind farm parameterization in the model. This study looked at two simulations (with and without a wind farm parameterization) from HARMONIE-AROME, an operational weather model, and assessed the performance of the wind farm parameterization by using the simulation results for the Belgian wind farm zone in the North Sea, and comparing it with observational data from Sentinel-1 SAR, floating LiDARs, measured power as well as results from a large-eddy simulation. The data was also composited based on wind direction and atmospheric stability and analysed. Most importantly, it was found, after comprehensive analysis, that the wind farm parameterization caused a marked improvement in the results of the model especially in the region downwind of a wind farm where the effects are most severely experienced. Specifically, the simulation with the wind farm parameterization reduced the overall wind bias to  $-0.028$  m/s from  $0.602$  m/s when compared with observational data for the selected region. The overall power bias was also found to be approximately  $1.92\%$ . Several hypotheses based on existing literature were also tested, and along with the composite analysis, indicated that the simulation with the wind farm parameterization performed well in most stability regimes with the exception of stable conditions. It was recommended that this be further explored to determine the cause. Recommendations for expanding the study to look at wind farm effects on surface fluxes in offshore regions have also been made.



---

## ACKNOWLEDGEMENTS

---

I would like to take the time and space here to express, in writing, my deepest gratitude for all those who have helped me in this endeavour. The past nine to ten months would have been impossible if it was not for the support and encouragement of my chair supervisor, Prof.dr. A.P. Siebesma. He has been instrumental in keeping my spirits raised both with his vision with regards to the thesis and his genuine concern for my overall well-being. He has also been a wonderful mentor, teacher, and advisor during my two and a half years at TU Delft.

I would like to thank Dr. Sukanta Basu. He has taught me so much more than can be recorded here. His patient advice, attention to detail and rigorous assessment has been a real blessing. I am especially grateful for his time, his openness and his sincere interest in helping me make the most of my Master thesis.

I am also deeply indebted to Dr.ir. Bart van Stratum without whom this thesis literally would have not been possible. I thank him for his work in incorporating the wind farm parameterization in HARMONIE-AROME and running the model simulations. I have deep appreciation for his technical prowess and for his excellent work ethic. I also thank Dr.ir. Remco Verzijlbergh whose kind cooperation allowed me to use Whiffle's GRASP LES data. His comments were always thought-provoking and he always motivated me to explore different avenues in my thesis. Additionally, I would like to thank Prof.Dr.ir. C.J. Simão Ferreira whose insights shed new light on the results and provided a great deal of objectivity for evaluating my work.

This thesis would not have been possible if it was not for the Royal Netherlands Meteorological Institute (KNMI) and especially Ine Wijnant. Her kindness, energy and spiritedness is unparalleled. She always made my work feel valued.

I also would like to thank the teams at Whiffle, Denmark Technical University (DTU), Fugro and the Netherlands Enterprise Agency, and Elia, the Belgian transmission operator, for their data-sets.

I cannot fail to mention a note of gratitude to my father. He has worked tirelessly to ensure that I am able to pursue my dreams without inhibition. Everything I am today, I owe it entirely to him.

Finally, I would like to thank my colleagues, work mates in room 3.53, close friends, housemates and the rest of my family for their never-ending support and boundless affection. Last but not least, a note to record names of those who have in their own ways stood by my side through it all: Yomi Tadfor, Nikhil Nayar, Priyanka Thad-  
daeus.



---

## CONTENTS

---

1	INTRODUCTION	1
1.1	Topic and Relevance . . . . .	1
1.2	Research Questions and Methodology . . . . .	3
1.3	Organisation of Thesis . . . . .	4
2	LITERATURE REVIEW	5
2.1	Background . . . . .	5
2.1.1	Numerical Weather Prediction Models . . . . .	5
2.1.2	Parameterizations . . . . .	7
2.1.3	Obukhov Length and Atmospheric Stability . . . . .	7
2.2	Studies on Wind Farm Parameterization . . . . .	10
2.2.1	Wind Farm Parameterization Development in Literature . . . . .	13
2.2.2	Relevant Outcomes from Previous Wake Studies . . . . .	15
2.3	Construction of Hypotheses . . . . .	19
3	METHODOLOGY	21
3.1	Data-sets . . . . .	21
3.1.1	Observational Data-sets . . . . .	21
3.1.2	Models . . . . .	24
3.2	Analysis Procedure . . . . .	28
3.2.1	Delimitation of the Study (Spatial and Temporal Domain) and Indicators . . . . .	28
3.2.2	Data Processing . . . . .	31
3.2.3	Checks and Balances . . . . .	35
3.3	Limitations, Assumptions and Range of Validity . . . . .	35
4	RESULTS	37
4.1	Qualitative Analysis: An Overview . . . . .	37
4.1.1	HRM vs HRM-WF: A Benchmark Analysis . . . . .	37
4.1.2	Comparisons of HRM-WF and Measured Wind Data . . . . .	40
4.2	Qualitative Analysis: A Composite View . . . . .	50
4.2.1	Atmospheric Stability Composite Results . . . . .	50
4.2.2	Wind Direction Composite Results . . . . .	64
4.3	Quantitative Analysis . . . . .	67
4.3.1	Descriptive Statistics: A Tabular Overview . . . . .	70
4.3.2	Descriptive Statistics: A Composite View . . . . .	72
5	DISCUSSION	75
5.0.1	Summary . . . . .	75
6	CONCLUSION AND RECOMMENDATIONS	79
6.1	Research Outcomes . . . . .	79
6.2	Recommendations . . . . .	80
	BIBLIOGRAPHY	83

A	DATA SOURCES	87
A.1	Access to Model Simulations . . . . .	87
A.2	Access to Observational Data-sets . . . . .	87
B	SUPPLEMENTARY RESULTS	89
B.1	Descriptive Statistics: A Tabular Composite View . . .	89
B.2	Inverse Obukhov Length from the New European Wind Atlas . . . . .	95
B.3	Spatial Plots for Wake Phase Diagram Construction . .	95
B.4	Additional Figures . . . . .	102

---

## LIST OF FIGURES

---

Figure 1	THE PROPOSED DUTCH WIND FARMS AND BELGIAN WIND FARMS. ADAPTED FROM RVO.NL ( <a href="http://Offshorewind.rvo.nl">Offshorewind.rvo.nl</a> ) The red, green, and pink zones are already commissioned wind farms by Belgium. The other colours are wind farms that are yet to be commissioned. The Borssele Wind Farm Zone is adjacent to the Belgian wind farms shaded in grey. . . . .	2
Figure 2	THE PROPOSED BORSSELE WIND FARM ZONE AND FULLY COMMISSIONED BELGIAN WIND FARM. ADAPTED FROM RVO.NL ( <a href="http://Offshorewind.rvo.nl">Offshorewind.rvo.nl</a> ) A closer look at the region of interest with the different wind operators of the Belgian wind farm highlighted in different colours and the proposed sites within the Borssele Wind Farm Zone. . . . .	3
Figure 3	THE RELATIONSHIP BETWEEN STABILITY PARAMETERS ( $z/L$ ) AND ATMOSPHERIC VARIABLES. ADAPTED FROM MOENE AND DAM (2014) As the figure indicates, $z/L$ close to 0 indicates neutral regimes, positive values imply stable regimes and negative values indicate unstable regimes. In the latter regime, low wind speeds but a positive sensible heat flux is expected. In the former, a negative sensible heat flux is expected. Neutral regimes are usually well-mixed with high wind speeds. . . . .	9
Figure 4	AN ILLUSTRATION OF LIFT AND DRAG FORCES ON A WIND TURBINE BLADE The lift force allows the turbine blade to be lifted and the drag force is exerted in the direction parallel to the flow of the wind. . . . .	10
Figure 5	AN ILLUSTRATION OF POWER AND THRUST CURVES OF A VESTAS 112 WIND TURBINE AS FUNCTIONS OF WIND SPEED The $x$ -axis is the wind speed and the $y$ -axis shows the values for the the thrust and power coefficients. These curves are often provided by wind turbine manufacturers. . . . .	11
Figure 6	AVERAGE VELOCITY DEFICIT FOR REFERENCE AND WAKE TRANSECT FOR ONSHORE AND OFFSHORE WINDS. ADAPTED FROM (CHRISTIANSEN AND HASAGER, 2005) The shaded region indicates the location of the wind farm. Areas in the graph to the left and to the right are upstream and downstream distance respectively. . . . .	16

Figure 7	VELOCITY DEFICIT FROM SAR DATA DURING UNSTABLE AND NEAR-NEUTRAL CONDITIONS. ADAPTED FROM (CHRISTIANSEN AND HASAGER, 2005) <i>The shaded region indicates the location of the wind farm. Areas in the graph to the left and to the right are upstream and downstream distance respectively.</i> . . . . .	17
Figure 8	HORIZONTAL WAKE STRUCTURE IN THE MORNING AND EVENING. ADAPTED FROM (FITCH, LUNDQUIST, AND OLSON, 2013) <i>The structure of the wake is visible during the labelled time periods at hub height depicting the difference in wind speed between a wind farm and no-wind farm case. On the top row, a) 0530 local time b) 0600 local time c) 0630 local time. On the bottom row, a) 1600 local time b) 1800 local time c) 2300 local time.</i> . . . . .	18
Figure 9	TIME-AVERAGED WIND SPEED CONTOURS IN m/s SLICED HORIZONTALLY AT THE TURBINE HUB HEIGHT FOR DIFFERENT STABILITY CONDITIONS. ADAPTED FROM (ABKAR AND PORTÉ-AGEL, 2015B) <i>The x axis is normalised downwind distance, y axis is normalised lateral distance. The topmost plot is for a Convective Boundary Layer (CBL) condition, the middle plot is for a Neutral Boundary Layer (NBL) and the lowest plot is for a Stable Boundary Layer (SBL)</i> . . . . .	19
Figure 10	SAR DATA RETRIEVED USING GOOGLE EARTH ENGINE (THE GOOGLE EARTH ENGINE CODE TO EXTRACT THE RELEVANT DATA WAS PROVIDED AS A COURTESY BY DR. S.L.M. (STEF) LHERMITTE) ( <i>User Guides - Sentinel-1 SAR - Overview - Sentinel Online</i> ) <i>This snapshot shows the wakes from the Belgian wind turbines as captured by Sentinel-1 and displayed on the Google Earth Engine viewer.</i> . . . . .	22
Figure 11	SAMPLE WAKE IMAGE FROM THE SAR DATA-SET <i>The colorbar indicates wind speed in m/s. This figure illustrated is for 5th February 2016.</i> . . . . .	23
Figure 12	THE DUTCH OFFSHORE WIND ATLAS DOMAINS (ALONG WITH THE PREVIOUS VERSION OF THE ATLAS: KNW (IS NOT RELEVANT TO THIS THESIS) ADAPTED FROM (KNMI, 2019) <i>The area shaded in red was the model output that was used for this work and further zoomed in to focus on just the Borssele wind-farm region in the North Sea.</i> . . . . .	24

Figure 13	WIND FARM ZONES IN THE NORTH SEA. PROVIDED BY BART VAN STRATUM. (VAN STRATUM, PERSONAL COMMUNICATION, OCTOBER 21, 2019) <i>The red points indicate wind farm areas. The arrows point to observation locations. Out of the three, only the Borssele LiDARs are utilised in this study.</i> . . .	26
Figure 14	SCHEMATIC SETUP OF GRASP LES. ADAPTED FROM APPENDIX D OF (PONDERA ET AL., 2019) . . . . .	27
Figure 15	ILLUSTRATION OF LiDAR LOCATIONS AND MODEL GRID POINTS USED FOR COMPARISON <i>The top panel illustrates the grid lines of the high LES resolution and the bottom panel illustrates the grid lines of the coarser HARMONIE-AROME resolution. The legends indicate the locations in the model that were closest to the actual LiDAR coordinates.</i> . . . . .	32
Figure 16	HUB-AVERAGED WIND SPEEDS BETWEEN HRM AND HRM-WF ON 5TH FEB 2016 <i>The top panel shows a spatial hub averaged wind speed plot for HRM and the bottom panel shows the same for HRM-WF. The Belgian wind farm location has noticeably weaker average wind speeds (around 12 m/s).</i> . . . . .	38
Figure 17	HRM vs HRM-WF: SPATIAL TKE PROFILES <i>The top 2 rows show a spatial TKE plot for HRM and the bottom 2 rows show the same for HRM-WF. Note that the upper limit of the colorbar was adjusted to clearly illustrate the increase in TKE over the BWFZ as we approach hub height and subsequent decrease.</i> . . . . .	39
Figure 18	SPATIAL WIND CONTOUR MAPS - 5TH FEB 2016 <i>The left panel shows explicit wake trails from the Belgian wind farms captured at 10m height in an image from SAR on 5th Feb 2016 at 6 AM. The right panel shows the spatial wind contour map at 10m height by HRM-WF. The atmosphere was stable at this time and date.</i> . . . . .	40
Figure 19	WAKE SIGNATURE AT 10M CAPTURED BY HRM-WF <i>The wakes are represented here in yellow. The black dots depict the wind farms and the colour is unrelated to the colorbar.</i> . . . . .	41
Figure 20	SPATIAL WIND CONTOUR MAPS - 5TH MAR 2016 <i>The leftmost panel is a SAR image, the middle panel is HRM-WF with a colorbar comparable to the SAR image and the last rightmost panel is HRM-WF with a tweaked colorbar to highlight the wakes.</i> . .	41

Figure 21	SPATIAL WIND CONTOUR MAPS - 12TH MAR 2016 <i>The leftmost panel is a SAR image, the middle panel is HRM-WF with a colorbar comparable to the SAR image and the last rightmost panel is HRM-WF with a tweaked colorbar to highlight the wakes.</i> . . . . .	42
Figure 22	SPATIAL WIND CONTOUR MAPS - 24TH MAR 2016 <i>The leftmost panel is a SAR image, the middle panel is HRM-WF with a colorbar comparable to the SAR image and the last rightmost panel is HRM-WF with a tweaked colorbar to highlight the wakes.</i> . . . . .	42
Figure 23	SPATIAL WIND CONTOUR MAPS - 4TH JUN 2016 <i>The leftmost panel is a SAR image, the middle panel is HRM-WF with a colorbar comparable to the SAR image and the last rightmost panel is HRM-WF with a tweaked colorbar to highlight the wakes.</i> . . . . .	42
Figure 24	SPATIAL WIND CONTOUR MAPS - 12TH JUN 2016 <i>The leftmost panel is a SAR image, the middle panel is HRM-WF with a colorbar comparable to the SAR image and the last rightmost panel is HRM-WF with a tweaked colorbar to highlight the wakes.</i> . . . . .	42
Figure 25	WAKE LENGTHS (AT 10M) CATEGORISED ACCORDING TO SPEED AND STABILITY CLASS. . . . .	44
Figure 26	WIND SPEED AT HUB HEIGHT (100M) AT FAR LIDAR LOCATION . . . . .	44
Figure 27	WIND SPEED AT HUB HEIGHT (100M) AT NEAR LIDAR LOCATION . . . . .	45
Figure 28	HISTOGRAMS OF FAR-LIDAR AND NEAR-LIDAR <i>The leftmost panel is a histogram between the far and near LiDARs. The middle panel is a histogram comparison of the models and the observational data-set for the far-lidar. The rightmost panel is the histogram comparison between the near-lidar observational data-set and the models.</i> . . . . .	45
Figure 29	DIURNAL CYCLE AT FAR-LIDAR <i>The panels depict data from top to bottom in the following order: LiDAR, GRASP LES, HRM-WF, HRM.</i> . . . . .	46
Figure 30	DIURNAL CYCLE AT NEAR-LIDAR <i>The panels depict data from top to bottom in the following order: LiDAR, GRASP LES, HRM-WF, HRM.</i> . . . . .	47
Figure 31	WIND SHEAR AT THE NEAR AND FAR LIDARS <i>The panels depict wind shear profiles for different hours of the day in the following order: 0000 hrs, 0600 hrs, 1200 hrs, 1800 hrs.</i> . . . . .	48

Figure 32	A TIME SERIES OF POWER PRODUCTION IN THE BELGIAN WIND FARMS FROM MARCH - MAY 2016 FOR HRM-WF AND ACTUAL POWER . . . . .	49
Figure 33	A TIME SERIES OF POWER PRODUCTION IN THE BELGIAN WIND FARMS FROM MARCH - MAY 2016 FOR GRASP LES AND ACTUAL POWER . . . . .	50
Figure 34	A 2D HISTOGRAM OF POWER PRODUCTION IN THE MODEL AND OBSERVATIONAL DATA-SETS <i>The left panel depicts HRM-WF vs Elia and the right panel depicts GRASP LES vs Elia.</i> . . . . .	50
Figure 35	PROPORTIONS OF VARIOUS ATMOSPHERIC STABILITY REGIMES FROM MARCH - MAY 2016 <i>The top panel is the stability percentages for the far lidar location and the bottom panel represents the near lidar location.</i> . . . . .	51
Figure 36	HISTOGRAMS FOR 'VERY UNSTABLE' REGIME <i>The leftmost panel is a histogram between the far and near LiDARs. The middle panel is a histogram comparison of the models and the observational data-set for the near-lidar. The rightmost panel is the histogram comparison between the far-lidar observational data-set and the models.</i> . . . . .	52
Figure 37	HISTOGRAMS FOR 'UNSTABLE' REGIME <i>The leftmost panel is a histogram between the far and near LiDARs. The middle panel is a histogram comparison of the models and the observational data-set for the near-lidar. The rightmost panel is the histogram comparison between the far-lidar observational data-set and the models.</i> . . . . .	52
Figure 38	HISTOGRAMS FOR 'STABLE' REGIME <i>The leftmost panel is a histogram between the far and near LiDARs. The middle panel is a histogram comparison of the models and the observational data-set for the near-lidar. The rightmost panel is the histogram comparison between the far-lidar observational data-set and the models.</i> . . . . .	52
Figure 39	HISTOGRAMS FOR 'VERY STABLE' REGIME <i>The leftmost panel is a histogram between the far and near LiDARs. The middle panel is a histogram comparison of the models and the observational data-set for the near-lidar. The rightmost panel is the histogram comparison between the far-lidar observational data-set and the models.</i> . . . . .	53

Figure 40	HISTOGRAMS FOR 'NEUTRAL' REGIME <i>The left-most panel is a histogram between the far and near LiDARs. The middle panel is a histogram comparison of the models and the observational data-set for the near-lidar. The rightmost panel is the histogram comparison between the far-lidar observational data-set and the models. . . . .</i>	53
Figure 41	FAR-LIDAR DIURNAL WIND SPEED CYCLE <i>The top left panel is the diurnal cycle for a very unstable regime. The top right panel is the diurnal cycle for an unstable regime. The bottom panel is the diurnal cycle for a neutral regime. . . . .</i>	54
Figure 42	FAR-LIDAR DIURNAL WIND SPEED CYCLE <i>The top panel is the diurnal cycle for a stable regime. The bottom panel is the diurnal cycle for a very stable regime. . . . .</i>	55
Figure 43	NEAR-LIDAR DIURNAL WIND SPEED CYCLE <i>The top left panel is the diurnal cycle for a very unstable regime. The top right panel is the diurnal cycle for an unstable regime. The bottom panel is the diurnal cycle for a neutral regime. . . . .</i>	56
Figure 44	NEAR LIDAR- DIURNAL WIND SPEED CYCLE <i>The top panel is the diurnal cycle for a stable regime. The bottom panel is the diurnal cycle for a very stable regime. . . . .</i>	57
Figure 45	FAR-LIDAR DIURNAL WIND SHEAR CYCLE <i>The top left panel is the diurnal shear for a very unstable regime. The top right panel is the diurnal shear for an unstable regime. The bottom panel is the diurnal shear for a neutral regime. . . . .</i>	59
Figure 46	FAR-LIDAR DIURNAL WIND SHEAR CYCLE <i>The top panel is the diurnal shear for a stable regime. The bottom panel is the diurnal shear for a very stable regime. . . . .</i>	60
Figure 47	NEAR-LIDAR DIURNAL WIND SHEAR CYCLE <i>The top left panel is the diurnal shear for a very unstable regime. The top right panel is the diurnal shear for an unstable regime. The bottom panel is the diurnal shear for a neutral regime. . . . .</i>	61
Figure 48	NEAR-LIDAR DIURNAL WIND SHEAR CYCLE <i>The top panel is the diurnal shear for a stable regime. The bottom panel is the diurnal shear for a very stable regime. . . . .</i>	62

Figure 49      *HEXBIN PLOTS FOR POWER PRODUCTION The leftmost panel is for a very unstable regime. The middle panel is for an unstable regime. The rightmost panel is for a neutral regime. From top to bottom, the panels are HRM-WF and GRASP LES. . . . .*      63

Figure 50      *HEXBIN PLOTS FOR POWER PRODUCTION The left panel is for a stable regime. The right panel is for a very stable regime. From top to bottom, the panels are HRM-WF and GRASP LES. . . . .*      64

Figure 51      *PERCENTAGE OF WIND ORIGINATING FROM VARIOUS DIRECTION DURING THE MARCH - MAY 2016 PERIOD. The left panel is for the far-lidar. The right panel is for the near-lidar. . . . .*      64

Figure 52      *WIND SPEED BIAS VS. DIRECTION The top panel is for the far-lidar. The bottom panel is for the near-lidar. . . . .*      65

Figure 53      *NE AND SW WIND SPEED BIAS VS REGIME FOR THE FAR LIDAR LOCATIONS The top panel is wind speed bias vs regime for the NE wind direction and the bottom panel is for the SW wind direction. . . . .*      66

Figure 54      *BIAS VS RMSE' DIAGRAM. The top panel is for HRM and the bottom panel for HRM-WF at far-lidar location. . . . .*      68

Figure 55      *BIAS VS RMSE' DIAGRAM. The top panel is for HRM and the bottom panel for HRM-WF at near-lidar location. . . . .*      69

Figure 56      *WIND SPEED BIAS VS. STABILITY The top panel is for the far-lidar location and the bottom panel for the near-lidar location. . . . .*      72

Figure 57      *POWER BIAS VS. STABILITY. The bias is expressed as a percentage of nameplate capacity of the wind farm which is 684.59 MW. See Appendix B for power bias in terms of MW. . . . .*      73

Figure 58      *FUTURE WIND FARMS IN THE NORTH SEA. As the figure illustrates, there are 6 upcoming wind farm projects in the pipeline including the Borssele Wind Farm Zone which was the area of interest in this study. . . . .*      81

---

## LIST OF TABLES

---

Table 2	THE LOCATIONS OF THE TWO FLOATING LiDARs ( <i>Offshorewind.rvo.nl</i> ) The ‘far-lidar’ is referred to as Lot 1 in official documentation and is around 17.63 km from the Belgian wind farms. The ‘near-lidar’ is Lot 2 and 6.4 km away. . . . .	21
Table 3	CHARACTERISTICS OF OPERATIONAL BELGIAN WIND TURBINES ( <i>Offshorewind.rvo.nl</i> ). This table provides turbine data which is relevant for discussion and interpretation of results from Chapter 4. . . . .	29
Table 4	FLOATING LiDAR DATA AVAILABILITY ( <i>Offshorewind.rvo.nl</i> ) As depicted, an overlap of the two data-sets is present only in 2016. . . . .	30
Table 5	RATIO OF CURTAILED POWER IN THE BELGIAN WIND FARM The ratio of curtailed power production for the selected temporal domain has been presented. . . . .	34
Table 6	DESCRIPTIVE STATISTICAL OVERVIEW OF MODEL PERFORMANCE AT FAR-LIDAR FOR HUB HEIGHT. . . . .	70
Table 7	DESCRIPTIVE STATISTICAL OVERVIEW OF MODEL PERFORMANCE AT NEAR-LIDAR FOR HUB HEIGHT. . . . .	70
Table 8	DESCRIPTIVE STATISTICAL OVERVIEW OF MODEL PERFORMANCE FOR POWER PRODUCTION. The rated power of the wind farm is 684.59 MW. . . . .	71
Table 9	INTRA-MODEL PERFORMANCE INDICATING LEAST BIAS CONDITIONS AND MOST BIAS CONDITIONS. This table illustrates a model’s least and most bias conditions when compared with its bias values for all the stability regimes. . . . .	77

---

## LIST OF ACRONMYS

---

BWFZ	Belgian Wind Farm Zone. <a href="#">28</a>
CBL	Convective Boundary Layer. <a href="#">xii</a> , <a href="#">19</a>
DTU	Denmark Technical University. <a href="#">22</a>
E	East. <a href="#">34</a>
GPU	Graphical Processing Unit. <a href="#">26</a>
HRM	HARMONIE-AROME without wind farm parameterization. <a href="#">24</a> , <a href="#">87</a>
HRM-WF	HARMONIE-AROME with wind farm parameterization. <a href="#">25</a> , <a href="#">87</a>
IPCC	Intergovernmental Panel on Climate Change. <a href="#">1</a>
KNMI	Royal Netherlands Meteorological Institute. <a href="#">2</a>
LES	Large-Eddy Simulation. <a href="#">2</a> , <a href="#">3</a>
NBL	Neutral Boundary Layer. <a href="#">xii</a> , <a href="#">19</a>
NE	North-East. <a href="#">34</a>
NW	North-West. <a href="#">34</a> , <a href="#">35</a>
NWP	Numerical Weather Prediction. <a href="#">5-7</a>
RMSE	Root Mean Squared Error. <a href="#">30</a>
SAR	Synthetic Aperture Radar. <a href="#">15</a> , <a href="#">22</a>
SBL	Stable Boundary Layer. <a href="#">xii</a> , <a href="#">19</a>
SE	South-East. <a href="#">34</a>
SW	South-West. <a href="#">34</a>

TKE	Turbulent Kinetic Energy. <a href="#">7</a> , <a href="#">8</a>
UTC	Coordinated Universal Time. <a href="#">23</a>
W	West. <a href="#">34</a>
WFP	Wind Farm Parameterization. <a href="#">35</a>
WRF	Weather Research and Forecasting. <a href="#">18</a>

---

## INTRODUCTION

---

*In this chapter, a succinct discussion of the field of research is presented. The relevance of the research, its broader implications and the main objectives are addressed. It also concisely outlines the contents of this document.*

### 1.1 TOPIC AND RELEVANCE

From time immemorial, mankind has always taken a keen interest in predicting the future. Whether it is looking up at the stars or looking down at our palms, numerous disciplines have evolved from this primary urge. Out of all these, only some fields have achieved the mathematical and scientific rigour necessary to be taken seriously and among these is weather forecasting.

This outcome is a result of years of development of a myriad of mathematical models and simulations. Some of which has allowed us to look at climatology, others short-range forecasts and so on and so forth. These models provide us with data on different things related to the weather at different levels of temporal and spatial resolutions: atmospheric variables such as daily wind speeds or temperature as well as more complex long-term reports such as the carbon dioxide concentration over several decades. The latter, after close monitoring by the [Intergovernmental Panel on Climate Change \(IPCC\)](#) for several years has been the catalyst for the steady shift towards renewable energy consumption which includes solar, wind and other such energy production.

As on date, the Netherlands is fortunately poised to capitalise on such a shift since it has already launched plans to install wind farms, particularly in the North Sea, with the interest of meeting the demands of the Paris agreement. Thus, with more projects in the pipeline, wind farms are becoming a significant feature in our horizon both literally and figuratively ([Borssele Wind Farm Site V, Innovation Site | RVO.nl](#)).

Furthermore, to aid a better understanding of the wind resource on the North Sea, a weather atlas, namely the Dutch Offshore Wind Atlas (the atlas is the data output by HARMONIE-AROME - a model that was developed by the ALADIN-HIRLAM consortium and which is used operationally in ten countries) by the Royal Netherlands Mete-

orological Institute (KNMI), was released in early 2019 (KNMI, 2019). Currently, the region of interest in the North Sea already has several wind farms that are operated by various wind operators who supply electricity to Belgium's power grid (see Figure 1).

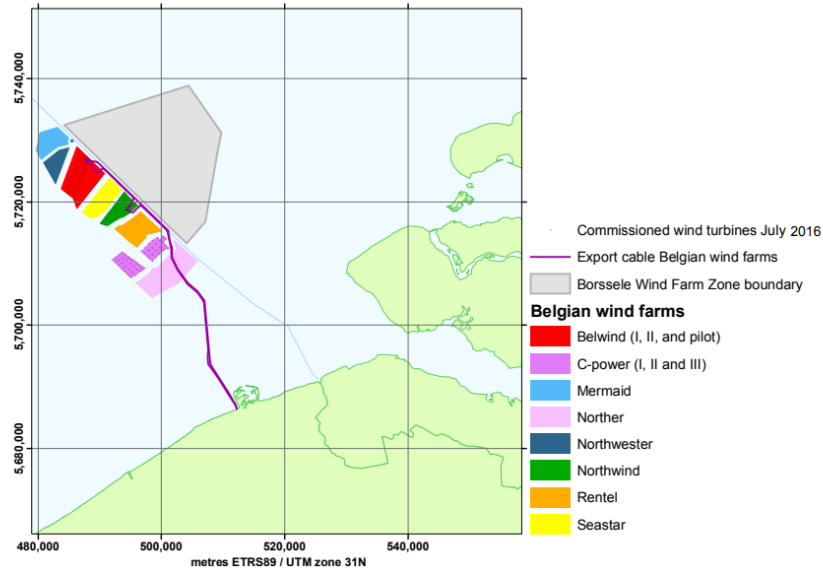


Figure 1: THE PROPOSED DUTCH WIND FARMS AND BELGIAN WIND FARMS. ADAPTED FROM RVO.NL ([Offshorewind.rvo.nl](http://Offshorewind.rvo.nl)) The red, green, and pink zones are already commissioned wind farms by Belgium. The other colours are wind farms that are yet to be commissioned. The Borssele Wind Farm Zone is adjacent to the Belgian wind farms shaded in grey.

This information is important to consider when performing a wind resource assessment since literature studies [Fitch, Lundquist, and Olson (2013) and Roy, Pacala, and Walko (2004)] show that wind farms have a significant effect on atmospheric flow with practical implications such as energy extraction by upwind turbines affecting the power output of downwind turbines. Specifically, Figure 2 illustrates the wind farm projects that have been planned by the Dutch government. They are placed adjacent to Belgian wind farms that have already been fully commissioned and hence will have an impact on the future Dutch wind farms. To appropriately assess the Borssele wind farm region, floating LiDAR observations by Fugro were dispatched in the region. However, point measurements need to be supplemented with model data. Additionally, as Roy, Pacala, and Walko (2004)'s work rightly demonstrates, there are advantages of mesoscale modelling as a source of valuable information especially since it not being as computationally expensive as higher resolution models, i.e. [Large-Eddy Simulation \(LES\)](#).

Thus, the Dutch Offshore Wind Atlas needs to account for the atmospheric effects of the wind farms and this has been done by including

a set of equations in the (HARMONIE-AROME) model which will mathematically represent the physical effects of a wind farm (this will be elaborated in detail in a following section). This thesis is an attempt to validate the model output against meteorological and turbine power data from the Belgian wind farms.

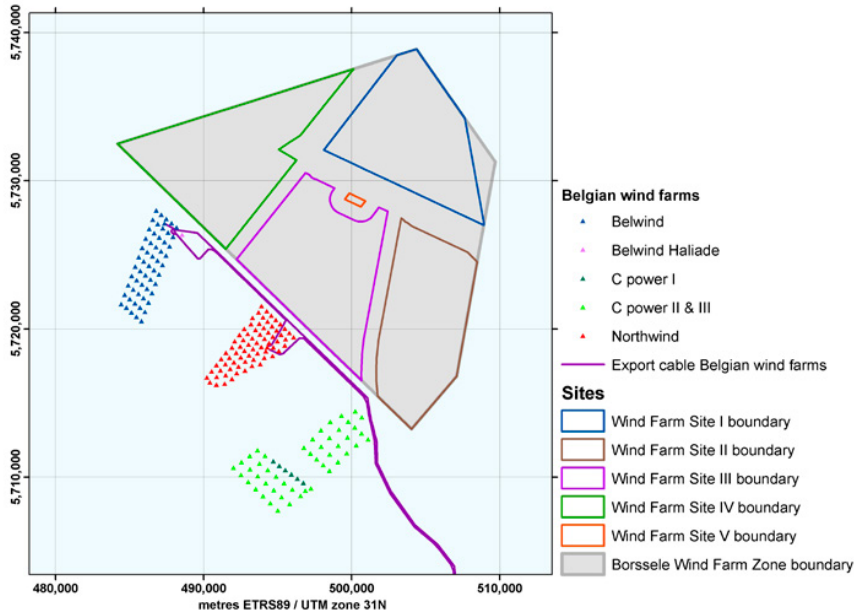


Figure 2: THE PROPOSED BORSSELE WIND FARM ZONE AND FULLY COMMISSIONED BELGIAN WIND FARM. ADAPTED FROM RVO.NL ([Offshorewind.rvo.nl](http://offshorewind.rvo.nl)) A closer look at the region of interest with the different wind operators of the Belgian wind farm highlighted in different colours and the proposed sites within the Borssele Wind Farm Zone.

## 1.2 RESEARCH QUESTIONS AND METHODOLOGY

Primarily, the validation is structured to answer the following questions:

- HOW DOES THE WIND FARM PARAMETRIZATION (WFP) IN HARMONIE-AROME PERFORM? This question will be answered by evaluating model results with observational data-sets which include wind speed, power production, as well as comparisons with a data-set generated by a [Large-Eddy Simulation \(LES\)](#).
- HOW CAN THE CURRENT WFP IN HARMONIE-AROME BE FURTHER IMPROVED? The results of the model vs observations comparisons will provide insights on model performance. Furthermore, composite analysis based on atmospheric stability, wind

direction and aerial wake samples will highlight the exact areas of improvement and aspects of the model that need to be fine-tuned or indicate an overall bias that requires a correction factor.

- **WHAT ARE THE METEOROLOGICAL INSIGHTS ONE CAN GAIN FROM THE SIMULATION RESULTS?** This is an open-ended question which will be answered by collating the model performance results and connecting it to existing literature to either corroborate or contradict previous results. Primarily, once the model is validated, model behaviour in various atmospheric stability regimes can provide additional understanding of the various atmospheric effects of wind farms.

A detailed methodology of research is elaborated in a following section.

### 1.3 ORGANISATION OF THESIS

This thesis comprises of five chapters (excluding this one) and follows a standard thesis format. Chapter 2 provides key background concepts to grasp the literature on wind farm parameterizations provided in the chapter. It also presents results from literature studies that have been conducted on similar scenarios and from which certain hypotheses or expectations for this thesis' results have been developed. This is followed by Chapter 3 which extensively details the methodology adopted for the performance evaluation to ensure that results are reproducible by third parties. Chapter 4 and 5 present the results of the work done by the author along with a discussion section where the results are placed in context of existing literature. Since, many of the results are pictorial in nature and to avoid cluttering the main text, appendices with figures have also been attached.

# 2

---

## LITERATURE REVIEW

---

*This chapter provides a concise background on the field of study by reviewing fundamental concepts such as the workings of a numerical weather prediction model, important terms and definitions in atmospheric physics. It also addresses what a wind farm parameterization is and how it has been developed and the results of incorporating it in a model according to literature.*

### 2.1 BACKGROUND

In this section, a limited overview of what numerical weather prediction models are and the mechanism of representing complex atmospheric processes in a simplified manner within a model (parameterization) is presented. It also discusses a relevant atmospheric physics concept of atmospheric stability and the meteorological indices used to describe it.

#### 2.1.1 Numerical Weather Prediction Models

The HARMONIE-AROME model that is being validated for its new parameterization in this thesis is an operational mesoscale [Numerical Weather Prediction \(NWP\)](#) model. In simpler terms, it is a type of weather prediction model that is a) in use, b) has a resolution that is between 1 - 10 km and c) is used to forecast weather by numerically approximating fundamental equations that are used to describe the atmospheric dynamics.

Such models are crucial to studying the atmosphere and the mesoscale impacts of various phenomenon. This is because there exist few reliable observational data sets. This is particularly true for observational data that record atmospheric impacts of wind farms (Fitch et al., 2012). Consequently, this implies that if the model behaviour is validated, it can be later utilised to provide a fresh perspective on local impacts of wind farms as well. A mesoscale model is a sub-category of [NWP](#) models. The equations that are used in a [NWP](#) prognose atmospheric variables such as temperature, humidity, wind etc whereby the initial state is usually arrived at by data assimilation (Haupt et al., 2017). Weather prediction, in general, is difficult since these atmospheric equations do not have an analytical solutions. Hence, NWP's, as the

name suggests, numerically approximate the solutions. There are two key parts to an NWP: a dynamic solver and physical parametrization schemes (Haupt et al., 2017). The dynamic solver, by algebraic approximation, solves for the advection, pressure gradient, Coriolis force and other terms. This is done either by finite difference methods or by spectral methods (Haupt et al., 2017).

The simplest models are diagnostic in nature but a NWP more often than not contains prognostic variables. In such models, there are often more unknowns than equations. Therefore, to solve for unknown variables, a mathematical technique known as a closure scheme is employed (Warner, 2011) where the remaining unknown terms are parameterized by representing them as some function of the known variables.

A closure scheme's order is identified by the degree of the moment of a predictive (or prognostic) equation. In other words, if there exists an equation for a mean variable such as temperature  $\bar{\theta}$  and the covariance term for temperature ( $\overline{w'\theta'}$ ) is in turn parameterized, this implies that the covariance is expressed in terms of  $\bar{\theta}$  and it is known as a first order closure (Warner, 2011). Mathematically, the equation for covariance of temperature is parameterized as:

$$\overline{w'\theta'} = -K_H \frac{\partial \bar{\theta}}{\partial z} \quad (1)$$

Where  $K_H$  is the diffusivity term. This allows us to solve for an equation such as (Warner, 2011):

$$\frac{\partial \bar{\theta}}{\partial t} = \dots - \frac{\partial \overline{w'\theta'}}{\partial z} \quad (2)$$

This is the most basic closure scheme for predicting variables like vertical fluxes (Holtstlag, 2015). Thus, it follows from this that in a second order closure scheme, prognostic equations for both the mean variable  $\bar{\theta}$  and its covariance ( $\overline{w'\theta'}$ ) exist and only a triple correlation is parameterized ( $\overline{w'w'\theta'}$ ) (Warner, 2011).

This can be summarized as follows as adapted from Warner (2011):

ORDER OF CLOSURE	UNKNOWNNS
Zero	$\bar{\theta}$
First	$\overline{w'\theta'}$
Second	$\overline{w'w'\theta'}$

An interesting scenario exists according to Warner 2011 when:

“in a prognostic equation for the first moments, some second moments on the right side may be parameterized

while others are predicted. If all the second moments are predicted, the closure would be second order. If they are all parameterized, it would be first order. Thus, in this case ...(wherein some of the terms in a particular moment category are parameterized and some are explicitly predicted)... it would be referred to as a 1.5 order method."

A 1.5 order closure scheme is the minimum mandatory requirement for prognosing **Turbulent Kinetic Energy (TKE)** (Holtslag, 2015). This can be understood by looking at the TKE equation (Equation (3)) for small scale fluctuations in the next section where  $\bar{\epsilon}$  is prognosed in terms of turbulent heat and momentum fluxes.

### 2.1.2 Parameterizations

The part of the NWP that is most relevant to this study are the parameterizations that along with a dynamic solver, form a **NWP**. As stated earlier, the purpose of a physical parameterization scheme is to represent the effects of processes that are not explicitly resolved in the model. In model terminology, the phrase "resolved" often refers to processes that do not need to be parameterized and these are often the primary inputs for parameterizations. Note that parameterization schemes can be incorporated either algorithmically or statistically (Haupt et al., 2017).

Furthermore, much like how the physical processes in the real world interact with each other and are interdependent, parameterization schemes should not be developed completely independently. These interactions determine the realistic accuracy of models (Haupt et al., 2017). In summary, parametrization schemes are incorporated in **NWPs** to model physical processes that cannot be resolved and/or are not well understood (Haupt et al., 2017). This includes radiation, land-surface interaction, turbulent mixing, convective clouds, microphysics and other such processes (Haupt et al., 2017).

### 2.1.3 Obukhov Length and Atmospheric Stability

In preceding sections and in the upcoming chapters, the phrase 'atmospheric stability' has been and will be used liberally. This section provides a limited recapitulation of this concept.

To understand 'atmospheric stability', it is necessary to review the equation for turbulent kinetic energy.

$$\frac{\partial \bar{\epsilon}}{\partial t} = -\overline{u'w'} \frac{\partial \bar{u}}{\partial z} + \frac{g}{\theta_v} \overline{w'\theta'_v} - \dots - \dots - \epsilon \quad (3)$$

Where,

$\overline{u'w'}$  is the turbulent momentum flux in  $\text{m}^2\text{s}^{-2}$

$-\overline{u'w'}\frac{\partial\bar{u}}{\partial z}$  is the shear production term in  $\text{m}^2\text{s}^{-3}$  (Let this be referred to as Term I)

$\overline{w'\theta'_v}$  is the is the turbulent heat flux in  $\text{m}^2\text{s}^{-2}$

$\frac{g}{\theta_v}\overline{w'\theta'_v}$  is the buoyancy term in  $\text{m}^2\text{s}^{-3}$  (Let this be referred to as Term II)

$\epsilon$  is the dissipation of TKE due to molecular diffusion at the small scales in  $\text{m}^2\text{s}^{-3}$

(...) are two omitted transport terms that are not relevant here but represent redistribution of TKE in space

The first term,  $-\overline{u'w'}\frac{\partial\bar{u}}{\partial z}$ , in the budget equation is a production term for TKE and the last term,  $\epsilon$ , is a loss term for TKE. On the other hand, buoyancy,  $\frac{g}{\theta_v}\overline{w'\theta'_v}$ , can either be a production or a loss term based on its sign.

The ratio of the buoyancy production term to the shear production term (Term II and Term I) is known as the Richardson (flux-Richardson) number and this gives us a measure of atmospheric stability by characterising the role of buoyancy in the production of turbulence (Moene and Dam, 2014):

$$\text{Ri}_f = -\frac{\text{buoyancy production}}{\text{shear production}} = \frac{\frac{g}{\theta_v}\overline{w'\theta'_v}}{\overline{u'w'}\frac{\partial\bar{u}}{\partial z}} \quad (4)$$

Specifically, four broad states have been distinguished as per Moene and Dam (2014): a neutral regime where there is no buoyancy production, an unstable regimes where TKE is produced by both the shear term and the buoyancy term (refer Equation (3)), a stable regimes where buoyancy destroys TKE produced by the shear term, and a very unstable or a very stable regime wherein the effect of shear production is dominated entirely by the effect of buoyancy.

Another such index used to classify the atmosphere into different regimes is the Obukhov length (L) and is later used in this thesis to parse data into different atmospheric regimes. The Obukhov length is the height below which shear dominates TKE production and above which buoyancy dominates TKE production (Moene and Dam, 2014). When the Obukhov length scale is used to scale the height above the ground  $z$ , we obtain the dimensionless parameter  $z/L$ .

Mathematically, adapted from Moene and Dam (2014):

$$z/L = -z\kappa\frac{g}{\theta_v}\frac{\overline{w'\theta'_v}}{\rho C_p} \frac{1}{u_*^3} \quad (5)$$

Where,

$z$  is the height above the ground in m

$\kappa$  is the von Karman constant historically considered to be 0.40 (although Moene and Dam (2014) argue that its value in the atmospheric surface layer is a point of contention)

$\frac{g}{\theta_v}$  is the buoyancy parameter where  $g$  (in  $\text{ms}^{-2}$ ) is the acceleration due to gravity and  $\theta_v$  is the virtual potential temperature (in K)

$\overline{w'\theta'_v}$  is the kinematic heat flux,  $C_p$  (in  $\text{J}/(\text{kg K})$ ) is the specific heat of moist air,  $\rho$  is the density (in  $\text{kgm}^{-3}$ )

$u^*$  is the friction velocity which is equal to  $\sqrt{\frac{\tau}{\rho}}$  where  $\tau$  (in Pa) is the surface shear stress or momentum transported towards the ground

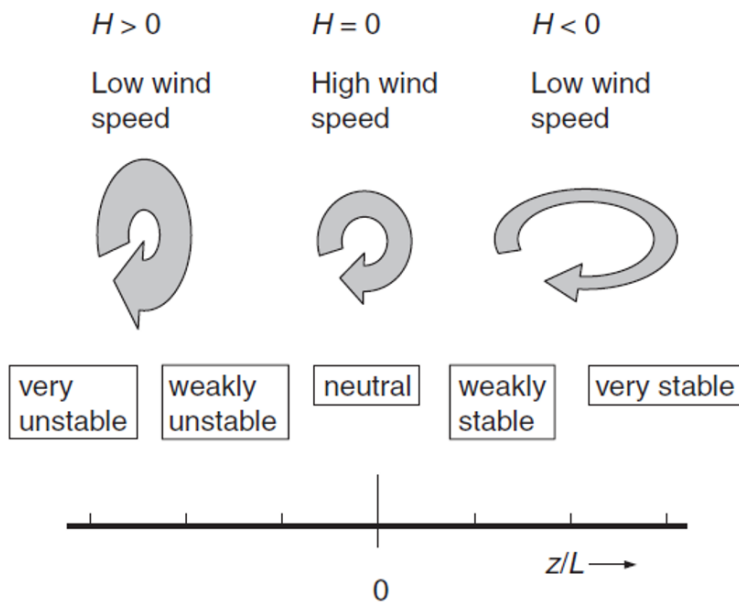


Figure 3: THE RELATIONSHIP BETWEEN STABILITY PARAMETERS ( $z/L$ ) AND ATMOSPHERIC VARIABLES. ADAPTED FROM MOENE AND DAM (2014) As the figure indicates,  $z/L$  close to 0 indicates neutral regimes, positive values imply stable regimes and negative values indicate unstable regimes. In the latter regime, low wind speeds but a positive sensible heat flux is expected. In the former, a negative sensible heat flux is expected. Neutral regimes are usually well-mixed with high wind speeds.

What is relevant here is that when  $z/L$  is positive, it indicates stable conditions or a suppression of turbulence by buoyancy whereas

negative values imply unstable conditions or an enhancement of turbulence by buoyancy. Simultaneously, when  $z/L = 0$ , it implies that we have neutral conditions where buoyancy does not play any role. This is explicitly illustrated in Figure 3 along with wind speed behaviour for associated classes (Moene and Dam, 2014).

The shape and thickness of the arrows indicate the effect of stability on turbulent motion and intensity of turbulent motion respectively. The 'H' represents the sensible heat flux and below that, the representative wind speeds in the regimes are provided (Moene and Dam, 2014). Thus, it is expected that the model wind speed outputs, when classified according to stability, will agree with the magnitude of wind speeds expressed here.

## 2.2 STUDIES ON WIND FARM PARAMETERIZATION

Wind energy extraction is based on the principle of transforming kinetic energy of the wind into electricity - which is carried out by wind turbines. This is possible because of the forces that act on a turbine blade. From an aerodynamic perspective, there are two components of the force that is exerted by the wind on a wind turbine blade: the lift and drag forces. They act perpendicular and parallel to the wind direction respectively (see Figure 4.) The lift force is used to overcome gravity and allows the mass to be lifted up from the ground (Hansen, 2008).

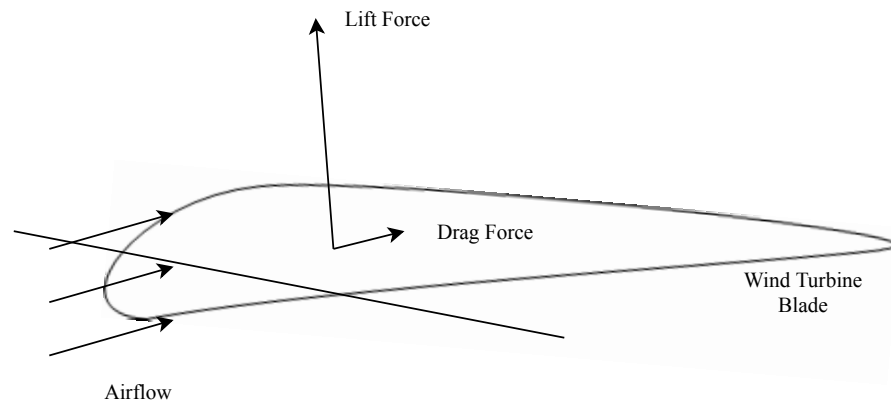


Figure 4: AN ILLUSTRATION OF LIFT AND DRAG FORCES ON A WIND TURBINE BLADE *The lift force allows the turbine blade to be lifted and the drag force is exerted in the direction parallel to the flow of the wind.*

In theory, one can calculate the maximum amount of power that can be extracted based on the wind speed. Practically, the actual power that can be generated is deduced with a coefficient, called

the power coefficient or  $C_p$  which is the ratio of the actual power obtained from a turbine to the maximum power available:

$$C_p = \frac{P}{\frac{1}{2}\rho V_o^3 A} \tag{6}$$

Where,

$\rho$  is the air density in  $\text{kgm}^{-3}$

$V_o$  is the upstream wind speed in  $\text{ms}^{-1}$

$A$  is the area of the rotor in  $\text{m}^2$

This coefficient is important since it plays an integral role in the parameterization of a wind farm. In some other words,  $C_p$  is also referred to as the ratio of the power output to the kinetic energy flowing through the rotor (Hansen, 2008).

There is also another recurring coefficient:  $C_T$  or the thrust coefficient which requires discussion. The thrust is the axial force applied by the wind on the rotor and consequently, by Newton’s first law of mechanics, the axial force applied by the wind turbine on the wind (Hansen, 2008). Mathematically, the thrust coefficient is the ratio of the force used to necessary to slow down the wind speed (to extract energy) to the ideal thrust:

$$C_T = \frac{T}{\frac{1}{2}\rho V_o^2 A} \tag{7}$$

Where the other terms hold the same meaning as Equation (6).

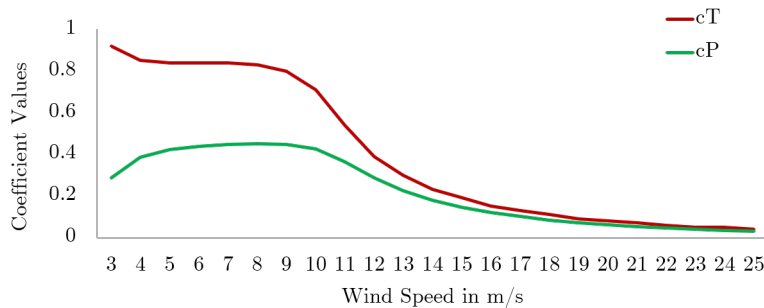


Figure 5: AN ILLUSTRATION OF POWER AND THRUST CURVES OF A VESTAS 112 WIND TURBINE AS FUNCTIONS OF WIND SPEED The x-axis is the wind speed and the y-axis shows the values for the the thrust and power coefficients. These curves are often provided by wind turbine manufacturers.

What is important is that both coefficients need to be highly accurate so that realistic results are generated. Usually all wind turbine

types have a unique power output curve which is provided by the manufacturer and expresses the power that can be generated as a function of wind speed at rotor hub height. An example is provide in Figure 5.

Theoretically, the maximum  $C_p$  value is 0.59. This is known as the Betz limit (Roy, Pacala, and Walko, 2004). This limit is the maximum efficiency of a wind turbine (in terms of power production) according to literature. However, in practice, as seen from Figure 5 this value is usually closer to 0.5.

#### 2.2.0.1 *Wind Farm Wake Effects on Local Meteorology*

In offshore wind energy-wind speed studies (and this thesis), the most interesting aspect of a wind farm is the region immediately behind the turbine rotor blades is known as a wake. As Vermeer, Sørensen, and Crespo (2003)'s work states, normally, the turbine wake is divided into a near and a far wake. The near wake is the area just behind the rotor up to 1 rotor diameter distance. In this region, properties of the rotor can be discriminated. The far wake is the region beyond the near wake, beginning between 1 and 3 rotor diameters (Vermeer, Sørensen, and Crespo, 2003). More often than not, wind farms are structured in such a way that turbines that are not at the edges are situated in the wake region of a turbine in front of them. As a result, downstream turbines experience slower winds and additional turbulence (Vermeer, Sørensen, and Crespo, 2003). This is because a percentage of the energy that upstream turbines are unable to transform into electricity, becomes turbulent kinetic energy. At the same time, wind turbines transform the energy into electricity by removing the momentum of the wind (Vermeer, Sørensen, and Crespo, 2003). Thus, these wake losses hamper the power predicted in wind farms and are an import area of research. Once we are sufficiently downstream, though, turbulent diffusion removes both the momentum deficit and the increase in TKE but these are dependent on the atmospheric stability conditions for most part and even during the best conditions, wake losses within a wind farm persist due to the spacing of turbines (Vermeer, Sørensen, and Crespo, 2003).

Aside from the impact of wake losses on power production, a lot of studies on the effects of wind farms on the local weather have been conducted. Among these, some papers quantify effects on local wind, turbulence, temperature, or moisture flux. For example, in the study conducted by Roy, Pacala, and Walko (2004), it was found that wind farms significantly reduce the wind speed at the turbine hub-height level and turbulence generation can cause mixing which in turn affects the shear profiles of variables such as temperature, humidity, surface sensible and latent heat fluxes. Furthermore, due to the nocturnal low-level jet, these impacts were found to be strongest at dawn or earlier. This is because the nocturnal boundary layer is

largely stable with large vertical gradients of wind speed, humidity and temperature. Hence, any mixing during this period has a more pronounced effect than in a well-mixed boundary layer. (Roy, Pacala, and Walko, 2004)

Regarding non-local effects, Keith et al. (2004)'s analysis suggests that wind farms do have significant impacts but to quantify and confirm this hypothesis, further research is required.

### 2.2.1 Wind Farm Parameterization Development in Literature

From literature, it was identified that there are two popular methods to parameterize wind farms in meso- or large-scale models. In the first method, they are modelled as an increase in roughness length and in the second they are represented as an elevated momentum sink and source of turbulence (Abkar and Porté-Agel, 2015a). The former approach works well with coarse vertical resolution atmospheric models but it has a drawback: it is often difficult to estimate the effective roughness length. In contrast, the latter method can be employed in any type of atmospheric model as long as the lowest grid point is below the turbine hub height. It considers the fact that wind turbines generate 'wake losses'. In aerodynamics, wake losses are losses of energy due to its transformation into turbulent kinetic energy (TKE). (Abkar and Porté-Agel, 2015a) This second method is most recently employed in numerical weather prediction models.

Roy, Pacala, and Walko (2004)'s method was one of the earliest proposals based on this concept. This was shortly followed by Blahak et. al who developed the early method to parameterize wind turbine induced drag forces as a feedback into the atmospheric system in a mesoscale weather model. This scheme is specifically developed for a situation where several layers of the model intersect the rotor area of the wind turbines and where the wind farm may span several adjacent model grid columns (Blahak, Goretzki, and Meis, 2010). In Blahak, Goretzki, and Meis (2010)'s paper, the parameterization modifies the one proposed by Roy, Pacala, and Walko (2004) by assuming that the TKE added by turbines is proportional to the extracted kinetic energy of the turbine. The derivation is not presented here but mathematically, the TKE source equation (in  $\text{m}^2/\text{s}^3$ ) is written as (for a model such as an LES),

$$\frac{\partial \text{TKE}}{\partial t} = n_t \alpha \frac{\frac{1}{2} C_P \langle \bar{u}_r \rangle_k^3 A_k}{z_{k+1} - z_k} \quad (8)$$

Where,

$n_t$  is the local number of wind turbines per area (inside a grid cell):  $\frac{N_t}{\Delta x_{\text{grid}} \times \Delta y_{\text{grid}}}$

$\alpha$  is the additional kinetic energy conversion from grid scale to sub-grid scale and is empirically set to 0.2

$C_p$  is the power coefficient

$\langle \tilde{u}_r \rangle_k$  is the grid-cell horizontal velocity magnitude at hub height where the over-bar and angle brackets denote time and spatial averaging respectively in m/s (The tilde denotes the LES filtering operation at scale  $\tilde{\delta}$  and is not relevant for HARMONIE-AROME)

$A_k$  is the cross sectional rotor area of one wind turbine within the model level  $k$  and  $k + 1$  in the grid cell in  $m^2$

$k, k+1$  are grid box notations (representing lower and upper heights of the grid cell)

$z$  is the height in m

Additionally, since the turbines also behaved as a momentum sink, the equation (in  $m^2/s^3$ ) was written as:

$$\langle \bar{f}_i \rangle = n_t (1 + \alpha) \frac{\frac{1}{2} C_p \langle \tilde{u}_r \rangle_k \langle \tilde{u}_i \rangle_k A_k}{z_{k+1} - z_k} \quad (9)$$

Where,

$\langle \tilde{u}_i \rangle_k$  is the grid-cell velocity in  $ms^{-1}$

The other terms hold the same meaning as in Equations (8).

In 2012, Fitch et al., 2012 improved on Blahak, Goretzki, and Meis, 2010's parameterizations by quantifying the fraction of kinetic energy extracted from the atmosphere (previously  $(1 + \alpha) * C_p$ ) as  $C_T$  or the thrust coefficient (see Equation (7)).

Therefore, the momentum sink tendency (in  $m^2/s^3$ ) is given by:

$$\langle \bar{f}_i \rangle = n_t \frac{\frac{1}{2} C_T \langle \tilde{u}_r \rangle_k \langle \tilde{u}_i \rangle_k A_k}{z_{k+1} - z_k} \quad (10)$$

This can also be written, as mentioned in Fitch et al., 2012, as the rate of loss of kinetic energy (in a grid cell) which is given by (in  $kg m^2/s^3$ ):

$$\frac{\partial KE_{drag}}{\partial t} = -\frac{1}{2} n_t \Delta x \Delta y C_T \rho \langle \tilde{u}_r \rangle_k^3 A_k \quad (11)$$

Furthermore, Fitch et al., 2012 states that the fraction of the extracted energy converted into electrical energy is denoted as  $C_p$  (the power coefficient, see Equation (6)). Thus, the power extracted by the

turbine which is converted to useful electric energy is given by (in  $\text{kg m}^2/\text{s}^3$  or in W):

$$P = \frac{1}{2} n_t \Delta x \Delta y C_P \rho \langle \bar{u}_r \rangle_k^3 A_k \quad (12)$$

Where,  $\rho$  is the air density (in  $\text{kg}/\text{m}^3$ )

Finally, the difference,  $C_T - C_p$ , is consumed as losses or contributes to the production of TKE such that  $C_{\text{TKE}} = C_T - C_p$  (Fitch et al., 2012). Therefore, the TKE source (the power extracted that is not converted into electricity and converted to TKE (in  $\text{m}^2/\text{s}^3$ )):

$$\frac{\partial \text{TKE}}{\partial t} = n_t \frac{\frac{1}{2} C_{\text{TKE}} \langle \bar{u}_r \rangle_k^3 A_k}{z_{k+1} - z_k} \quad (13)$$

Where, the terms hold the same meaning as in Equations (8) to (9). (All equations have been adapted from Fitch et al. (2012) and Abkar and Porté-Agel (2015a)'s papers). In Chapter 3, the method of incorporating Equations (13) and (10), which form the core of the wind farm parameterization in the model, will be elaborated upon.

### 2.2.2 Relevant Outcomes from Previous Wake Studies

The early 2000s had a lot of work that primarily focused on understanding the factors that affect wind farm wakes strongly.

CHRISTIANSEN AND HASAGER (2005): In Christiansen and Hasager (2005)'s paper, for example, an analysis of velocity deficits show that there are three factors that have an impact on the wake effects from wind farms: the free stream velocity, the atmospheric stability and the number of turbines in operation. In their work, they use *Synthetic Aperture Radar (SAR)* data to create two transects - one crossing the wind farm and the other 8km parallel to the first transect (with no wind farms) as a reference. The velocity deficit from the transect across the wind farm is denoted as VD whereas the velocity deficit from the reference transect is  $\text{VD}_{\text{ref}}$ . Both these terms are positive when the measured wake wind speed is below the free stream velocity. Mathematically, velocity deficit is defined as:

$$\text{VD (in \%)} = \frac{U_{\text{freestream}} - U_{\text{wake}}}{U_{\text{freestream}}} * 100 \quad (14)$$

where the freestream wind ( $U_{\text{freestream}}$ ) is the undisturbed mean wind speed far upstream of a wind farm and wake wind ( $U_{\text{wake}}$ ) is the wind speed measured in the wake of a wind farm.

From Figure 6, it can be determined that the average VD increases over the wind farms for offshore conditions albeit slower than onshore. Overall, a maximum of 3% deficit is observed where wind

farms end. It must be noted here that during the SAR overpasses, it was confirmed that more than a third of the wind turbines were operational - indicating that this is a factor that may affect wakes. However, a relationship between the velocity deficit and number of operational turbines could not be established (Christiansen and Hasager, 2005).

As for wake dependence on stability (shown in Figure 7), during the SAR passes, the atmospheric regime was mostly an unstable or a near neutral regime, and the former resulted in wind speeds that recovered over a downstream distance of 5km (to 2% of the free stream velocity) and the latter resulted in a 20km recovery distance. Overall, an average drop of 8-9% was observed in the SAR data as the wind passed through a wind farm.

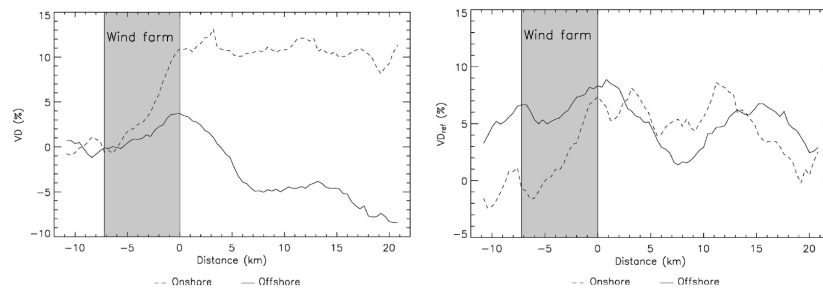


Figure 6: AVERAGE VELOCITY DEFICIT FOR REFERENCE AND WAKE TRANSECT FOR ONSHORE AND OFFSHORE WINDS. ADAPTED FROM (CHRISTIANSEN AND HASAGER, 2005) The shaded region indicates the location of the wind farm. Areas in the graph to the left and to the right are upstream and downstream distance respectively.

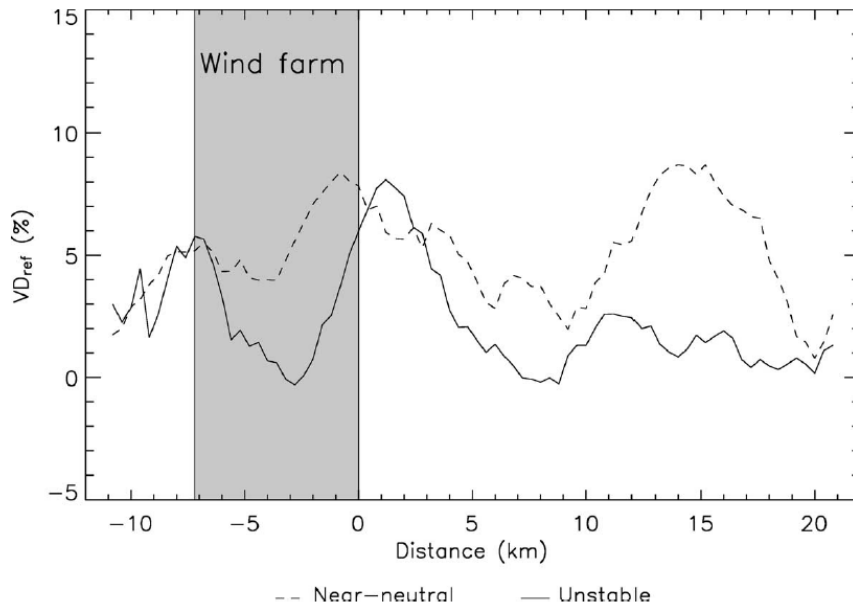


Figure 7: VELOCITY DEFICIT FROM SAR DATA DURING UNSTABLE AND NEAR-NEUTRAL CONDITIONS. ADAPTED FROM (CHRISTIANSEN AND HASAGER, 2005) The shaded region indicates the location of the wind farm. Areas in the graph to the left and to the right are upstream and downstream distance respectively.

In mid to late 2000s, more investigative studies on wakes were performed:

FITCH, LUNDQUIST, AND OLSON (2013): In 2013, a more quantitative study of the mesoscale influences of onshore wind farms by Fitch, Lundquist, and Olson (2013) produced the following conclusions. Due to strong mixing in the daytime thanks to an unstable boundary layer, it was observed that the momentum deficit is dissipated throughout the depth of the boundary layer and hence, a smaller drop in wind speed is observed. In numbers, a (maximum) reduction of 10% in the magnitude of wind speeds at hub height was observed during the day, which increased three-fold at night, to 30% since the nighttime stable layer results in lesser mixing due to stratification and leads to shallower wakes with higher wind speed reductions (See Figure 8).

ABKAR AND PORTÉ-AGEL (2015B): Abkar and Porté-Agel (2015b) also conducted an exhaustive large eddy simulation investigation on the influence of atmospheric stability on wind turbine wakes. Their results pointed out that atmospheric stability has a significant effect on three characteristics of a wake: the mean velocity deficit in terms of its spatial distribution, turbulence in the wake region and the meandering of the wake itself. Classifying atmospheric stability broadly as unstable, stable and neutral, the paper concludes qualitatively that

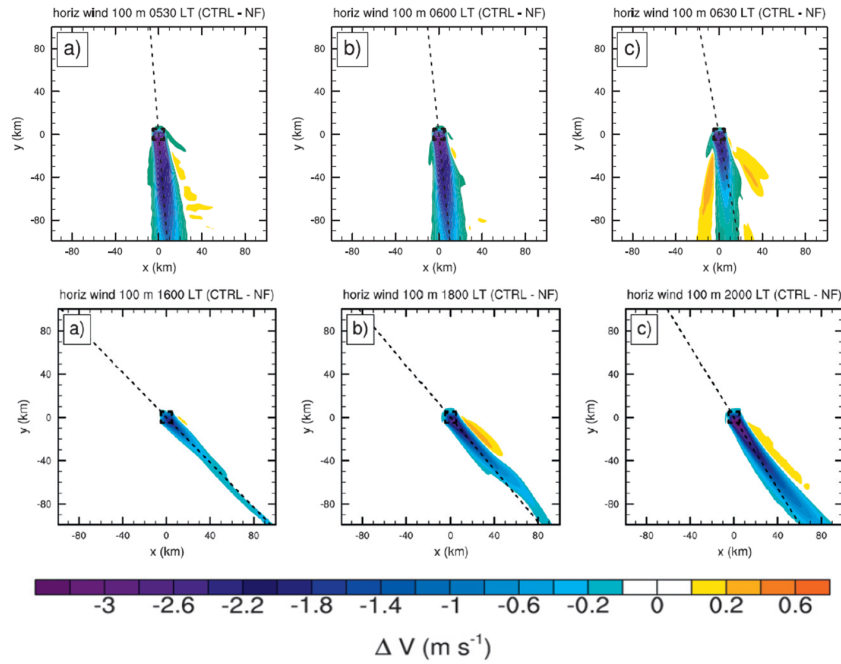


Figure 8: HORIZONTAL WAKE STRUCTURE IN THE MORNING AND EVENING. ADAPTED FROM (FITCH, LUNDQUIST, AND OLSON, 2013) *The structure of the wake is visible during the labelled time periods at hub height depicting the difference in wind speed between a wind farm and no-wind farm case. On the top row, a) 0530 local time b) 0600 local time c) 0630 local time. On the bottom row, a) 1600 local time b) 1800 local time c) 2300 local time.*

the wakes recover faster in convective conditions as compared to neutral and stable cases as illustrated in Figure 9.

Abkar and Porté-Agel (2015b) also stated that wake meandering was found to be stronger in convective conditions. It is to be noted here that according to (Larsen, 2007),

“The downstream advection of a wake from the emitting turbine describes a stochastic pattern known as wake meandering. It appears as an intermittent phenomenon, where winds at downwind positions may be undisturbed for part of the time, but interrupted by episodes of intense turbulence and reduced mean velocity as the wake hits the observation point.”

Interestingly, Abkar and Porté-Agel (2015b) also discovered that turbulence production and dissipation reached a peak around the upper edge of the wake. This was attributed to the presence of higher wind shear and turbulent fluxes in that region.

LEE AND LUNDQUIST (2017): Finally, in Lee and Lundquist (2017) 's most recent work (a paper evaluating a wind farm parameterization), a [Weather Research and Forecasting \(WRF\)](#) model with Fitch et al.

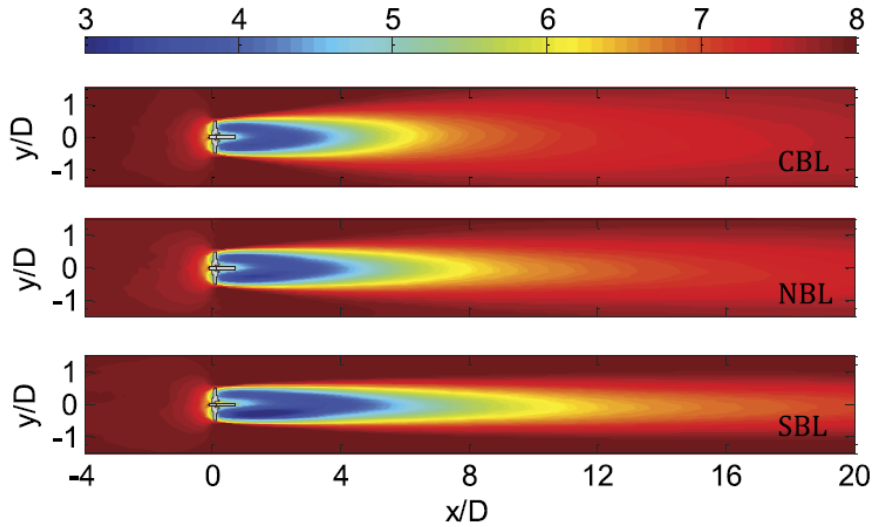


Figure 9: TIME-AVERAGED WIND SPEED CONTOURS IN m/s SLICED HORIZONTALLY AT THE TURBINE HUB HEIGHT FOR DIFFERENT STABILITY CONDITIONS. ADAPTED FROM (ABKAR AND PORTÉ-AGEL, 2015B) The  $x$  axis is normalised downwind distance,  $y$  axis is normalised lateral distance. The topmost plot is for a *Convective Boundary Layer (CBL)* condition, the middle plot is for a *Neutral Boundary Layer (NBL)* and the lowest plot is for a *Stable Boundary Layer (SBL)*

(2012)'s WFP was evaluated for a period of 24th to 27th August 2013. Although the goal of this evaluation was to quantify the far-wake impacts of multiple rows of turbines in staggered and aligned grid formations, some of their results are pertinent to this study.

In their paper, the WRF model setup simulated a central Iowa wind farm with 200 turbines and a total nameplate capacity of around 300 MW, and was compared to a profiling LiDAR, a scanning LiDAR, and a surface flux station. Their results concluded that in windy, stable and less turbulent conditions, the wake effects seemed to be overestimated in the model and hence the power production was underestimated.

These results indicate that an analysis of the model outputs in terms of atmospheric stability would provide insightful information on the latter's parameterization performance.

### 2.3 CONSTRUCTION OF HYPOTHESES

Based on reviewed literature and our expectations from the wind farm parameterization, certain hypotheses were constructed and specifically tested during the data analysis.

To determine the pure effect of the incorporation of the wind farm parameterization a benchmark evaluation between HARMONIE-AROME

with wind farm parameterization and HARMONIE-AROME without wind farm parameterization was conducted and it was expected to yield the following results:

- The undisturbed model results (HRM) at the near LiDAR will not account for wake effects unlike HRM-WF
- In a no-wind farm or an undisturbed region, for example, Cabauw, the two model runs' wind speed results will be nearly identical

Since a succinct comparison between HRM-WF and WRF was performed as a sanity check (Stratum et al., 2019), it was reasonable to assume that the results of Lee and Lundquist (2017)'s evaluation may have a bearing for the performance study of HRM-WF. Therefore, it was hypothesised that:

- In stable regimes, HRM-WF's power production (and/or wind speed) will be underestimated.

Other results in literature enabled to construct the following hypotheses:

- The wind farm will have an effect on the TKE/mixing
- The wind farm will cause a slowing down of wind speeds at hub height
- Turbulence generation can cause mixing which in turn affects atmospheric variables and will have the strongest impact during the early hours of the day (Roy, Pacala, and Walko, 2004)
- Wakes will recover faster in convective conditions compared to neutral and stable conditions

The hypotheses and the outcomes will be explicitly addressed at the end of Chapter 4.

# 3

---

## METHODOLOGY

---

*In this chapter, the methods used in conducting research are described and justified. Specifically, information on the data-sets and the various ways they were processed to help in evaluating the performance of the wind farm parameterization is provided. A list of hypotheses and the limitations and assumptions that have affected this work have also been discussed.*

### 3.1 DATA-SETS

#### 3.1.1 Observational Data-sets

- Fugro LiDAR: Fugro has conducted met-ocean measurement campaigns by deploying two floating LiDARs in the Borssele Wind Farm Zone. The data-sets are not continuous and include gaps due to irregular servicing needs. The locations of the two LiDARs are:

LiDAR	LONGITUDE (IN E)	LATITUDE (IN N)	DISTANCE FROM BELGIAN WIND FARMS (IN KM)
LOT 1 (FAR-LIDAR)	3.019157	51.71556	approx. 17.63
LOT 2 (NEAR-LIDAR)	2.9422162	51.650032	approx. 6.4

Table 2: THE LOCATIONS OF THE TWO FLOATING LiDARs ([Offshorewind.rvo.nl](http://Offshorewind.rvo.nl))  
*The 'far-lidar' is referred to as Lot 1 in official documentation and is around 17.63 km from the Belgian wind farms. The 'near-lidar' is Lot 2 and 6.4 km away.*

The data provided by Fugro include wind speed, wind direction, wind gust and turbulent intensity every 10 minutes at 30m, 40m and then up to 200m at 20m intervals. According to an analysis report on these Fugro LiDARs, (Dhirendra and Crockford, 2016), the uncertainty of measurements at hub height is around 0.45%.

- Sentinel-1 SAR: The Sentinel - 1 is a radar mission by Copernicus EU. It provides images in the C-band and has a high 20 m resolution with a wide swath of 250 km. Satellite Aperture Radar (SAR imagery) allows us to observe wakes qualitatively and provides a good representation of the wind turbine effects on the local environment (*User Guides - Sentinel-1 SAR - Overview - Sentinel Online*). A sample is attached in Figure 10. To obtain SAR imagery for the relevant time period, Google Earth Engine was employed to examine snapshots where wind farm wakes were observable. The data for the selected dates were downloaded from [Denmark Technical University \(DTU\)](#)'s portal for Satellite Winds. The data provided by (*Methodology - Synthetic Aperture Radar (SAR)*) are SAR wind maps that show the equivalent neutral wind speeds at 10 m above the sea surface. The wind retrieval is performed by several geophysical model functions that have been purposefully developed empirically for ocean wind retrieval from radar measurements. It is also noted that these functions are built on the assumption that wind speed increases logarithmically with height. While this is valid for neutrally stratified atmospheric stability regimes, a disclaimer is provided that for stable stratification an underestimation is observed while in unstable regimes an overestimation is expected. (*Methodology - Synthetic Aperture Radar (SAR)*)



Figure 10: SAR DATA RETRIEVED USING GOOGLE EARTH ENGINE (THE GOOGLE EARTH ENGINE CODE TO EXTRACT THE RELEVANT DATA WAS PROVIDED AS A COURTESY BY DR. S.L.M. (STEF) LHERMITTE) (*User Guides - Sentinel-1 SAR - Overview - Sentinel Online*) This snapshot shows the wakes from the Belgian wind turbines as captured by Sentinel-1 and displayed on the Google Earth Engine viewer

The SAR images were parsed for wakes and then the following dates were selected since they captured the wakes. A sample visual representation is provided in Figure 11:

– 5th February 2016

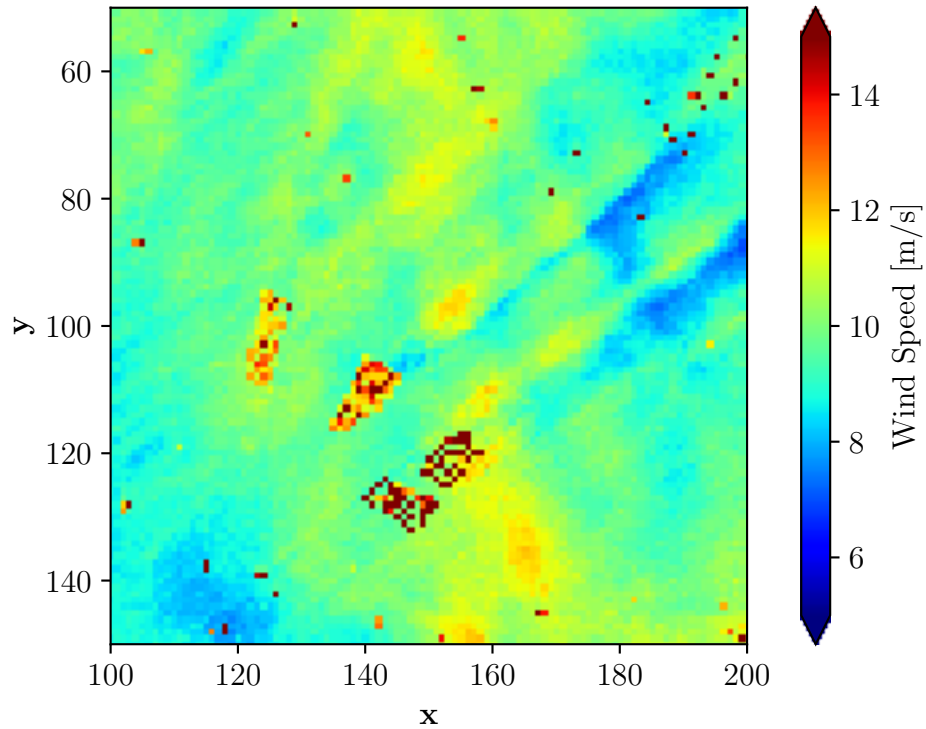


Figure 11: SAMPLE WAKE IMAGE FROM THE SAR DATA-SET *The colorbar indicates wind speed in m/s. This figure illustrated is for 5th February 2016.*

- 5th March 2016
  - 12th March 2016
  - 24th March 2016
  - 4th June 2016
  - 12th June 2016
- Elia Power Production: Belgium's transmission operator, Elia, provides measured and forecast-ed power data for the entire year of 2016 with no data gaps. The power output is reported every 15 minutes and measured in MW. In the power production data-sets, negative power values of around -1.17 MW were observed irregularly across the data-set. This strange anomaly was removed so as to avoid any effect on the statistical analysis. The corresponding timestamps in the models were also removed to ensure uniformity. This data-set was also converted from its local time to UTC ([Coordinated Universal Time](#)) before any comparison was conducted. The website from where the data was downloaded is: <https://www.elia.be/en/grid-data/power-generation/wind-power-generation>

### 3.1.2 Models

#### 3.1.2.1 HARMONIE-AROME (with and without a wind farm parameterization)

The HARMONIE-AROME model is an operational mesoscale numerical weather prediction model that was made available in 2012. Specifically, the model serves to develop short-range forecasts for important European cooperation projects. The original ERA5-HARMONIE domain comprises of 789x789 points but we will be using a sub-domain of 217x234 points. As for the the vertical resolution of the model, a hybrid sigma vertical grid is used. This consists of 65 vertical levels and a tapering spacing such that near the surface the grid spacing is around 20m subject to terrain, height, surface pressure etc. [(Simmons and Burridge, 1981; Untch and Hortal, 2004); (van Stratum, personal communication, October 28, 2019)].

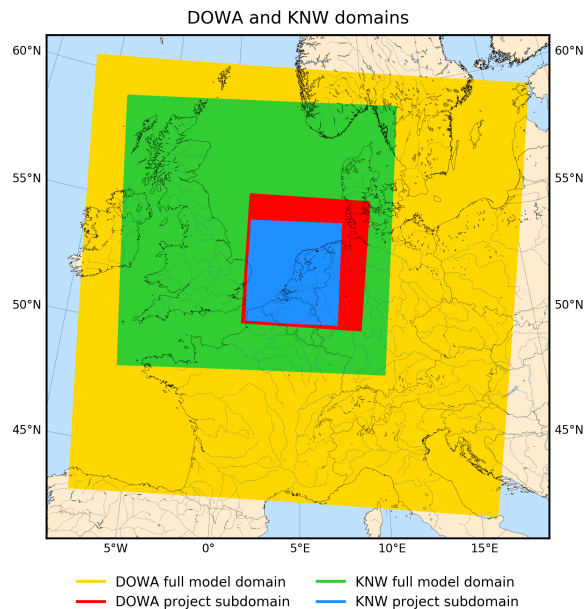


Figure 12: THE DUTCH OFFSHORE WIND ATLAS DOMAINS (ALONG WITH THE PREVIOUS VERSION OF THE ATLAS: KNW (IS NOT RELEVANT TO THIS THESIS) ADAPTED FROM (KNMI, 2019) The area shaded in red was the model output that was used for this work and further zoomed in to focus on just the Borssele wind-farm region in the North Sea.

These model details regarding domain and resolution apply to both versions of HARMONIE-AROME used in this thesis: with and without the wind farm parameterization (which was used to contrast the effect of the parameterization). This model, without the wind farm parameterization, is referred to, henceforth, as HRM and the HARMONIE-AROME run with the wind farm parameterization will

be referred to as [HRM-WF](#). HRM was obtained from the Dutch Off-shore Wind Atlas data-set which provides hourly data for all the grid points in the given region. The temporal resolution of the outputs of these models is hourly with a spatial resolution of 2.5 km. Specifically, HRM runs are labelled as ‘HARMONIE-AROME Cycle 40h1.2.tg2’ and HRM-WF runs are labelled as ‘HARMONIE-AROME Cycle DOWA\_40h12tg2\_fERA5\_WF2019’ in KNMI’s documentation (KNMI, 2019). It is important to note that the data in this thesis represented as HRM and HRM-WF runs are reanalyses, with a 3-hourly 3D-var data assimilation cycle (which is different from a HARMONIE forecast). The reanalysis is initialised with ERA5 data (at the start of 2016 for the run) and then consequently it provides information at the lateral boundaries of the model every hour (KNMI, 2019).

According to Bengtsson et al. (2017), both runs use “a framework with a prognostic equation for the turbulent kinetic energy (TKE) combined with a diagnostic length scale”. The TKE equation includes source and sink terms due to wind shear (sink), buoyancy (source), transport and dissipation of TKE (sink) as presented in Equation 3.

### 3.1.2.2 Incorporation of the wind farm parameterization in HARMONIE-AROME

The wind farm parameterization in (Fitch et al., 2012) considers wind turbines to be momentum sinks and sources of turbulent kinetic energy (see Equations (13) and (10) in Chapter 2). In HARMONIE-AROME, this is encoded by introducing a subroutine called ‘WIND-FARM’ (Stratum et al., 2019). This subroutine calculates the tendencies of U and V due to drag by wind turbines/farms, and TKE production due to efficiency losses

Algorithmically, SUBROUTINE WINDFARM:

- Calculates absolute wind speed at hub height
- Interpolates the power and thrust curves to the wind speed at hub height
- Calculates the difference between power production based on the mean wind speed at hub-height and the vertical integral wind speed over the wind turbine. This is a correction factor that has been included and is not part of (Fitch et al., 2012)’s WFP
- Calculates the corrected wind speed (u and v) tendencies (after calculating turbine area). The corrected tendencies for wind speed account for drag by having a term that removes momentum and the TKE tendency term accounts for additional TKE due to the wind farm.

It must be noted that this simulation incorporated not just the Belgian wind turbines near the Borssele Wind Farm Zone but several wind farms in the North Sea as Figure 13 illustrates.

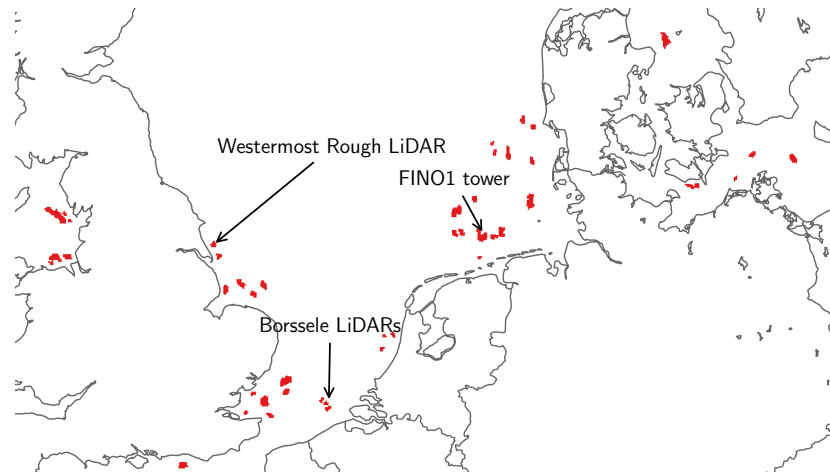


Figure 13: WIND FARM ZONES IN THE NORTH SEA. PROVIDED BY BART VAN STRATUM. (VAN STRATUM, PERSONAL COMMUNICATION, OCTOBER 21, 2019) The red points indicate wind farm areas. The arrows point to observation locations. Out of the three, only the Borssele LiDARs are utilised in this study.

### 3.1.2.3 GRASP LES

GRASP LES (GPU-Resident Atmospheric Simulation Platform Large-Eddy Simulation) is Whiffle's own GPU-based ([Graphical Processing Unit](#)) LES model. As Schalkwijk et al. (2015)'s work explains, a GPU is a processor that allows parallel computing to take place and hence has a massive computational advantage over a central processing unit (CPU). In general, LES models perform many computations that are nearly identical and this is handled by the (GPUs') parallel processing method as: firstly, any given equation solved for every grid node is the same and second, the data is ordered in a structured manner which allows each parallel GPU core to perform the same command but on the successive data element.

The LES model that runs on Whiffle's GPU core is based on the Dutch Atmospheric Large Eddy Simulation (DALES). The simulation used in this study has a domain of  $512 \times 512$  points with 25 vertical levels of 20m at the lower levels that increases to 30m by a height of 550m. ERA5 has been used to set the initial conditions, the dynamic surface roughness at the bottom of the domain, and large-scale boundary conditions (Appendix D of (Pondera et al., 2019)). However, the large scale boundary conditions are prescribed only as tendencies

and the model is usually run with periodic boundary conditions (Appendix B of (Pondera et al., 2019)).

The wind turbines in GRASP LES have been parameterized according to the disk actuator method (Appendix B of (Pondera et al., 2019)). The information required for this parameterization to work is: the power curve, thrust curve, rotor diameter and hub height. The parameterization calculates the forces on a turbine blade (drag and rotational) based on the information provided as well as the local wind speed (Appendix B of (Pondera et al., 2019)). Since the simulation domain is small, re-circulation of wakes need to be avoided and this is done by a running a simulation without wind farms whose boundaries are prescribed to the simulation with wind turbines. Furthermore, this allows for the development of wakes. This is illustrated in Figure 14.

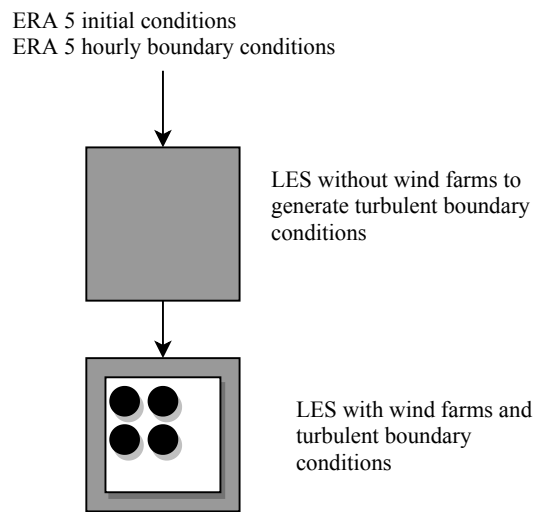


Figure 14: SCHEMATIC SETUP OF GRASP LES. ADAPTED FROM APPENDIX D OF (PONDERA ET AL., 2019)

The LES data, much like in (Abkar and Porté-Agel, 2015a) could provide insights on model behaviour when its performance is contrasted with HRM, HRM-WF. This is supported by recent work by Ciaran et al., 2019 where the GRASP LES model was specifically evaluated at the Horns Rev I wind farm in Denmark and results indicated that information from LES models, in tandem with standard models, could be very useful in improving skill of the forecasts. For this thesis, the model data was provided in three NetCDF files; a horizontally sliced data set provided the spatial wind field at two levels - at 10m and at 92.90m for the selected time period in hourly time steps, a power production data set that provided power in MW in 10 minute intervals, a profile data-set at the two floating LiDAR locations that provided wind speed in m/s at 10 minute intervals. The tower data is originally sampled once per time step which is typically a cou-

ple of seconds. These samples are averaged into 10-minute intervals and the time stamp is placed at the end of each interval contains all the samples that precede it up to 10 minutes. (e.g. time stamp 15.20 contains all samples between 15.10 and 15.20). (E. Wiegant, personal communication, July 16, 2019 )

### 3.2 ANALYSIS PROCEDURE

The following steps were undertaken to produce the results reported in the following chapter. The choices made have been justified with references to literature. Firstly spatial and temporal delimitation was imposed based on availability of observation data. This narrowed down the indicators for the study. The data was processed for missing values and any other discrepancies as well as to make it comparable with one another. Finally, a set of checks and balances were performed to ensure consistency across various results.

#### 3.2.1 *Delimitation of the Study (Spatial and Temporal Domain) and Indicators*

##### 3.2.1.1 *Temporal and Spatial Domain*

Since HARMONIE-AROME's domain is limited (being a mesoscale model), the wind farm that met the criteria of having several usable observational data-set and also being within the mesoscale domain was the Borssele Wind Farm Zone. The Borssele Wind Farm Zone (BWFZ) has, in close proximity, two observational data-sets from floating LiDAR buoys that were dispatched by Fugro to two different locations in regular intervals to record various wind variables such as speed, direction, gust and turbulent intensity. Furthermore, the power grid connected to this region, run by the Belgian transmission operator, Elia, publishes verified data on the measured power output.

Over the BWFZ, available Sentinel-1 SAR data also provided useful qualitative wake data despite the limited frequency of snapshots of a single time-step once every few weeks.

The Borssele Wind Farm zone is comprised of wind turbines from three different suppliers. In total, there are five types of wind turbines with different cut in and cut out speeds:

The choice of the time period for any time series evaluation was motivated by the availability of continuous LiDAR data. The location of the LiDAR that is further away from the wind farm, position 1, had buoys recording the variables on these dates:

Since the closer LiDAR at position 2 has data only from 2nd December to 22nd June 2016 (02.12.2016 - 22.06.2016), the subset of available data from both LiDARs, the months from February to June in 2016, was chosen as the time period for evaluating HARMONIE-AROME.

NAME	HUB HEIGHT (IN M)	CUT IN (M/S)	CUT OUT (M/S)
VESTAS 90	76	4	25
VESTAS 112	72/84	3	25
SENVION 6.2M	95	4	30
SENVION 5M	94	4	30
HALIADÉ	100	4	25

Table 3: CHARACTERISTICS OF OPERATIONAL BELGIAN WIND TURBINES ([Offshorewind.rvo.nl](http://Offshorewind.rvo.nl)). This table provides turbine data which is relevant for discussion and interpretation of results from Chapter 4.

The LiDAR data had to be processed to remove the invalid (NaN) values that occurred intermittently. In this analysis, March - May was considered since it had the least data gaps. To ensure consistency and ease of comparison, the same time period was selected for the power production data-sets.

### 3.2.1.2 Selection of Evaluation Metrics

To evaluate the performance of the HARMONIE-AROME model with the new parameterization, atmospheric variables that illustrated the effect of a wind farm parameterization as well variables for which it was possible to obtain observed data had to be chosen. As discussed in the previous sections, the impact of a wind farm is mostly illustrated by changes in wind speed and the power production data. Since these two variables are available in all the data-sets involved, the primary indicators for the evaluation were narrowed down to spatial wind speed fields that illustrate the wake signature, time series/shear profiles at the LiDAR locations and time series of power production. Secondary indicators such as wind direction, turbulent kinetic energy were also used to establish certain benchmarks or filter the data. These variables were used to generate figures that provided an overview as well as a composite view of the data. A composite view of the data was created by classifying the data-sets into several stability regimes based on Obukhov length as well as into wind direction sectors based on, evidently, the wind direction. This is elaborated upon in a following sections.

### 3.2.1.3 Description of Figures

Specifically, to study ambient flow, time-height contours such as those presented in Lee and Lundquist (2017)'s work were created. For a closer look at the behaviour of the model at hub height in a short time period, monthly time series of wind speed from both the models and

	FAR-LIDAR (LOT 1)
4*AVAILABLE DATES	11th June to 26th December 2015 (11.06.2015 - 26.12.2015)
	12th February to 20th July 2016 (12.02.2016 - 20.07.2016)
	20th July to 9th December 2016 (20.07.2016 - 09.12.2016)
	12th December 2016 to 27th February 2017 (12.12.2016 - 27.02.2017)
	NEAR-LIDAR (LOT 2)
AVAILABLE DATES	2nd December 2015 to 22nd June 2016 (02.12.2015 - 22.06.2016)

Table 4: FLOATING LIDAR DATA AVAILABILITY (*Offshorewind.roo.nl*) As depicted, an overlap of the two data-sets is present only in 2016.

the observational data-set was used. To study wake characteristics, a spatial contour plot of the wind speed at 10m height at the time of the SAR overpass was generated and compared with the satellite data. To characterise the wakes further, a temporal average of spatial winds at hub height was performed. It is pertinent to note that to establish the working of the parameterization, HRM data was juxtaposed against HRM-WF results in the Belgium Wind Farm zone as well as in a no-wind farm region. Moreover, a spatial animation plot to show the wake behaviour was constructed to better observe the behaviour of the wind fields in the presence of a wind farm parameterization. To check if the model truly represented real world behaviour, a comparison of the diurnal cycles was made. Diurnal shear profiles generated also provided additional insights. As for the power production, time series, scatter plots, and 2D histograms were used to determine the performance of the parameterization.

For quantifying the performance of the model, a statistical analysis was performed. Histograms and bias vs. root mean squared error (RMSE) figures of the selected heights for the two key variables were generated to illustrate the behaviour of the model at different heights. Plots that represented the bias as a function of time and height were also used to evaluate the model. To clarify, in this thesis, bias is the difference between modelled data and observational data. For e.g., a positive bias implies that the model overestimates and vice versa.

Since the various data-sets were from different sources, with different resolutions, they required pre-processing before direct comparisons could be made. This is elaborated on in the upcoming section.

### 3.2.2 Data Processing

The wind speed variable in HRM/HRM-WF's NetCDF files is provided as vectors:  $u$  and  $v$  of 4 dimensions each ( $y$ ,  $x$ , height and time). Thus, wind speed was calculated ( $|V| = \sqrt{u^2 + v^2}$ ) and extracted for heights from 40m to 200m at 20m intervals for comparisons with the lidar. For spatial results, 10m and 100m heights were extracted. For HRM, wind speed data was a scalar variable. For GRASP LES, the spatial winds were provided at two heights: 10m and 92.90m (for comparisons, the data was interpolated to 100m).

For the profile data, in HRM-WF and HRM, the coordinates closest to the LiDAR coordinates was calculated using the Euclidean distance method as:

$$\text{distance} = \sqrt{(\text{longitude array} - \text{target longitude})^2 + (\text{latitude array} - \text{target latitude})^2} \quad (1)$$

Note: the latitude and longitude variables are two dimensional arrays thus making it necessary to calculate the distance to the nearest point instead of locating the nearest point in the latitude and longitude array independently.

This method was selected after exploring several other ways (i.e. Orthodromic, Spherical) to calculate the smallest distance between the target coordinates and the model coordinates. The Euclidean distance method resulted in the closest coordinate point and hence was selected (see Figure 15). It is also consistent with the method employed by Whiffle to extract profile data from the LES model.

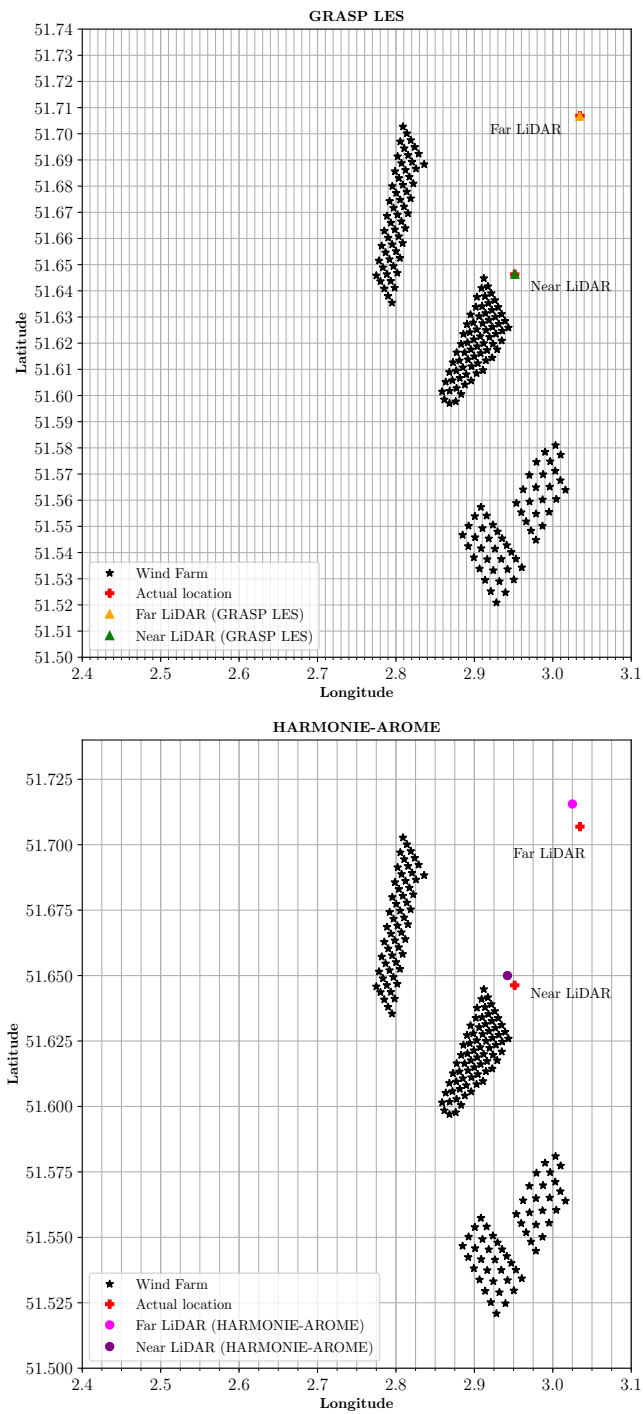


Figure 15: ILLUSTRATION OF LiDAR LOCATIONS AND MODEL GRID POINTS USED FOR COMPARISON The top panel illustrates the grid lines of the high LES resolution and the bottom panel illustrates the grid lines of the coarser HARMONIE-AROME resolution. The legends indicate the locations in the model that were closest to the actual LiDAR coordinates.

For the time series and other profile plots, 9 heights were selected: 40, 60, 80, 100, 120, 140, 160, 180, 200. GRASP LES data was received in non-standard heights and hence, the data was interpolated to these heights.

In this work, the phrase 'hub height' is used to refer to 100m since a majority of the turbines in Table 3 are around this height and it is one of the standard heights provided in the HRM/HRM-WF model.

For performing statistical analyses, the data-sets were averaged into hourly time-steps, if the resolution was finer. There were two ways this could be performed. An asymmetric or forward averaging was the average of the 5 time-steps leading up to the next hour, i.e. wind speed at 16:00 is an average of the wind speeds from 16:00 to 16:50. A symmetric averaging method averaged the time-steps +/- 30 minutes for a given hour, i.e. wind speed at 16:00 would be the average of wind speeds from 15:30 to 16:30. The model data-sets were also processed to remove timestamps that were invalid in the observational data-sets - this includes NaN values or negative power values.

For HARMONIE-AROME's power production data, it was necessary to calculate the sum of power per grid cell and this was done by masking all the grid points outside of latitudes from 51.44 to 51.9 N and longitudes from 2.5 to 3.2 E followed by a summation of the unmasked grid point power values.

For both HRM-WF and GRASP LES, it was necessary to account for a curtailment of power production that was observed in the power measurement data-sets. Several hypothesis to explain this have been made but none have been confirmed. Nevertheless, this has been accounted for in the selected time period. This was done by calculating the active wind turbines from the Elia data-set. The ratio of maximum observed power with respect to maximum possible power was calculated. Later, this fraction was multiplied with the nameplate capacity to derive the maximum power generated in the given month. This value was used to parse the model data in such a manner that any data points above this value would be capped to the maximum observed power thus eliminating the bias that was observed due to the model's assumption that power production occurred at full capacity whereas the measurements by the transmission operator indicated that the wind farm was operating at sub-capacity. The following Table 5 illustrates the active wind turbine percentage during the relevant months.

### 3.2.2.1 *Generation of Composites based on Stability Regimes*

To obtain a composite view of the data which would further aid in assessing the performance of the wind farm parameterization, the data-sets were binned into several stability regimes. As evidenced in research by Abkar and Porté-Agel (2015a), atmospheric stability has a strong influence on wake effects. The stability classification based

MONTHS	MARCH	APRIL	MAY
FRACTION OF CURTAILED POWER	0.946	0.961	0.957

Table 5: RATIO OF CURTAILED POWER IN THE BELGIAN WIND FARM *The ratio of curtailed power production for the selected temporal domain has been presented.*

on Monin-Obukhov length that was used is based on M. Motta, R. J. Barthelmie, and P. Vølund (2005) since the paper derived said classification after observations from four offshore sites with air temperature and wind sensors at various heights:

- Very Unstable :  $-200 < L < 0$
- Unstable :  $-1000 < L < -200$
- Neutral :  $|L| > 1000$
- Stable :  $200 < L < 1000$
- Very Stable :  $0 < L < 200$

The Monin-Obukhov length variable was obtained from the New European Wind Atlas (NEWA) data-set and it was chosen for two reasons: since it directly provided Inverse Obukhov Length ( $1/L$ ) values which was relatively easier to use than computing it as well as because an unbiased, undisturbed stability variable would provide no undue advantage to any of the models (as opposed to computing stability with the atmospheric variables generated by the model). On the NEWA website, the Borssele/Belgian wind-farm region was selected; an area of  $14,821.94 \text{ km}^2$ , with the center at  $51.67678 \text{ N}$ ,  $3.00201 \text{ E}$ . (It is to be noted here that using a Python IDE may sometimes result in the inverse Obukhov length variable having its negative values masked and this needs to be corrected. This has, to the author's knowledge, no bearing on the results once the issue has been rectified.)

For classifying the power production data-set, the near-LiDAR Obukhov length values were utilised. The range of  $L$  over the region did not vary extensively and hence, using a single point for the stability classification of the entire region was justified (See Appendix B). (Note that, NEWA provides an undisturbed stability variable)

### 3.2.2.2 Generation of Composites based on Wind Direction

The data sets were also classified based on wind direction. Six wind direction sectors, 60each, were chosen. The models were binned based on direction measurements from the two LiDAR locations into North-East (NE), East (E), South-East (SE), South-West (SW), West (W), North-

West (NW) directions. They were also further classified per wind direction sector into various stability classes as explained in the previous section.

### 3.2.2.3 Construction of a Wake Phase Diagram

An attempt to qualitatively categorise the length of the wakes based on stability and wind speed was attempted since it was deemed useful for further research. Two spatial plots for two different time steps in every six hour period on a given day (00:00 - 6:00, 6:00 - 12:00, 12:00 - 18:00, 18:00 - 00:00) were collected. This implies that 8 samples per stability class were used to make the assessment. It was ensured that for the selected time-steps, winds originated from the South Westerly direction for maximum wakes. Usually, it was preferred that consecutive hours were selected. Furthermore, when no wakes were apparent, the wind speed data point that was used represents the wind speed around the wind farm. It must be noted here that when winds were below cut in speed, any wakes that appeared were considered to be due to the roughness of the wind turbines.

### 3.2.3 Checks and Balances

To justify the results and choice of data processing methods, several internal consistency checks were applied. Since the volume of data was quite large and the number of results that could be generated even with a limited number of indicator variables equally voluminous, it was important to ensure that the various results were consistent with each other.

## 3.3 LIMITATIONS, ASSUMPTIONS AND RANGE OF VALIDITY

In performing this research, a number of general assumptions were made. Firstly, it was assumed that the resampling does not corrupt the data and that the comparisons are valid. The power and thrust curves obtained from the manufacturers were assumed to be accurate, the Inverse Obukhov Length variable obtained from the New European Wind Atlas was also assumed to be accurate as is possible, and that the WFP was incorporated correctly in GRASP LES. Finally, blockage effects due to wind turbines (which is essentially a slowing down of wind just upstream of wind turbines (Bleeg et al., 2018)) were ignored while making inferences based on wind direction composite results.

Apart from assumptions, there were certain limitations to this analysis as well. The floating LiDARs had a large number of missing time steps (even within the selected temporal period) that had to be accounted for. Furthermore due to this short time period, the seasonal

patterns could not be investigated. This is also linked to the number of available SAR snapshots that allow comparison of spatial wind contours. Additionally, due to the size of the data and the number of data-sets, all the available model variables were not thoroughly explored. This was compounded by the fact that there were no TKE measurements available in the region. In the same vein, the power production data from Elia had anomalies such as negative values that had to be cleaned and the actual values for those data points remain unknown.

Most importantly though, the curtailment of the power production in the Belgian wind farms remains a point of concern. Elia, the organisation, when approached (Vanhecke M., personal communication, 25th October 2019) state that they receive the power production data from the individual wind farm operators and only oversee the injection of electricity into the main grid and hence, to confirm any hypothesis on the curtailment, the wind farm operators need to be contacted. As a result, the statistical analysis on the power production data must be accepted and interpreted keeping this in mind.

# 4

---

## RESULTS

---

*In this chapter, the results from the analysis conducted are published and interpreted. Fundamentally, the chapter strives to answer the research questions and test the constructed hypotheses with the obtained results and present the findings.*

### 4.1 QUALITATIVE ANALYSIS: AN OVERVIEW

This qualitative overview analysis provides the different model results of the selected key indicator variables (wind speed and power production) across the spatial and temporal domains that have been selected.

#### 4.1.1 HRM vs HRM-WF: A Benchmark Analysis

Before any comparisons between HRM-WF and observational data or other models were made, it was necessary to establish that the wind farm parameterization has been included correctly. The benchmark analysis results aim to establish that the observed changes between HRM and HRM-WF's model output data can solely be attributed to the wind farm parameterization. To this end, spatial wind contour maps of hub height averaged wind speed, 2-D cross-sections of TKE at various heights, and the hub height wind speed time series at Cabauw (an undisturbed wind farm region) were produced.

An averaging of hub height wind speeds was performed to exclude any effects due to the model's sensitivity to initial conditions and as Figure 16 depicts, there is indeed a parameterization effect represented by slowing wind speeds in the area where the Belgian wind farm is located. Since a WFP is represented as a momentum sink in the model (Fitch et al., 2012), it can be confidently stated that the weakening of wind speeds in just that particular region is a parameterization effect.

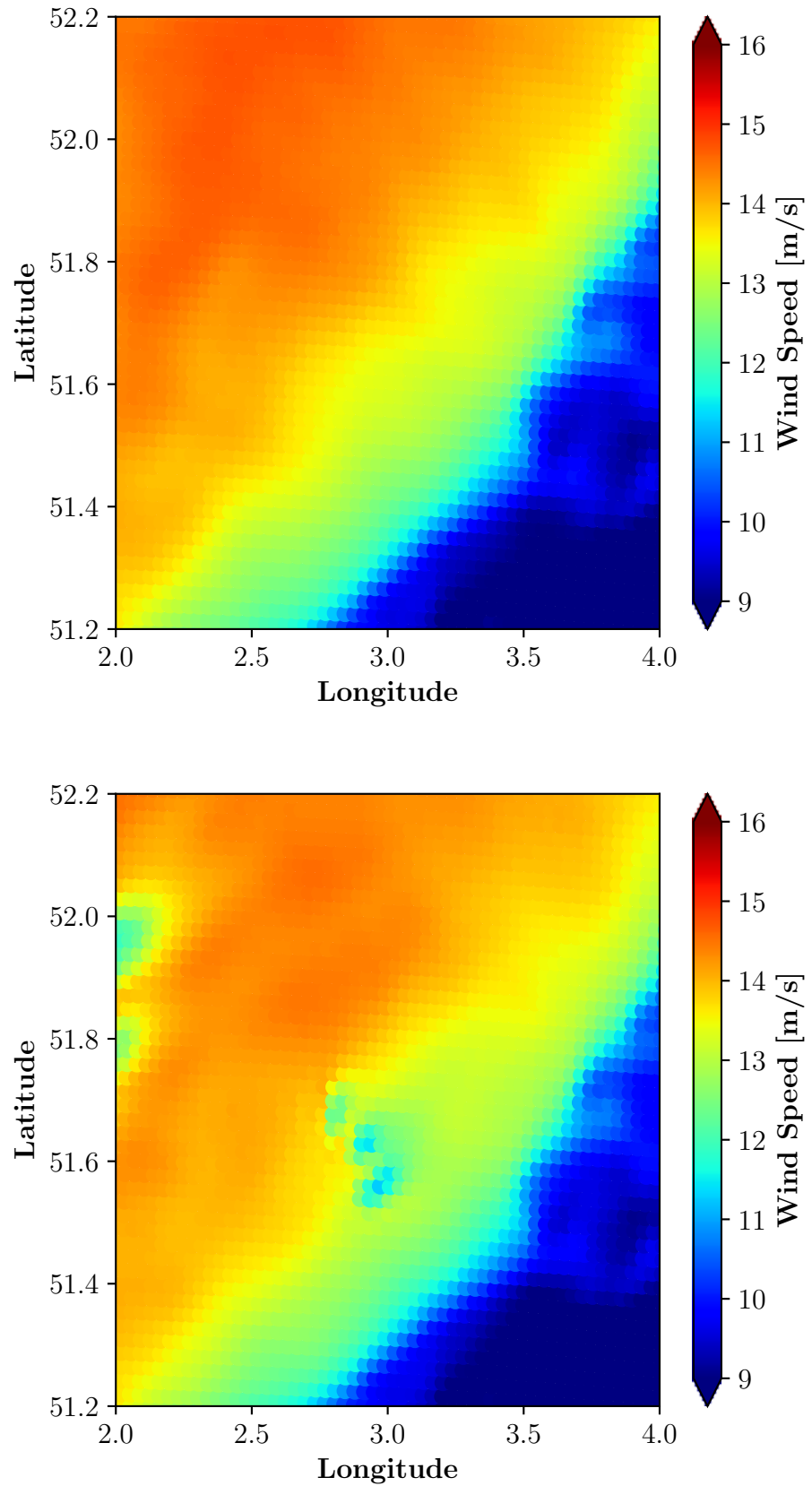


Figure 16: HUB-AVERAGED WIND SPEEDS BETWEEN HRM AND HRM-WF ON 5TH FEB 2016 The top panel shows a spatial hub averaged wind speed plot for HRM and the bottom panel shows the same for HRM-WF. The Belgian wind farm location has noticeably weaker average wind speeds (around 12 m/s).

A complementary result is obtained when the wind speeds at hub height for an undisturbed region (undisturbed by wind farm effects) were analysed. For the Cabauw location, an onshore coordinate where KNMI's wind mast observatory is situated, it was hypothesised that the HRM and HRM-WF results for hub height winds will be very similar. When this analysis was performed, the hub height wind speeds were not just very similar but nearly identical further satisfying the benchmark analysis that any differences in wind speeds at BWFZ is parameterization dependant (See Appendix B).

Finally, since the WFP acts not only as a momentum sink but also as a source of TKE (Fitch et al., 2012), the TKE profile was analysed for differences between the two runs. In Figure 17, HRM shows little to no TKE over the BWFZ as opposed to the HRM-WF run which has clearly outlined TKE fingerprints at hub height confirming that the WFP was indeed behaving as a momentum sink and a TKE source. Note that the maximum TKE in the colorbar was manipulated to show the effects clearly. The regions in red have TKE values of  $0.25 \text{ m}^2/\text{s}^2$  or greater.

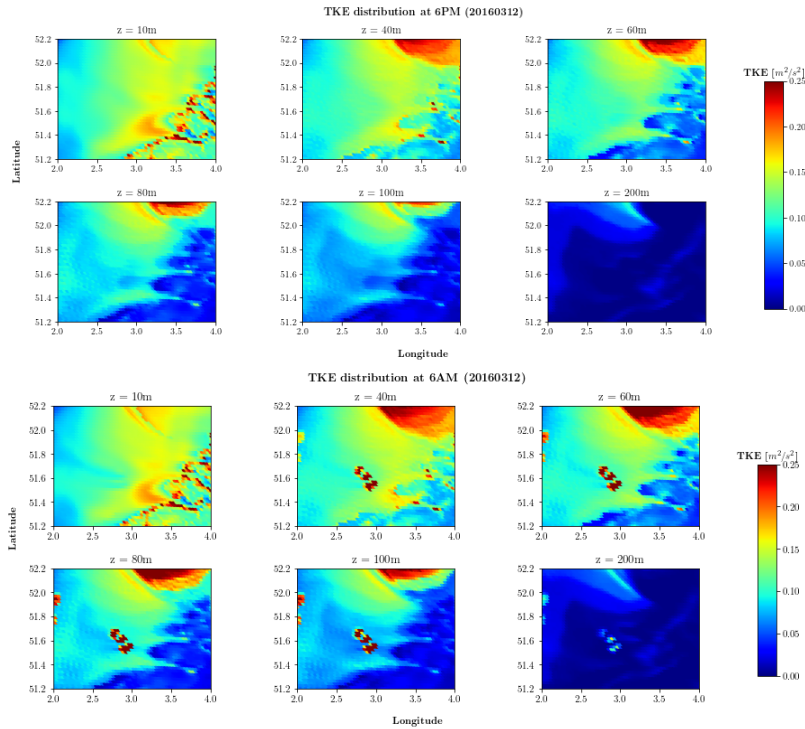


Figure 17: HRM vs HRM-WF: SPATIAL TKE PROFILES The top 2 rows show a spatial TKE plot for HRM and the bottom 2 rows show the same for HRM-WF. Note that the upper limit of the colorbar was adjusted to clearly illustrate the increase in TKE over the BWFZ as we approach hub height and subsequent decrease.

#### 4.1.2 Comparisons of HRM-WF and Measured Wind Data

One of the methods employed to ascertain the quality of HRM-WF against observations was spatial maps. These allowed the study of wind contours and wake signatures. Some of the other methods include the histograms for wind speed at hub height which will provide an insight into the difference between the two LiDAR locations. The patterns observed in the diurnal cycle and shear profiles and the model's ability to reproduce the same will also be discussed.

##### 4.1.2.1 Spatial Wind Contour Maps and Wake Signatures

The spatial wind contour maps were generated to validate whether HRM-WF was able to represent the wakes qualitatively. Since SAR imagery is sparse and only certain snapshots among those available in any selected time period have indications of wakes, the temporal domain adopted for LiDAR observations was abandoned and SAR imagery from February and June is also considered.

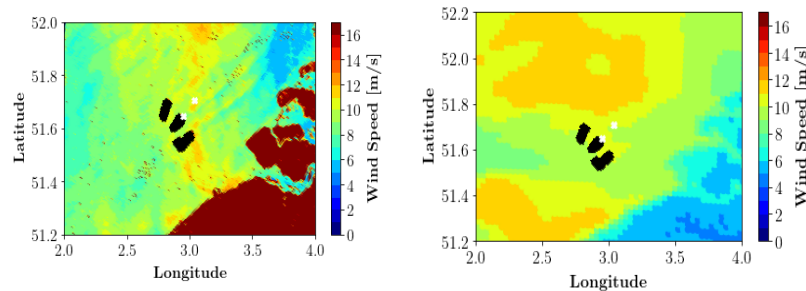


Figure 18: SPATIAL WIND CONTOUR MAPS - 5TH FEB 2016 The left panel shows explicit wake trails from the Belgian wind farms captured at 10m height in an image from SAR on 5th Feb 2016 at 6 AM. The right panel shows the spatial wind contour map at 10m height by HRM-WF. The atmosphere was stable at this time and date.

Since SAR images depict equivalent neutral wind speeds at 10m height, it is important to consider that in any other atmospheric stability regime, the wind speed accuracy is reduced. In Figure 18, the atmosphere is stable. According to the DTU SAR website (See Appendix A), underestimation is usually observed in stably stratified atmospheres. Also, the land regions are masked with very high values for clarity.

From Figure 18, it is noted that HRM-WF captures the wind speed contours with what appears to be a mild over estimation of about 1 m/s compared to SAR. Such a large bias can be duly accounted for by both, an underestimation in the SAR data in a non-neutral, stable regime, and model errors.

In this figure, it is also unclear whether the wakes that are explicitly captured by SAR are also reproduced. Since the resolution of HRM-

WF is much more coarser, the colorbar has been fine tuned to bring out the wake fingerprints as depicted in Figure 19.

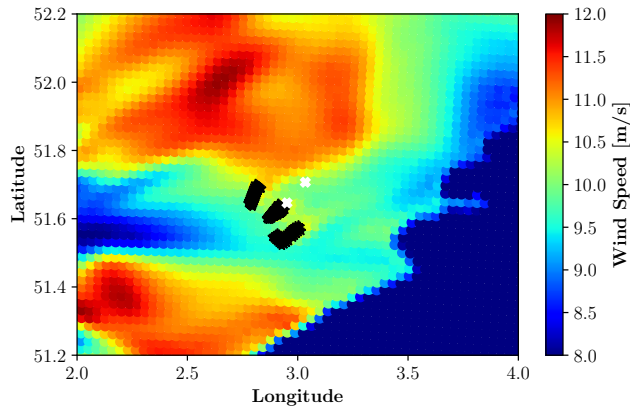


Figure 19: WAKE SIGNATURE AT 10M CAPTURED BY HRM-WF The wakes are represented here in yellow. The black dots depict the wind farms and the colour is unrelated to the colorbar.

In the area surrounding the wind farm (depicted here in blue), a weak wake fingerprint is seen in yellow with a speed of 10.5 m/s. This corresponds with the magnitude depicted by SAR. It is interesting to note that SAR captures an acceleration at the center of the wake which is not represented in HRM-WF. Furthermore, the length of the wake in SAR is much more longer. This is plausible since literature shows that stable regimes are prone to lesser mixing and wakes take longer to dissipate (Abkar and Porté-Agel, 2015b). Since these images show wind speed at a height much lower than hub height, it is hypothesised that wind speeds at the center of wakes may accelerate as opposed to decelerating as witnessed at hub height in Figure 16 due to increased vertical mixing when the turbines are operational. This is yet to be substantiated.

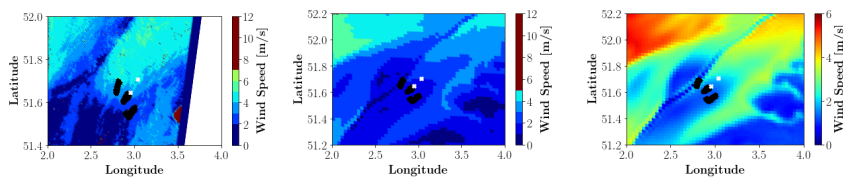


Figure 20: SPATIAL WIND CONTOUR MAPS - 5TH MAR 2016 The leftmost panel is a SAR image, the middle panel is HRM-WF with a colorbar comparable to the SAR image and the last rightmost panel is HRM-WF with a tweaked colorbar to highlight the wakes.

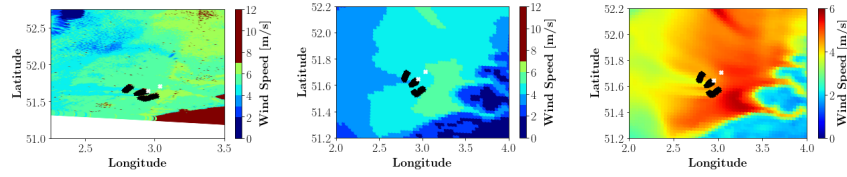


Figure 21: SPATIAL WIND CONTOUR MAPS - 12TH MAR 2016 *The leftmost panel is a SAR image, the middle panel is HRM-WF with a colorbar comparable to the SAR image and the last rightmost panel is HRM-WF with a tweaked colorbar to highlight the wakes.*

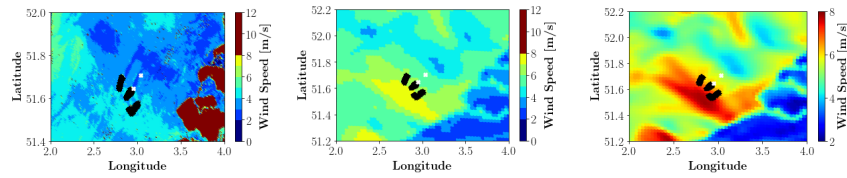


Figure 22: SPATIAL WIND CONTOUR MAPS - 24TH MAR 2016 *The leftmost panel is a SAR image, the middle panel is HRM-WF with a colorbar comparable to the SAR image and the last rightmost panel is HRM-WF with a tweaked colorbar to highlight the wakes.*

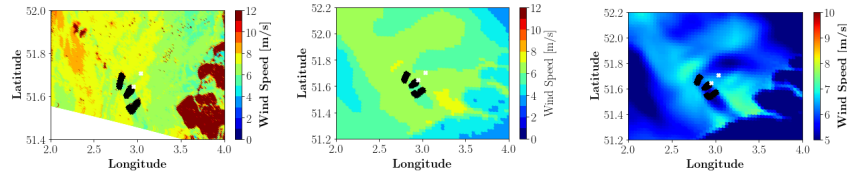


Figure 23: SPATIAL WIND CONTOUR MAPS - 4TH JUN 2016 *The leftmost panel is a SAR image, the middle panel is HRM-WF with a colorbar comparable to the SAR image and the last rightmost panel is HRM-WF with a tweaked colorbar to highlight the wakes.*

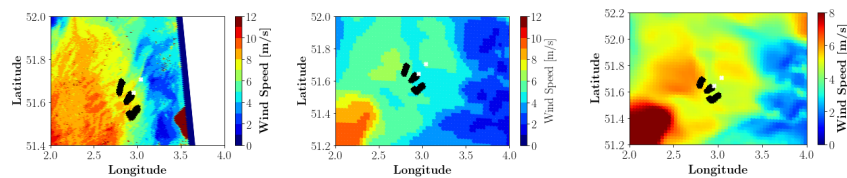


Figure 24: SPATIAL WIND CONTOUR MAPS - 12TH JUN 2016 *The leftmost panel is a SAR image, the middle panel is HRM-WF with a colorbar comparable to the SAR image and the last rightmost panel is HRM-WF with a tweaked colorbar to highlight the wakes.*

On 5th March, Figure 20 illustrates a very unstable atmospheric regime. It also appears as though there is a discrete band dissecting the map which could perhaps imply a meeting point of two fronts. This is present in both the observations and the model. HRM-WF also mildly underestimates winds but is able to capture, albeit coarsely, the wind systems in the region. It is harder to make inferences based on the wake signature plot but the wind speeds appear to be lower than the cut in speed which indicates that the wind farm is not operational and wind farm wakes due to rotating turbines will not be present.

On 12th March, Figure 21 also depicts a very unstable regime. From the HRM-WF plot, it is evident the wind contours are very well represented with a slight under-estimation in the magnitude. The wake signature is also reproduced excellently and it is fair to expect wakes since the wind speed moving towards BWFZ is slightly above cut in speed (3-4 m/s).

In a neutral regime, Figure 22, HRM-WF overestimates the wind speeds but a patch of higher wind speeds near the BWFZ is present in both the SAR and HRM-WF plots. The wake signature plot shows short wakes in the same direction as the ones that can be seen in the SAR.

In yet another very unstable regime, SAR Figure 23 depicts medium wakes towards the shore which are reproduced by HRM-WF. The model does not seem to pick up on any of the wind speed systems though. In the same month, a very stable regime captured by SAR on Figure 24 shows a wind system that is lagging in HRM-WF resulting in wind speeds near or below the average cut in speeds (3-4 m/s) and thus accounting for the absent or minimum wakes.

#### 4.1.2.2 *Sample Wake Phase Diagram Construction*

To summarise the wake signatures from HRM-WF, a qualitative assessment on wake lengths was performed. The wakes were visually classified in to short, medium and long wakes by eyeballing the number of degrees they spanned.

In Figure 25, HRM-WF's spatial plot results (see Appendix A) were sampled into different stability classes and the corresponding wake lengths were recorded to identify existing patterns, if any. This qualitative appraisal yielded results that are consistent with HRM-WF's wake behaviour in preceding sections. The results establish that most wakes occur in the 7.5 - 15 m/s wind speed range (which is also within the cut in and cut out speeds of wind turbines), with most wakes being short in length. Furthermore, wake lengths increase with increase in wind speed magnitude. With respect to mixing, wake lengths have more nuanced patterns. In general, very unstable regimes have none to short wakes. Unstable regimes also have short wakes even at medium wind speeds and medium wakes at higher wind

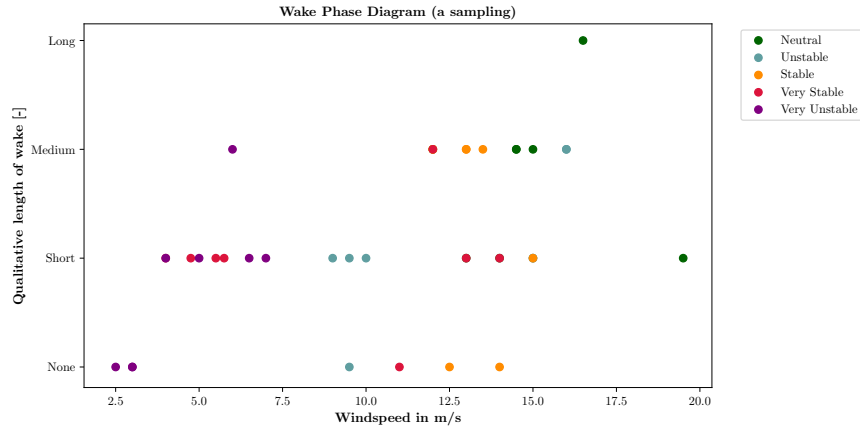


Figure 25: WAKE LENGTHS (AT 10M) CATEGORISED ACCORDING TO SPEED AND STABILITY CLASS.

speeds. Stable regimes have none to medium wakes within the same wind speed range so any direct inferences about speed and mixing are difficult to make. Very stable regimes appear to have a lot of short, low wind wakes. Neutral regimes result in the most long wakes. Overall, this implies that a well-mixed, high wind speed boundary layer may be the right combination for long wakes and that wind speed may be a stronger factor in determining wake length than mixing.

#### 4.1.2.3 Wind Speed at Hub Height (100m)

At the two LiDAR locations, wind speeds at hub height were compared to establish the overall performance of the model.

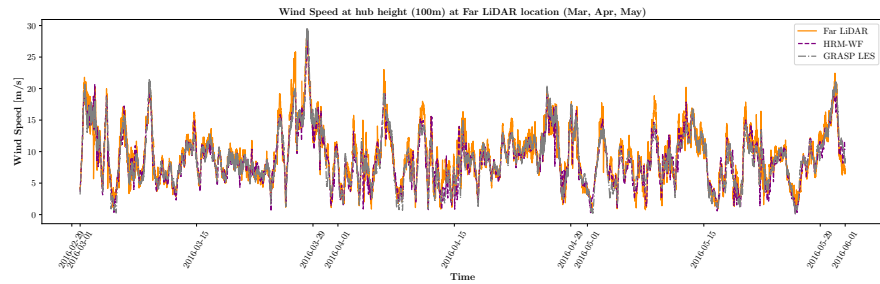


Figure 26: WIND SPEED AT HUB HEIGHT (100M) AT FAR LiDAR LOCATION

From Figures 26 and 27 it can be stated that HRM-WF's hub height wind speeds in March, April, and May 2016 align closely with observed as well as GRASP LES wind speeds. In general, there appears to be a mildly positive or a mildly negative bias at several time steps amounting to an overall bias  $\sim 0.6$  m/s. The two LiDARs have similar wind speeds but there is a perceptible time shift, especially noticeable if they are overlaid on top of each other. The histograms quantify this magnitude shift and is presented in the following section.

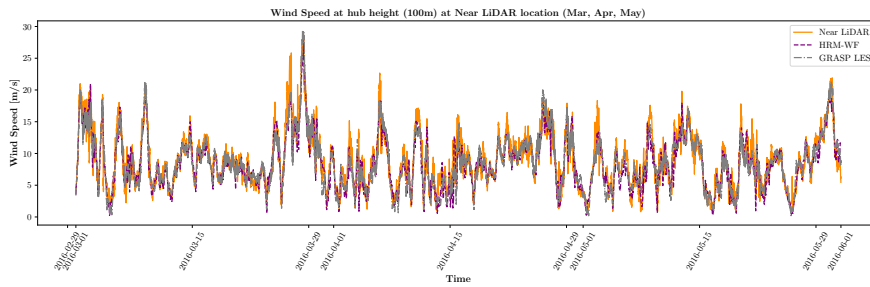


Figure 27: WIND SPEED AT HUB HEIGHT (100M) AT NEAR LiDAR LOCATION

#### 4.1.2.4 Histograms of Wind Speeds at Hub Height

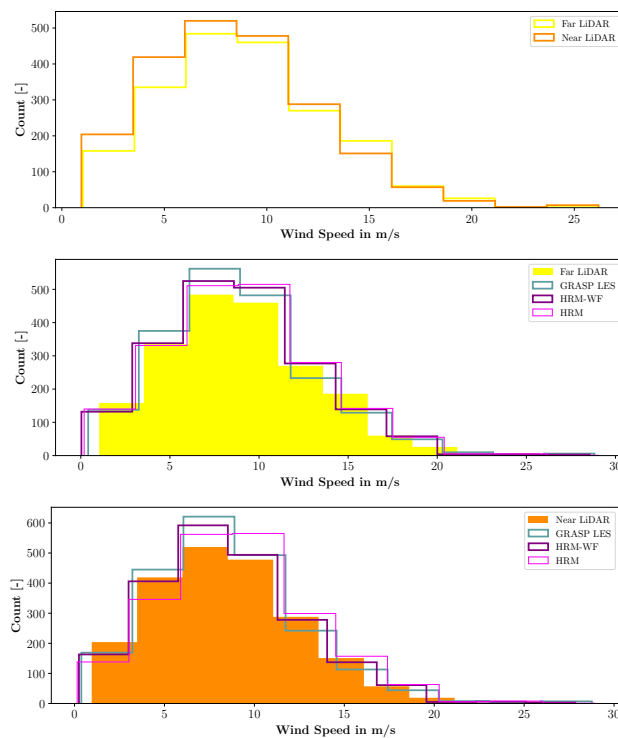


Figure 28: HISTOGRAMS OF FAR-LIDAR AND NEAR-LIDAR *The leftmost panel is a histogram between the far and near LiDARs. The middle panel is a histogram comparison of the models and the observational data-set for the far-lidar. The rightmost panel is the histogram comparison between the near-lidar observational data-set and the models.*

The utility of studying the two observational locations is underlined in Fitch et al. (2012)'s paper which states that very few observational data-sets on the atmospheric impact of wind farms exist. From Figure 28, it was noted that the differences between wind speeds at the two LiDAR locations is minimal. The near-lidar's histogram appears to be shifted slightly towards the left and this may be the result of weakening winds originating in the South-West or West as they cross the BWFZ.

The second plot in Figure 28 illustrates the histogram for the far-lidar. The models have a higher value than the observational data in the 6 - 12 m/s range. HRM-WF, HRM, and GRASP LES have performed similarly in this scenario.

In contrast, the third plot in Figure 28's results tell a different story. There is a marked difference between the histograms of HRM-WF and HRM. HRM has a higher count of wind speeds in the 7-10 m/s bins since it does not account for the presence of a wind farm.

#### 4.1.2.5 Diurnal Cycle of Wind

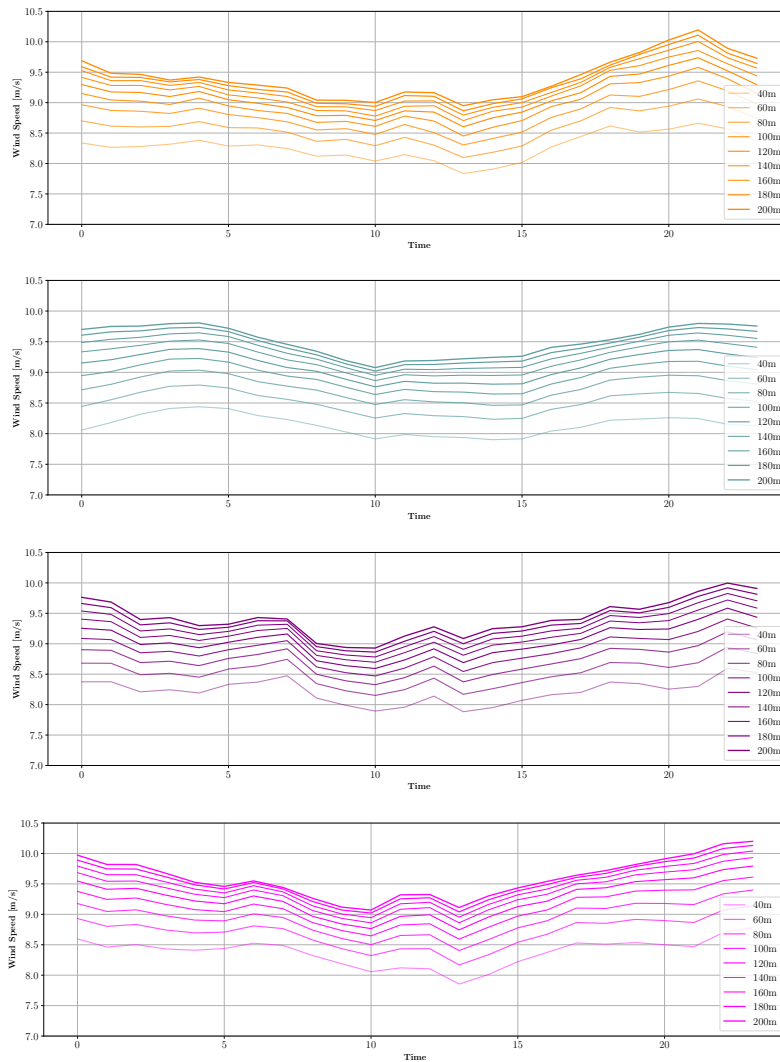


Figure 29: DIURNAL CYCLE AT FAR-LIDAR The panels depict data from top to bottom in the following order: LiDAR, GRASP LES, HRM-WF, HRM.

The diurnal wind speed cycle over the region is not larger than around 2 m/s at either lidar locations. Furthermore, in Figure 29, a pattern is noticeable where the wind speeds pick up after noon steadily rising up to 21:00 hrs after which the speed drops again.

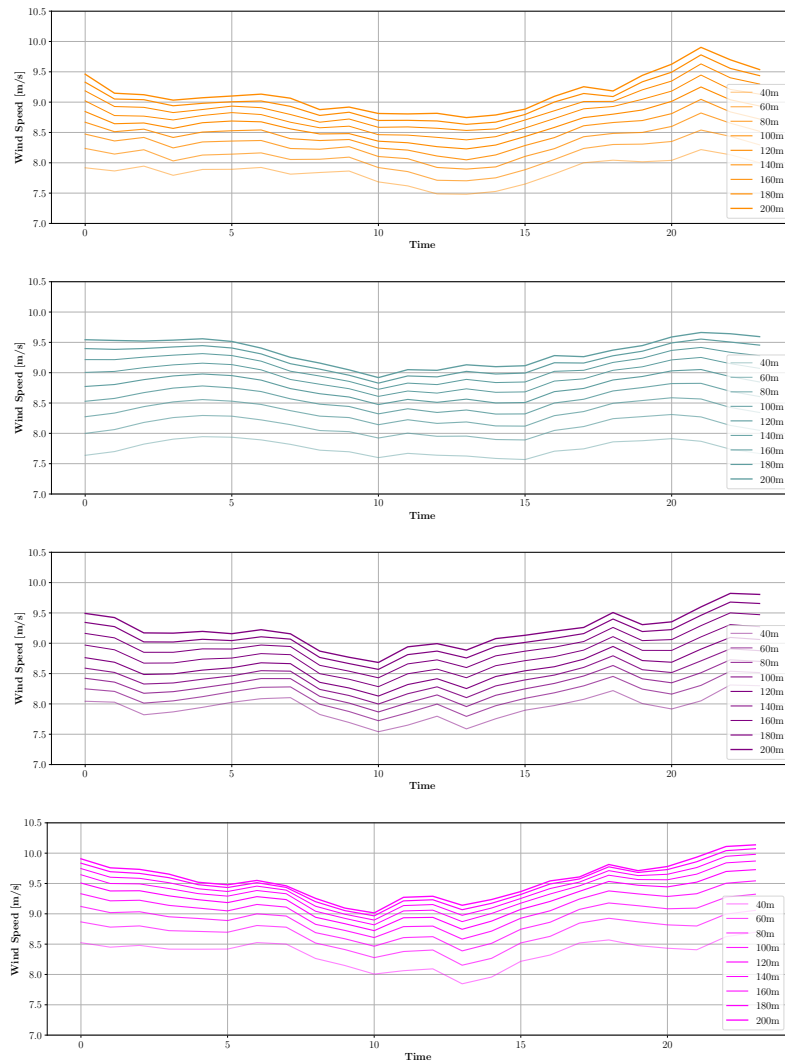


Figure 30: DIURNAL CYCLE AT NEAR-LIDAR *The panels depict data from top to bottom in the following order: LiDAR, GRASP LES, HRM-WF, HRM.*

The maximum wind speed at the far-lidar location is well after dusk. This behaviour is picked up by HRM-WF as well as HRM but the latter overestimates the magnitude considerably. GRASP LES accurately captures the magnitude but does not represent the mixing at higher heights. HRM-WF also loses the mixing at higher heights compared to HRM and the observations. It should be noted that HRM-WF also successfully captures the maximum wind speed around 21:00 hrs and the following sharp dip. Since the far-lidar has lesser undisturbed winds, HRM and HRM-WF have comparable performances with HRM capturing the overall shape better than HRM-WF. As we move closer to the wind farms, HRM loses this ability as is seen in Figure 30.

At the near-lidar location, Figure 30, there seems to be less pronounced mixing at higher heights and this is satisfactorily captured

by GRASP LES and HRM-WF. HRM performs less satisfactorily but this is an expected outcome since it does not account for any wake effects. The stratification at higher heights as compared to the far-lidar is an interesting development and it is uncertain whether it is only due to the presence of the BWFZ but they seem to be correlated in some way. There also seems to be a less sharp drop in wind speed after 21:00 hrs with lower diurnally averaged wind speeds - it hardly develops beyond 10 m/s. The LES also does not capture the dip in wind speeds after 1 or 2 AM and is consistently positively biased during that time period.

#### 4.1.2.6 Diurnally-averaged Wind Speed Shear Profiles

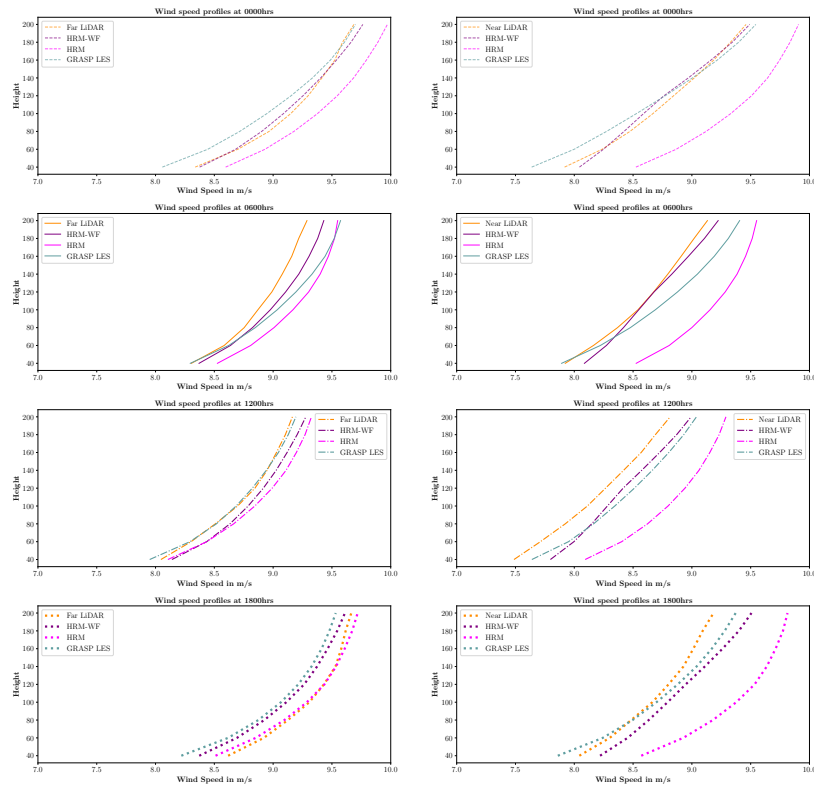


Figure 31: WIND SHEAR AT THE NEAR AND FAR LiDARs The panels depict wind shear profiles for different hours of the day in the following order: 0000 hrs, 0600 hrs, 1200 hrs, 1800 hrs.

The diurnally averaged wind speed shear profiles provide another perspective on the diurnal cycle and the model's performance in that category. Profiles for midnight, 6 AM, noon and 6 PM were selected since they are evenly spaced and provide an idea of the shear profile trends.

In Figure 31, at 00:00 hrs, HRM-WF and the far-lidar are nearly in complete overlap which is desirable. HRM has the same shear profile shape as HRM-WF but there is a consistent bias between the two that

seem to have been eliminated by the inclusion of the WFP. At 6:00 AM, the lower part of the shear profiles coincide well with the observations but the models increasingly over-estimate the wind speed from 100m and above. HRM has the largest bias at any given height. At noon, all the shear profiles are less steep with a weaker wind speed at lower heights compared to 12 AM and 6 AM. GRASP LES and the far-lidar are also nearly identical. Interestingly, at 6 PM, HRM coincides the most with the observational data-set. All the models also seem to overestimate at the lowest level but the bias reduces at upper levels.

For the near-lidar location, the differences between HRM and HRM-WF are a lot more drastic. Figure 31 illustrates this at all time steps. HRM shows a very strong positive bias - overestimating wind speeds - at all times and at all heights since it does not account for any wake effects. HRM-WF performs well at 00:00 hrs and 6:00 hrs but overestimates the wind speed slightly at noon and at 18:00 hrs. It also does not capture the shape at 18:00 hrs. Overall, GRASP LES and HRM-WF's results do not overlay the lidar observational data profiles but the overall bias is minute - especially at hub height.

These results also provide an insight into the behavior of the wind shear profile close to a wind farm zone. The observation profile at the near-lidar is less curved and appears to have more mixing than the one at the far-lidar. The range of wind speeds between 10m height and 200m height also seem to be reduced. It is possible that a wind farm zone not only damps the speed but also the natural mixing tendencies of the upper levels of the atmosphere (at and above hub height).

#### 4.1.2.7 Power Production over BWFZ

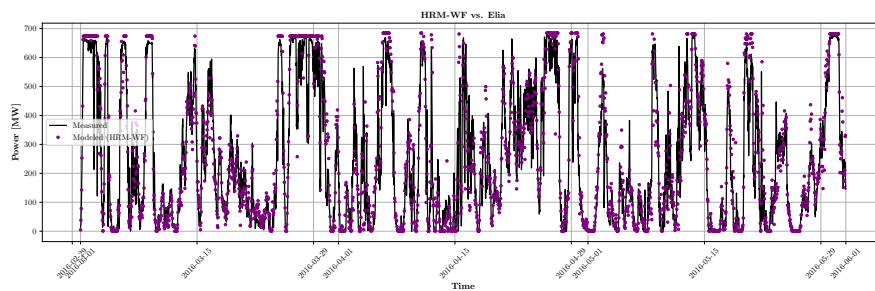


Figure 32: A TIME SERIES OF POWER PRODUCTION IN THE BELGIAN WIND FARMS FROM MARCH - MAY 2016 FOR HRM-WF AND ACTUAL POWER

The models perform very well after accounting for the curtailment of power as is evidenced by Figure 32 and Figure 33. Since the calculation of power in the models is dependant on the power and thrust curves, it is crucial to have accurate data on them. Usually, it is the wind turbines manufacturers who provide the data. As the figures

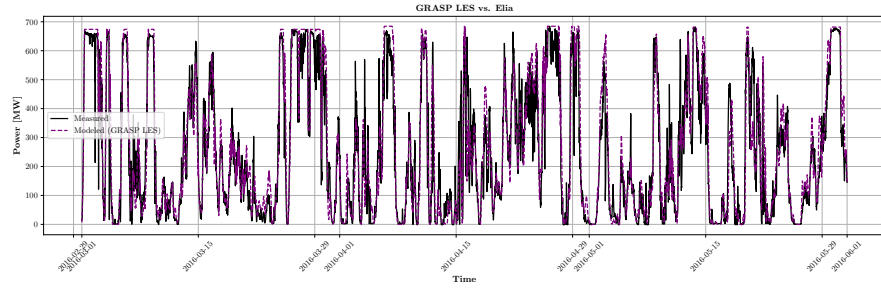


Figure 33: A TIME SERIES OF POWER PRODUCTION IN THE BELGIAN WIND FARMS FROM MARCH - MAY 2016 FOR GRASP LES AND ACTUAL POWER

illustrate, the models perform well with a mild bias within the 10-20 MW range.

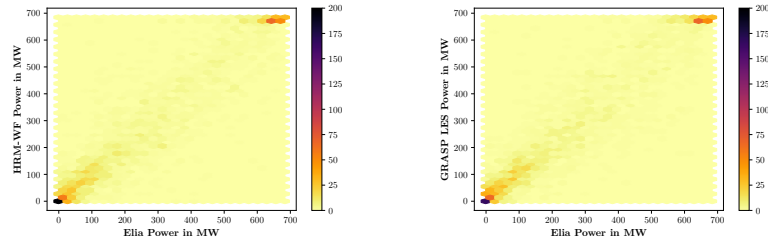


Figure 34: A 2D HISTOGRAM OF POWER PRODUCTION IN THE MODEL AND OBSERVATIONAL DATA-SETS *The left panel depicts HRM-WF vs Elia and the right panel depicts GRASP LES vs Elia.*

This hexbin plot (Figure 34) illustrates the correlation between measured and modelled power as well as the number of data points in a certain bin. We find that most of the data during this time period lie at the extremes - either the BWFZ is not operational or it is generating at full capacity. More insight into this is obtained when looking at composite hexbin plots in the following section.

#### 4.2 QUALITATIVE ANALYSIS: A COMPOSITE VIEW

##### 4.2.1 Atmospheric Stability Composite Results

The stability regime that is predominant in the BWFZ during March to May 2016 is the 'very unstable' regime according to Figure 35. Thus, statistically, a model's performance in this regime will skew its overall performance.

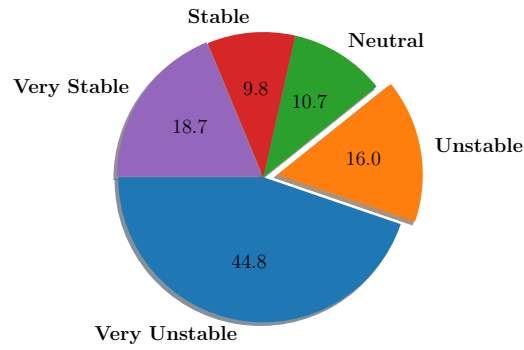


Figure 35: PROPORTIONS OF VARIOUS ATMOSPHERIC STABILITY REGIMES FROM MARCH - MAY 2016 The top panel is the stability percentages for the far lidar location and the bottom panel represents the near lidar location.

#### 4.2.1.1 Wind Speed Histograms for Hub Height

In Figure 36, very unstable near-lidar measurements have weaker wind speeds than the far-lidar. This is captured by GRASP LES but not HRM-WF. The model results are also more accurate for the far-lidar histogram.

In the unstable regime, both near and far lidar measurements have very different histograms with far-lidar having a prominent peak around 10 m/s whereas the near-lidar measurements are more equitably distributed across the bins. HRM-WF's histogram is the closest to the observational histogram for the far-lidar location while GRASP LES' histogram is the closest for the near-lidar location.

In stable regimes, far-lidar measurements have a peak further to the right than near-lidar measurements indicating weaker wind speeds at the latter location. This has been captured by the WFP in HRM-WF than in HRM (second figure, Figure 38). As for the far-lidar, all of the model's histograms are very different to the observational histogram.

The model's histograms at the near-lidar for very stable atmospheric regimes are also quite different from the observational histograms. Specifically, HRM-WF fails to capture the behaviour at the near-lidar. The models do reasonably at the far-lidar.

In neutral regimes, the leftward shift of the near-lidar observations is again predominant. The model histograms, at the near-lidar location, fall short with the exception of GRASP LES. At the far-lidar, there is no clear overlap between the models' and observational histograms. Overall, the models' histograms vary significantly from observed wind speed histograms especially at the near-lidar location.

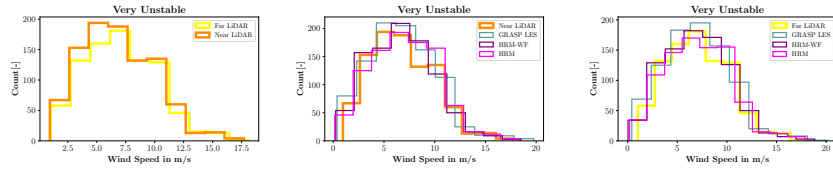


Figure 36: HISTOGRAMS FOR 'VERY UNSTABLE' REGIME The leftmost panel is a histogram between the far and near LiDARs. The middle panel is a histogram comparison of the models and the observational data-set for the near-lidar. The rightmost panel is the histogram comparison between the far-lidar observational data-set and the models.

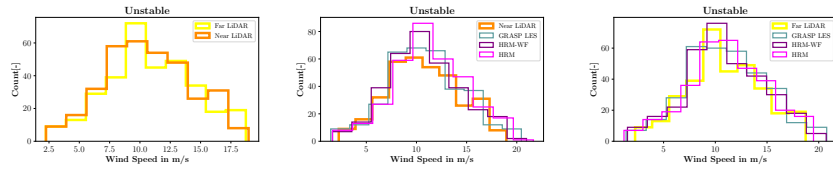


Figure 37: HISTOGRAMS FOR 'UNSTABLE' REGIME The leftmost panel is a histogram between the far and near LiDARs. The middle panel is a histogram comparison of the models and the observational data-set for the near-lidar. The rightmost panel is the histogram comparison between the far-lidar observational data-set and the models.

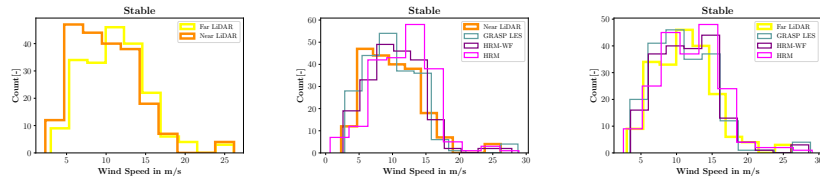


Figure 38: HISTOGRAMS FOR 'STABLE' REGIME The leftmost panel is a histogram between the far and near LiDARs. The middle panel is a histogram comparison of the models and the observational data-set for the near-lidar. The rightmost panel is the histogram comparison between the far-lidar observational data-set and the models.

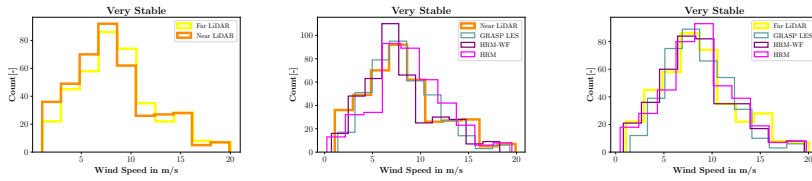


Figure 39: HISTOGRAMS FOR ‘VERY STABLE’ REGIME *The leftmost panel is a histogram between the far and near LiDARs. The middle panel is a histogram comparison of the models and the observational data-set for the near-lidar. The rightmost panel is the histogram comparison between the far-lidar observational data-set and the models.*

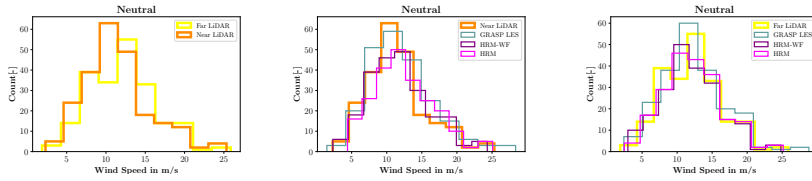


Figure 40: HISTOGRAMS FOR ‘NEUTRAL’ REGIME *The leftmost panel is a histogram between the far and near LiDARs. The middle panel is a histogram comparison of the models and the observational data-set for the near-lidar. The rightmost panel is the histogram comparison between the far-lidar observational data-set and the models.*

#### 4.2.1.2 Diurnal Wind Speed Cycle

From Figures 41 to 44, it is observed that the neutral and stable regimes have the highest wind speeds and variations on a daily basis. It can be discernibly noted that the models capture the mixing or rather lack of mixing in the different stability regimes appropriately. It is especially interesting to see that the peaks at around 3 AM in a neutral regime and peaks around 7 and 10 AM in a stable regime are represented accurately by HRM-WF. Furthermore, the WFP in the HRM-WF model appears to have contributed to reduced mixing at upper levels which matches the behaviour of the measurements in certain conditions, i.e. in stable regimes.

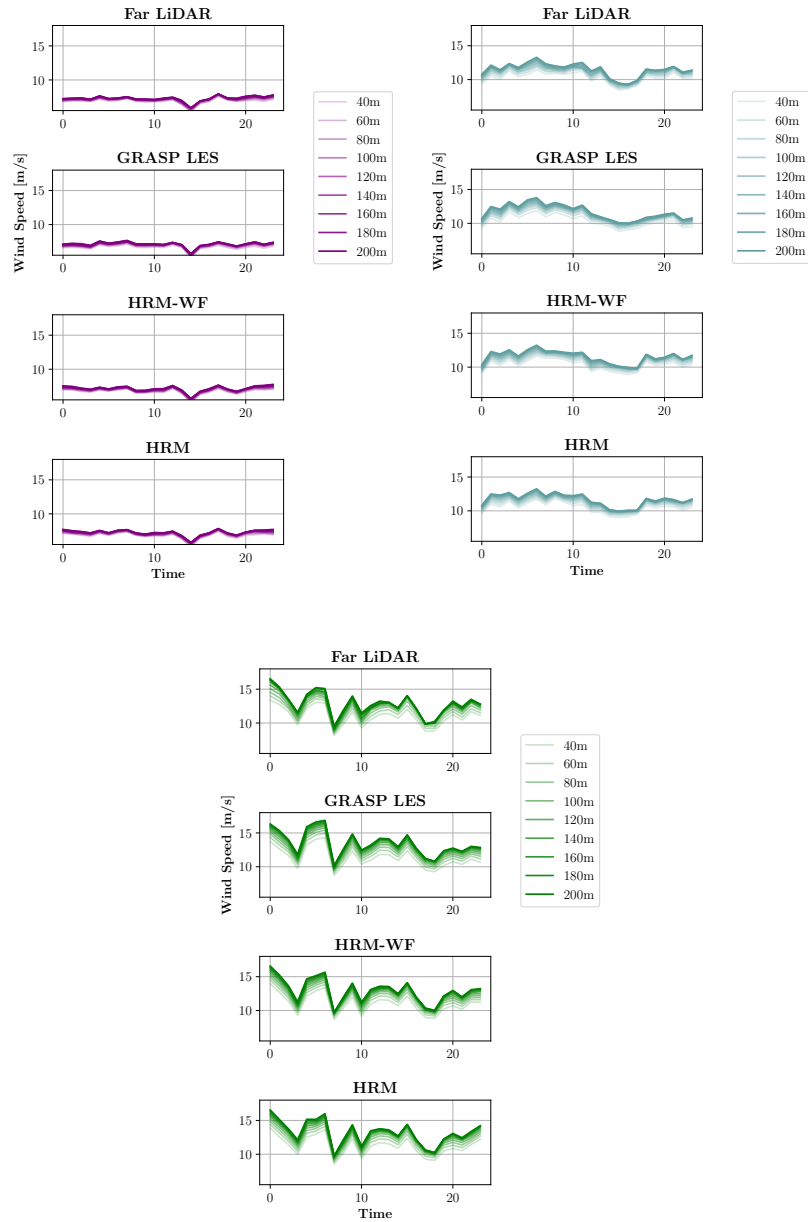


Figure 41: FAR-LiDAR DIURNAL WIND SPEED CYCLE The top left panel is the diurnal cycle for a very unstable regime. The top right panel is the diurnal cycle for an unstable regime. The bottom panel is the diurnal cycle for a neutral regime.

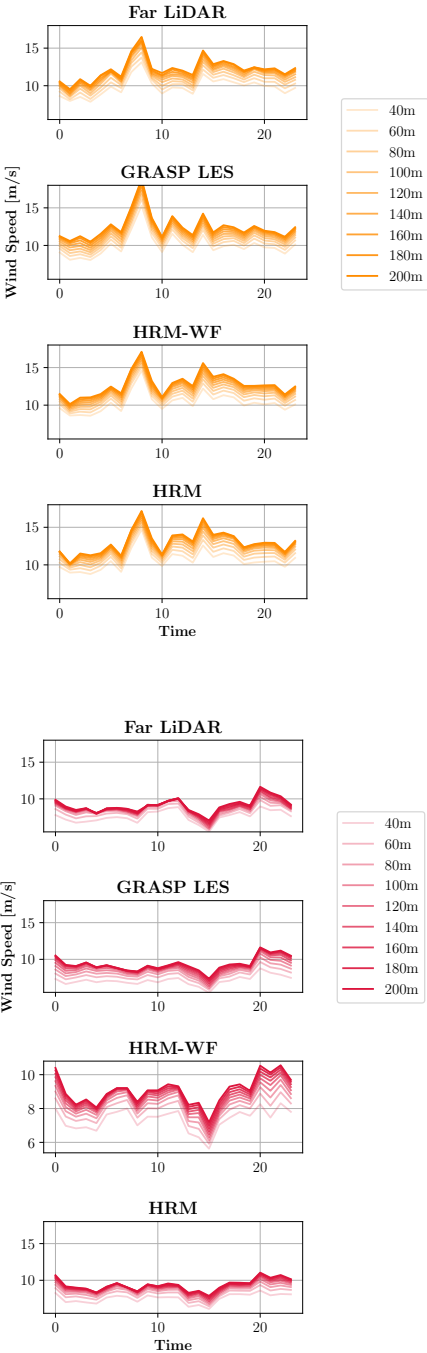


Figure 42: FAR-LIDAR DIURNAL WIND SPEED CYCLE *The top panel is the diurnal cycle for a stable regime. The bottom panel is the diurnal cycle for a very stable regime.*

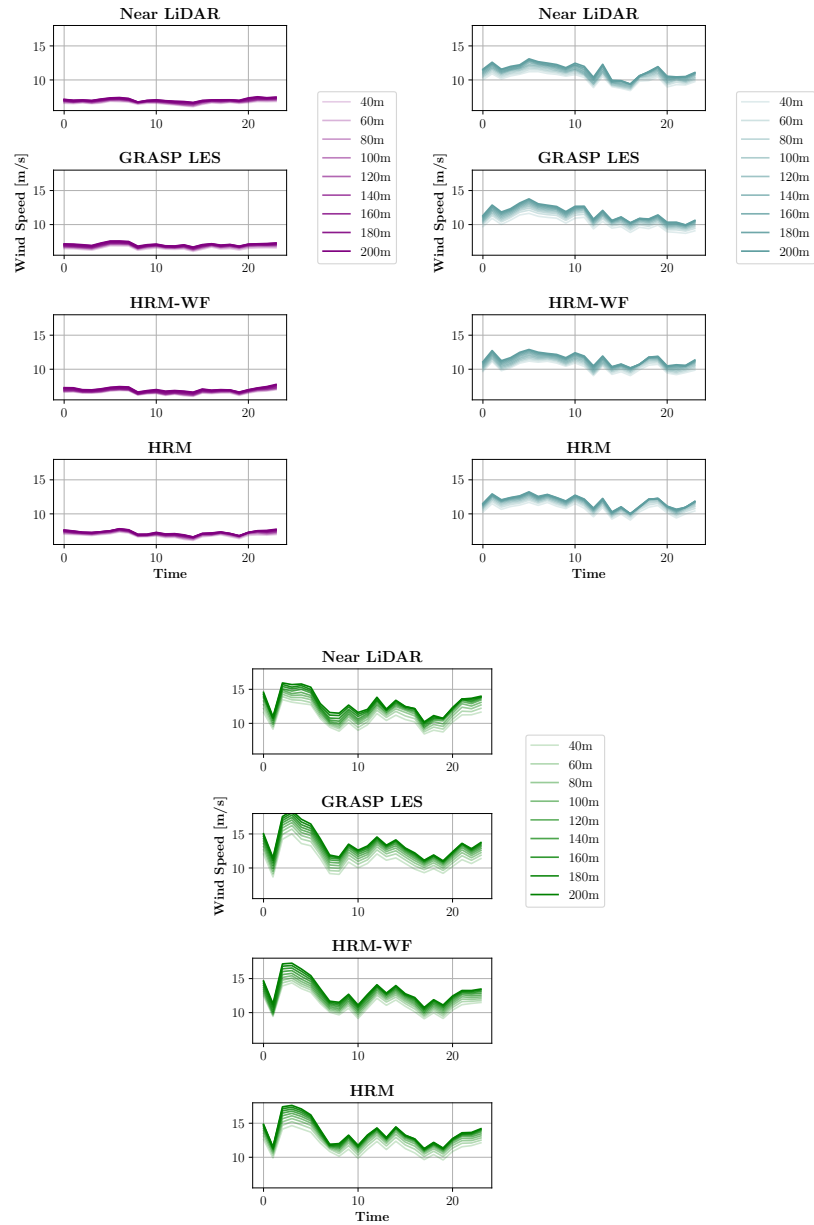


Figure 43: NEAR-LIDAR DIURNAL WIND SPEED CYCLE The top left panel is the diurnal cycle for a very unstable regime. The top right panel is the diurnal cycle for an unstable regime. The bottom panel is the diurnal cycle for a neutral regime.

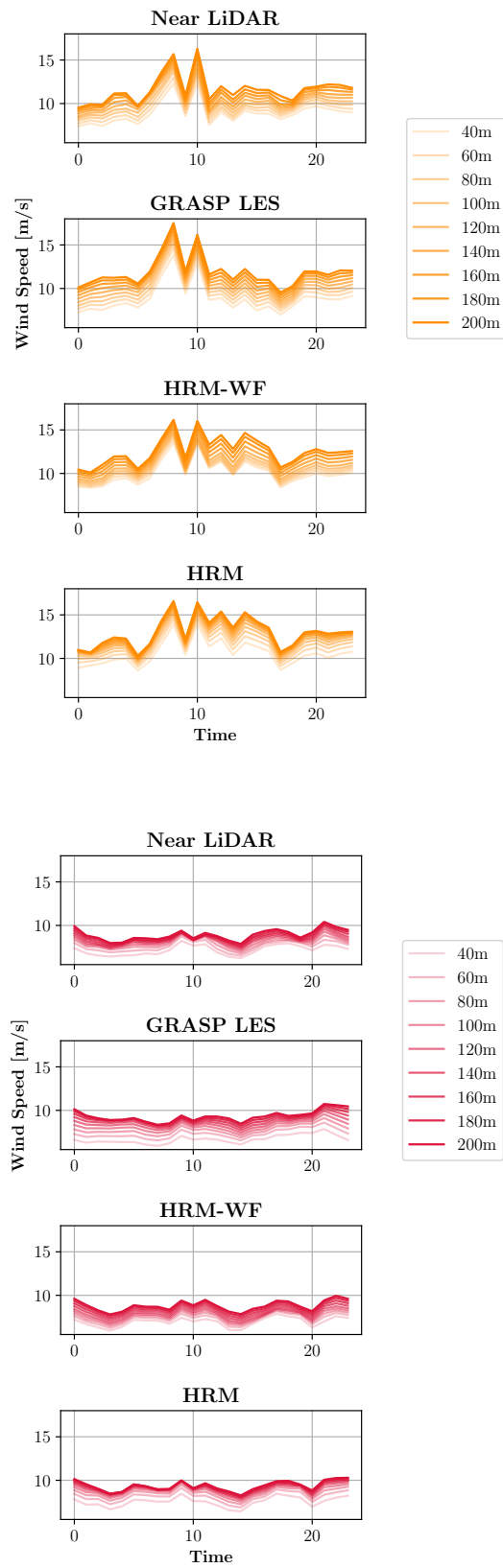


Figure 44: NEAR LiDAR- DIURNAL WIND SPEED CYCLE The top panel is the diurnal cycle for a stable regime. The bottom panel is the diurnal cycle for a very stable regime.

#### 4.2.1.3 *Diurnally-averaged Wind Speed Shear Profiles*

The shear profiles provide an interesting insight into the behaviour of wind speeds across different atmospheric regimes. In very unstable scenarios with potential for a lot of mixing, wind shear profiles are limited to speeds of 6-8 m/s. In very stable scenarios, the shear profiles at different hours of the day are not widely spread but the profiles have strong gradients that change from hour to hour. Neutral regimes see the most differences in magnitude from hour to hour. HRM-WF captures the qualitative order of the shear profiles for different hours of the day for unstable and neutrally stratified atmospheric regimes at the far-lidar.

At the near-lidar, the observations do not differ for 18:00 and 00:00 hrs in an unstable regime but the models do not reflect this behaviour. This is also the case for 6:00 and 12:00 hrs in stable regimes. This indicates that night-time conditions do not vary much during unstable regimes and day-time conditions are consistent in stable regimes. These trends are not reproduced in the models. In fact, HRM and HRM-WF results instead show a confluence between results for 06:00 and 18:00 hrs in unstable and stable regimes and this pattern ought to be investigated further.

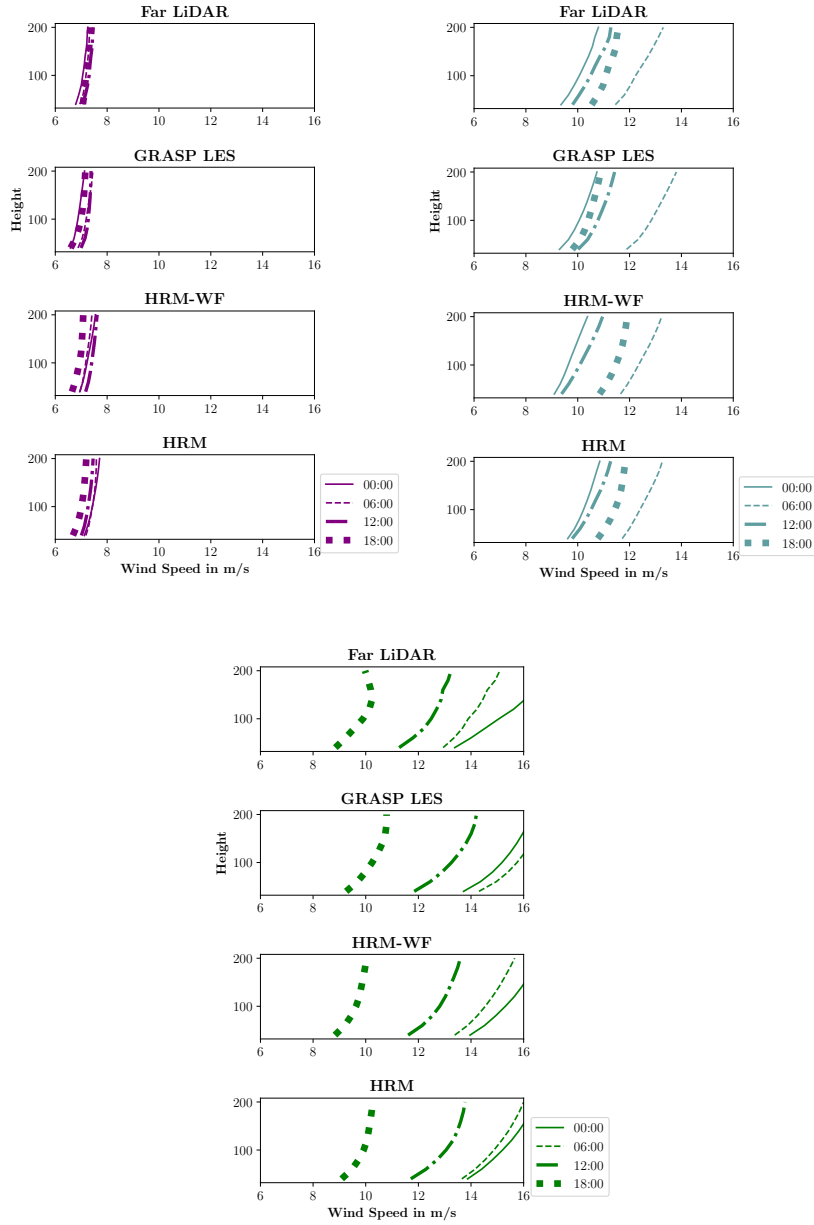


Figure 45: FAR-LiDAR DIURNAL WIND SHEAR CYCLE *The top left panel is the diurnal shear for a very unstable regime. The top right panel is the diurnal shear for an unstable regime. The bottom panel is the diurnal shear for a neutral regime.*

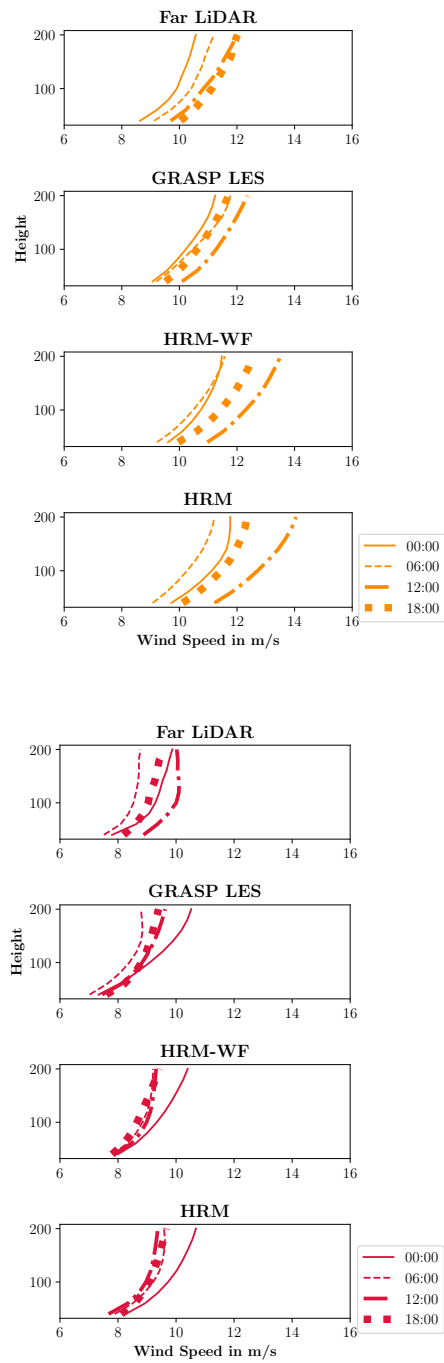


Figure 46: FAR-LiDAR DIURNAL WIND SHEAR CYCLE The top panel is the diurnal shear for a stable regime. The bottom panel is the diurnal shear for a very stable regime.

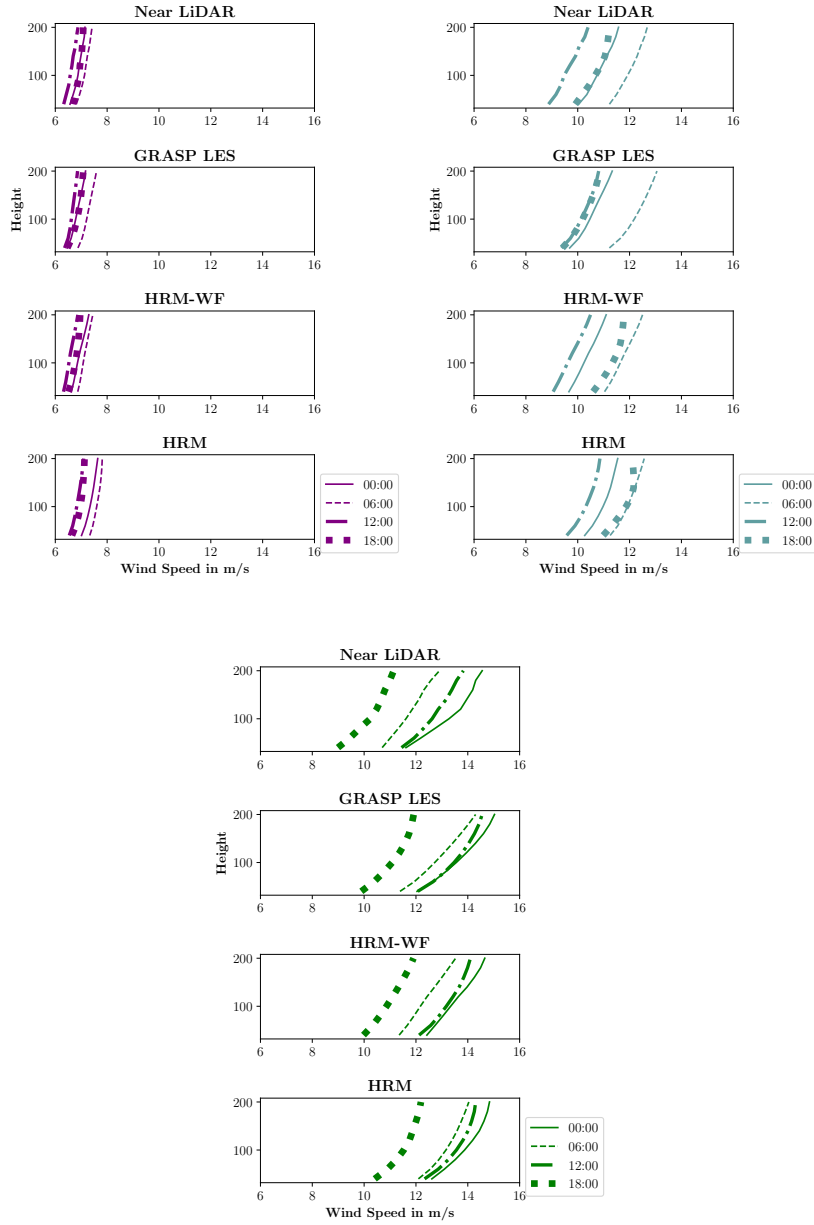


Figure 47: NEAR-LiDAR DIURNAL WIND SHEAR CYCLE *The top left panel is the diurnal shear for a very unstable regime. The top right panel is the diurnal shear for an unstable regime. The bottom panel is the diurnal shear for a neutral regime.*

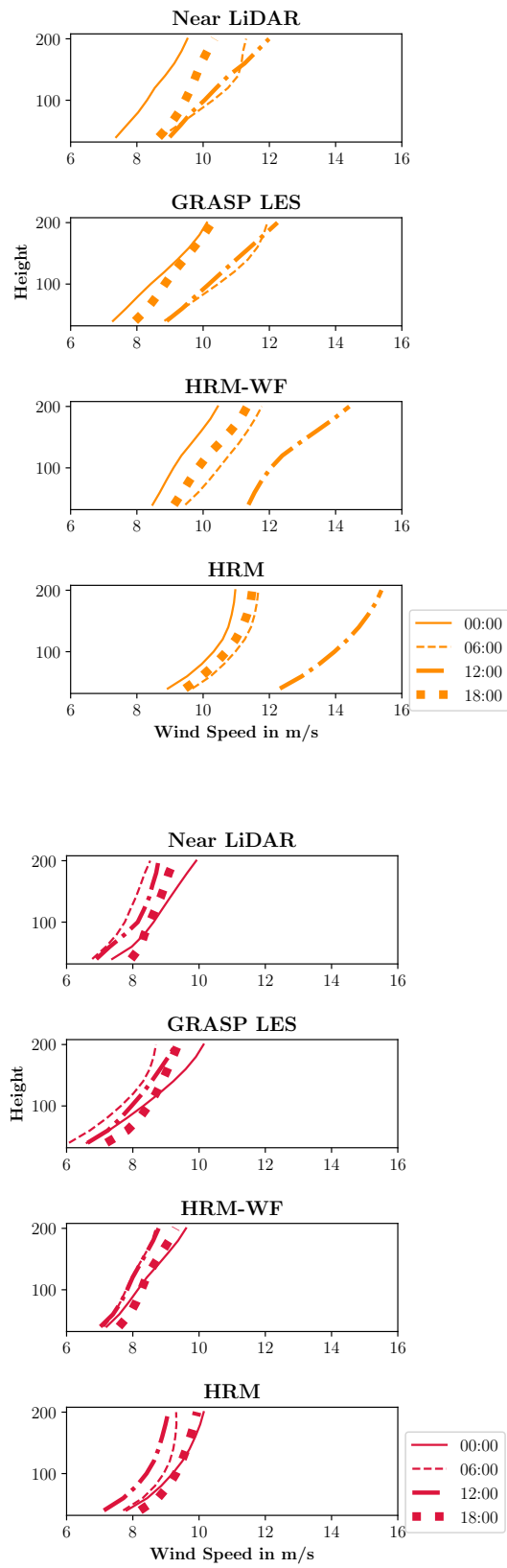


Figure 48: NEAR-LIDAR DIURNAL WIND SHEAR CYCLE The top panel is the diurnal shear for a stable regime. The bottom panel is the diurnal shear for a very stable regime.

## 4.2.1.4 Power Production over BWFZ

From Figures 36 and 39, it is evident that a good percentage of wind speeds in these two regimes are often below 3 - 4 m/s which is the cut in speed for the wind turbines to be operational. This explains the large number of data points at 0 MW for these two regimes. For unstable and neutral regimes, the bulk of the wind speed data points fall within the operational range of the wind turbines (4 - 25 m/s) thus we find most of the hexbin data points spread widely but also accumulated mostly in the upper left corner - maximum capacity (>600 MW). Figure 38 for stable regimes depicts two peaks: one between 5 -10 m/s and a smaller one at around 25 m/s which is the cut out speed for four of the turbine types mentioned in Chapter 3. This justifies the hexbin results for the stable regime: data points are present across the range but the number is few.

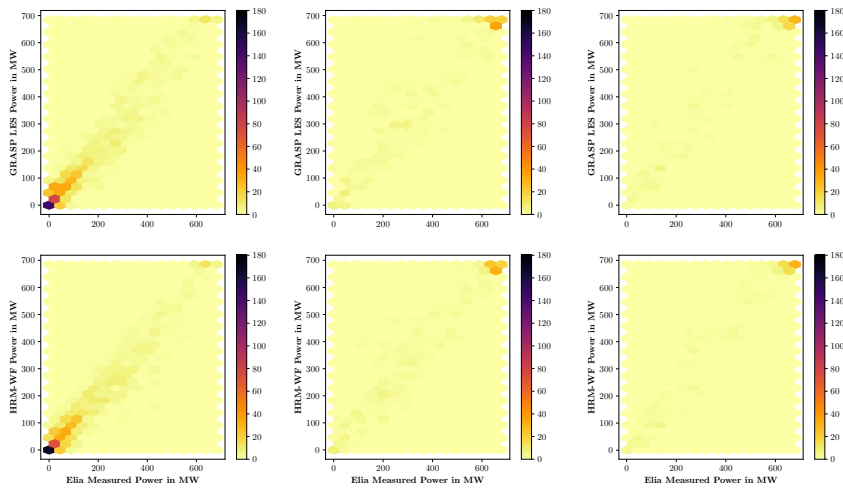


Figure 49: HEXBIN PLOTS FOR POWER PRODUCTION *The leftmost panel is for a very unstable regime. The middle panel is for an unstable regime. The rightmost panel is for a neutral regime. From top to bottom, the panels are HRM-WF and GRASP LES.*

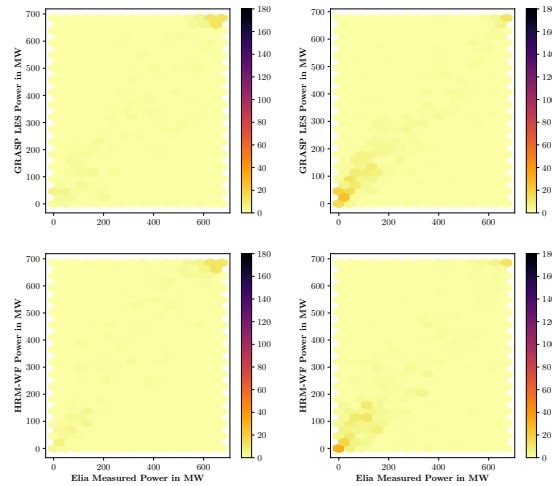


Figure 50: HEXBIN PLOTS FOR POWER PRODUCTION The left panel is for a stable regime. The right panel is for a very stable regime. From top to bottom, the panels are HRM-WF and GRASP LES.

#### 4.2.2 Wind Direction Composite Results

The model and observational data were composited into different directions to identify if the wind direction had any influence on the model bias and if any particular wind sector could be improved to minimise the bias. This work will allow the model improvement to happen in a focused manner.

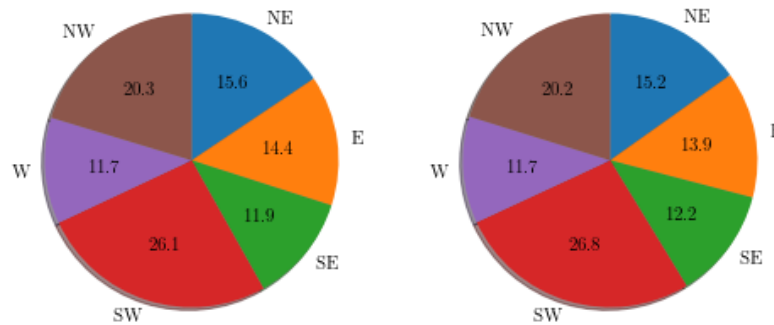


Figure 51: PERCENTAGE OF WIND ORIGINATING FROM VARIOUS DIRECTION DURING THE MARCH - MAY 2016 PERIOD. The left panel is for the far-lidar. The right panel is for the near-lidar.

As Figure 51 represents, the majority of the wind systems originate to the west of the wind farm. This explain why most of the wakes are in the North-East direction closely followed by wake trails towards the South-East. The parsing of wind direction also allows us to study the impact of the WFP at the far-lidar when undisturbed North-Easterly winds arrive at that location.

## 4.2.2.1 Wind Speed Bias per Direction

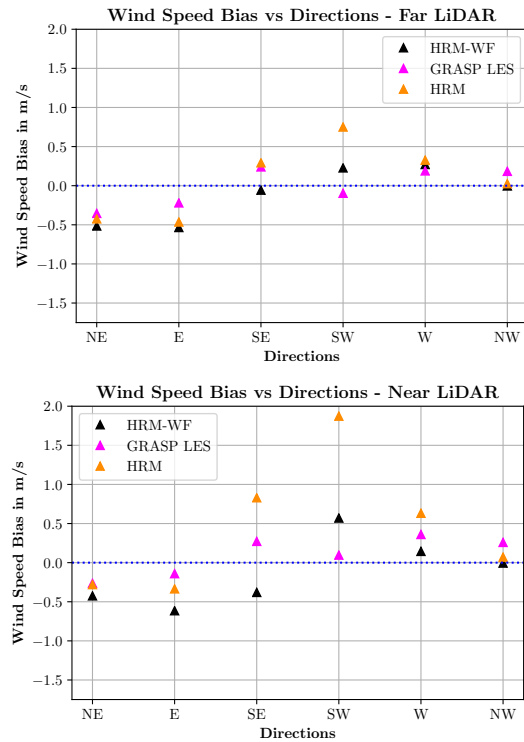


Figure 52: WIND SPEED BIAS VS. DIRECTION The top panel is for the far-lidar. The bottom panel is for the near-lidar.

It can be said that for directions NE, E, and SE, the wind arriving at the LiDARs is undisturbed (ignoring blockage effects) whereas for the rest of the directions, the wind arriving at the LiDARs is disturbed by wake effects of the wind turbines. With this presumption, Figure 52 illustrates that the difference in wind speed bias per direction between HRM and HRM-WF, for the far-lidar, is the maximum for the South Westerly winds and minimum for the North Westerly winds. For the latter, the difference in the bias is small as well as the absolute bias itself ( $\sim 0$  m/s). For the SW and W directions, HRM-WF has a lower bias than HRM but GRASP LES has the least bias out of all three. This is also the case for the NE and E directions. HRM also has a slightly smaller bias than HRM-WF in the undisturbed direction sector (NE, E) thus implying that the differences between the two models are solely the result of the wind farm parameterization. HRM-WF also performs the best for winds coming from the SE direction.

In Figure 52, the effect of wakes on the near-lidar winds is perceivable when looking at the bias of HRM-WF and HRM for winds emanating from the SW direction. A large difference also persists for winds from the SE direction. In most cases, however, HRM-WF outperforms HRM. With the exception of NE and E winds (which are undisturbed winds), HRM performs better. Overall, GRASP LES has

the best performance with the exception of W and NW cases. (Note that in the NE case, GRASP LES and HRM are superimposed on one another).

It is commendable however that the range of bias for HRM-WF is limited to -0.6 to 0.6 m/s in both LiDAR locations whereas the range of bias for HRM is -1.5 to nearly 2 m/s. Yet, GRASP LES has the smallest bias range with values from -0.4 to 0.4 m/s.

To further evaluate the difference between HRM and HRM-WF, the NE and SW originating wind speeds were classified into different stability regimes at the far-lidar location. Specifically, Figure 53 shows the wind speed bias for the two wind directions for the very unstable and very stable regimes. It was presupposed that these regimes would have maximum and minimum wake dissipation respectively. This would provide an insight into the way disturbed and undisturbed winds are represented in the two models across the two different atmospheric stability classes.

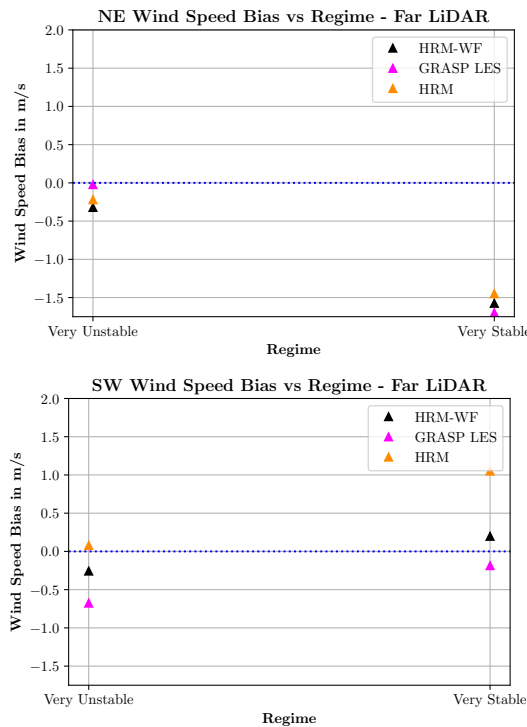


Figure 53: NE AND SW WIND SPEED BIAS VS REGIME FOR THE FAR LIDAR LOCATIONS The top panel is wind speed bias vs regime for the NE wind direction and the bottom panel is for the SW wind direction.

The most interesting result is that for disturbed SW winds at the far lidar, HRM has lower bias compared to HRM-WF for very unstable conditions. As for the very stable condition, HRM has a very large bias compared to HRM-WF. These results posit that the wind speed damping or the wake effect dissipates in very unstable conditions before the far lidar is reached and vice versa for stable conditions.

For undisturbed NE winds, the models have comparable biases for both the stability classes. The bias for the very stable regime is much higher than that for the very unstable regime. In the latter regime, all the models seem to be make quite big underestimations. This is evidently unrelated to the wind farm parameterization since HRM has a large bias and that seems to be present in HRM-WF as well. GRASP LES also exhibits this bias implying that perhaps the models' other parameterizations may play a role in this.

#### 4.3 QUANTITATIVE ANALYSIS

To summarise the the performance of the models against observational data, a descriptive statistical analysis was carried out. The main elements of this analysis includes evaluating measures of central tendency, measures of variability as well as noting the extremes (min, max). To illustrate the statistical advantage of including a wind farm parameterization, bias vs. RMSE' plots between HRM and HRM-WF for both lidar locations were created.

For the far-lidar, the statistical advantage is limited, as depicted in Figure 54. The bias at the lower levels up to 100m has changed sign with no real reduction in bias or RMSE' values. Above 200m, the models seem to have lower bias in terms of magnitude but also seem to be underestimating the wind speeds.

Figure 55 illustrates the advantage of including a WFP for locations impacted by wake effects - the near-lidar location. HRM has a very high bias at all levels with the smallest bias being around 0.4 m/s at 200m height. In contrast, HRM-WF has close to 0 m/s bias at hub height and an overall bias limited to -0.1 m/s to 0.1 m/s. This not only shows the marked improvement when including a WFP in HARMONIE-AROME but also that the current subroutine provides a quantitative improvement compared to HRM as well as compared to observations. The same figures were generated for GRASP LES and have been presented in Appendix B.

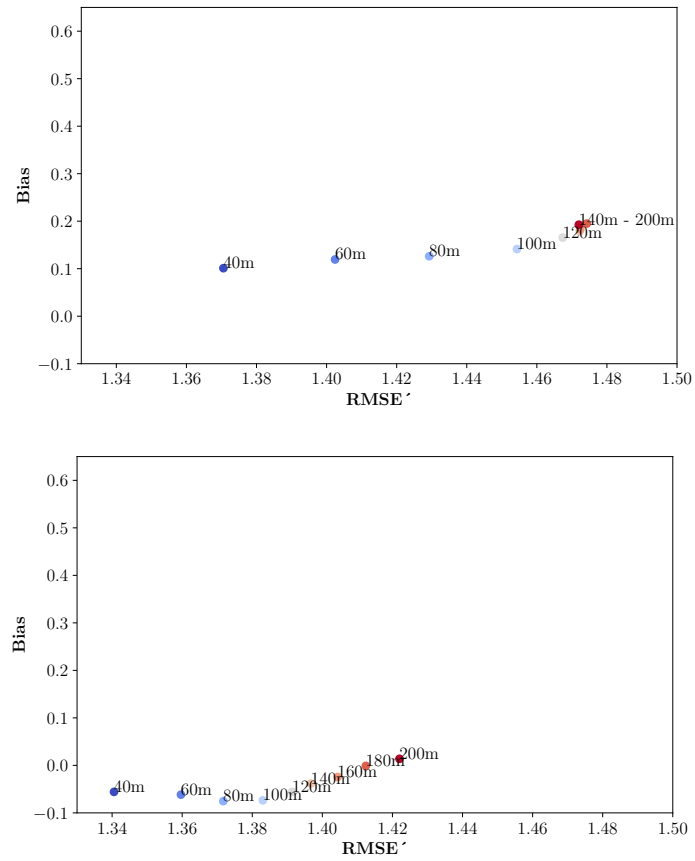


Figure 54: BIAS vs RMSE' DIAGRAM. The top panel is for HRM and the bottom panel for HRM-WF at far-lidar location.

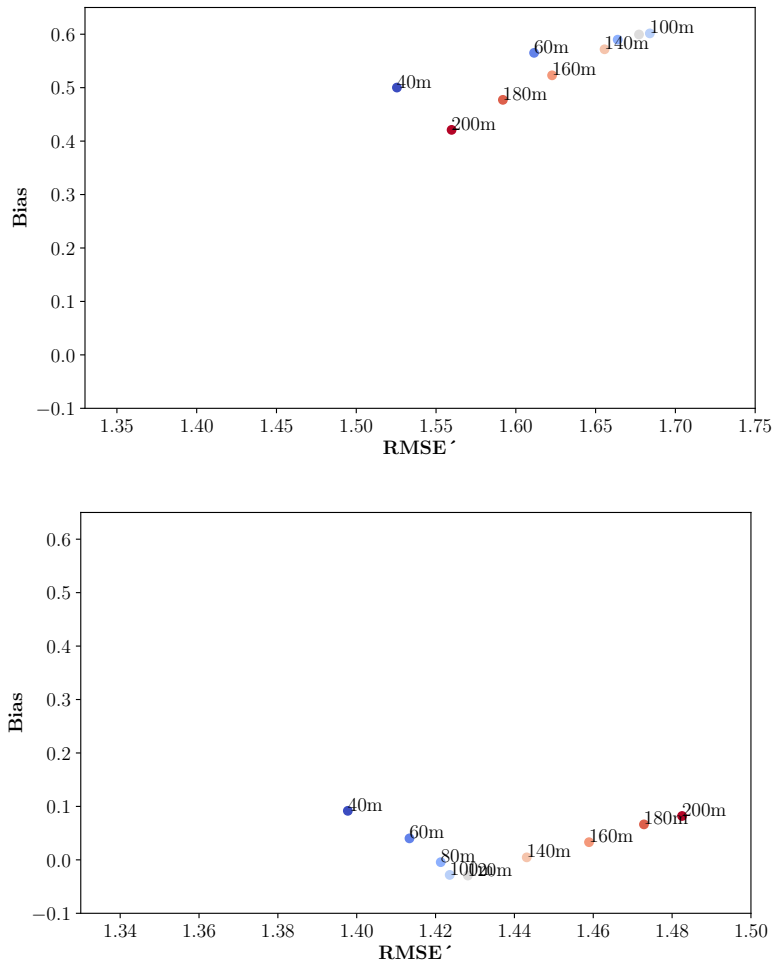


Figure 55: BIAS vs RMSE' DIAGRAM. The top panel is for HRM and the bottom panel for HRM-WF at near-lidar location.

### 4.3.1 Descriptive Statistics: A Tabular Overview

#### 4.3.1.1 Wind Speed - Far Lidar

In terms of overall bias at far-lidar location, HRM-WF fares better than HRM but GRASP LES has statistically lower bias compared to both. The models with the WFP have negative biases indicating that they underestimate the wind speeds and this may be due to the underestimation of wake recovery effects.

IN M/s	HRM-WF	GRASP LES	HRM	FAR-LIDAR
MEAN	8.89	8.93	9.101	8.96
MIN	0.034	0.41	0.19	1.03
MAX	28.56	28.82	29.05	26.15
BIAS	-0.074	-0.024	0.14	-
RMSE	1.38	1.46	1.46	-

Table 6: DESCRIPTIVE STATISTICAL OVERVIEW OF MODEL PERFORMANCE AT FAR-LIDAR FOR HUB HEIGHT.

#### 4.3.1.2 Wind Speed - Near Lidar

IN M/s	HRM-WF	GRASP LES	HRM	NEAR-LIDAR
MEAN	8.47	8.59	9.09	8.49
MIN	0.24	0.38	0.14	0.95
MAX	27.84	28.76	28.904	26.18
BIAS	-0.028	0.094	0.602	-
RMSE	1.42	1.39	1.78	-

Table 7: DESCRIPTIVE STATISTICAL OVERVIEW OF MODEL PERFORMANCE AT NEAR-LIDAR FOR HUB HEIGHT.

At the near-lidar location, as presented in Table 7, HRM-WF has the least overall bias compared to other models against wind observations from Fugro's LiDAR. The magnitude of the bias is also smaller than 0.1 m/s which is consistent with other observed results and patterns. Overall, HRM-WF successfully accounts for wake effects for distances equivalent to the one between the wind farm and the near-lidar.

4.3.1.3 *Power Production*

Wind speed and power production are interlinked in the wind farm parameterization and one can presuppose that better wind prediction near the wind farm would translate into better power forecasts. This is confirmed by the results presented in Table 8. HRM-WF, with the lower bias at near-lidar location for wind speed also has a lower bias in power production. Yet, the overall RMSE values are quite high since the parameter is sensitive to outliers and certain conditions such as ramp events (the simplest definition of a ramp is a large increase or decrease in energy output in a short time by Kamath (2010)) lead to measured power dropping to 0 MW but modelled power remaining at 600MW or more. This ability of models to capture ramp effects would greatly reduce the statistical errors.

in MW	HRM-WF	GRASP LES	ELIA
Mean	266.59	269.25	253.45
Min	0	0	0
Max	684.59	684.59	682.48
Bias	13.15	15.79	-
RMSE	81.47	81.68	-

Table 8: DESCRIPTIVE STATISTICAL OVERVIEW OF MODEL PERFORMANCE FOR POWER PRODUCTION. *The rated power of the wind farm is 684.59 MW.*

### 4.3.2 Descriptive Statistics: A Composite View

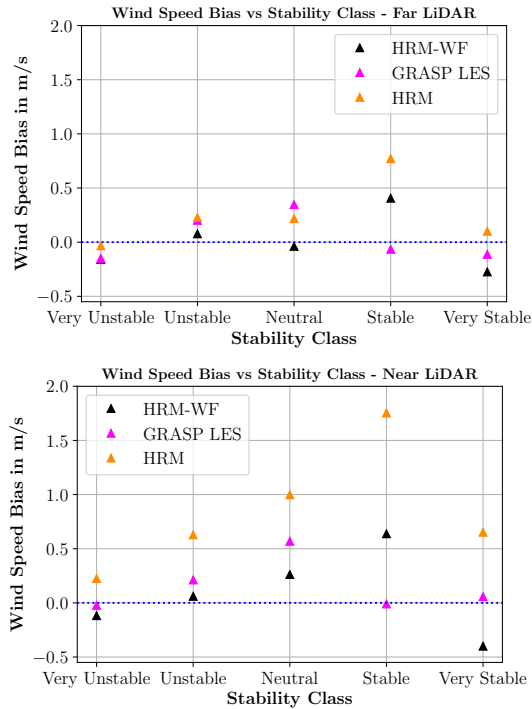


Figure 56: WIND SPEED BIAS VS. STABILITY The top panel is for the far-lidar location and the bottom panel for the near-lidar location.

#### 4.3.2.1 Wind Speed - Far Lidar

In very unstable and very stable conditions, we find that HRM has a lower bias than HRM-WF at the far-lidar (Figure 56). Hence, these two stability regimes were explored in tandem with wind direction composites to uncover any explanations. Between HRM-WF and GRASP LES, they outperform each other in 2 cases: HRM-WF performs well in unstable and neutral regimes whereas GRASP LES is able to perform well in stable and very stable regimes. This might indicate that HRM-WF may not be able to represent wake effects on wind speed for distances about 17km or above. In unstable and neutral regimes where mixing or well-mixed scenarios perhaps cause wake dissipation, HRM-WF outperforms GRASP LES.

As for HRM outperforming HRM-WF, in conjunction with the wind direction composites, an inference may be possible. Since the prevailing atmospheric stability regime is very unstable, any large biases in those regimes will have more weight-age in the overall bias. According to Figure 53, HRM has a lower bias than HRM-WF for disturbed winds (originating in the SW) in the very unstable regime. It also has an equivalently low bias for disturbed (originating in the NE) winds in the very unstable regime. This explains HRM bias <HRM-

WF bias in the very unstable regime. As for the very stable regime, HRM and HRM-WF have equally large and equally negative biases for NE (undisturbed) winds implying that this is an implicit model bias that needs attention. As for SW (disturbed) winds, HRM has a higher bias than HRM-WF but both are positive. It could be argued that the highly positive and the highly negative biases cancel each other out leaving overall HRM bias <HRM-WF bias for very stable regimes. This may explain the results in Figure 56.

#### 4.3.2.2 Wind Speed - Near Lidar

At the near-lidar location, HRM-WF performs the best in terms of bias in the unstable and neutral regimes. This result was represented by the spatial contour maps in Figure 22. GRASP LES, has the lowest bias values less than 0.1 m/s for three out of five stability regimes. HRM has the largest bias evidently because it does not represent any wake effects.

#### 4.3.2.3 Power Production

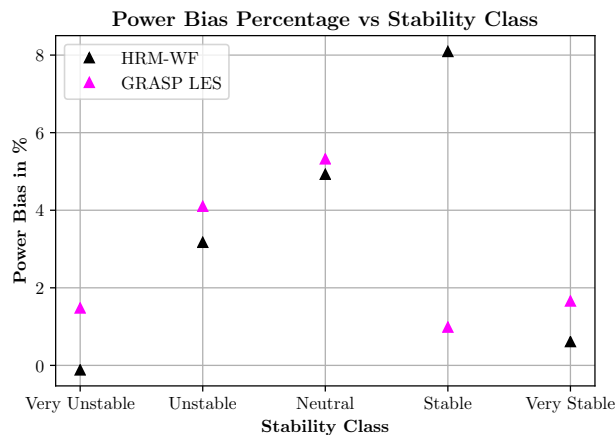


Figure 57: POWER BIAS VS. STABILITY. The bias is expressed as a percentage of nameplate capacity of the wind farm which is 684.59 MW. See Appendix B for power bias in terms of MW.

For power production, HRM-WF performs poorly in the stable regime compared to any other regime. Overall, the ranking of stability regimes in terms of wind bias at near lidar is valid here. Figure 57 demonstrates that GRASP LES and HRM-WF have comparable biases in most cases except for the stable regime. It is interesting to note that HRM-WF has the least power bias in the very unstable regime which accounts for majority of the state of the atmosphere and thus influences the overall power bias as seen in Table 8.



# 5

---

## DISCUSSION

---

### 5.0.1 *Summary*

From the results presented in this chapter, some of the key outcomes have been summarised in this section.

#### 5.0.1.1 *Qualitative Overview*

It was found from the results presented in Chapter 4 that HRM-WF captures spatial wind contours and wakes only in certain conditions. Next, it was confirmed that the hub height results between the model outputs (LES, HRM-WF) and the observations match very well. It was noticed that the Belgian wind farm seems to create enhanced mixing at the near-lidar and this was evident when comparing the near-lidar and far-lidar diurnal shear profiles. Finally, power production by the wind farm was captured well by HRM-WF as well as GRASP LES.

#### 5.0.1.2 *Qualitative Composite View*

In the diurnal cycle for stable regimes, it appears that the presence of the WFP results in less mixing and as expected, HRM-WF's results correspond better with observations than those of HRM. It was also observed that during unstable conditions, night-time and stable, day-time conditions, there was not a lot of variation in the magnitude of wind profiles. The histograms of the model's wind speed data vary significantly from observed wind speed data histograms especially at the near-lidar location. However, HRM-WF successfully captures the qualitative order of the shear profiles for different hours of the day for unstable and neutrally stratified atmospheric regimes at the far-lidar. Also, HRM-WF near-lidar results for disturbed winds (SW, W) are better than HRM. On the other hand, HRM-WF's results for undisturbed winds (NE, E) at the near-lidar has a greater bias than that of HRM. Finally, the wake effects at the far lidar for NE and E (undisturbed winds) show comparable results for HRM-WF and HRM but for SW and W winds (disturbed) at the far lidar, HRM-WF's performance is better than that of HRM.

### 5.0.1.3 Quantitative Overview

HRM-WF performs consistently well in unstable and neutral regimes but the reason for HRM outperforming HRM-WF in very unstable and very stable conditions needs to be explored. GRASP LES is statistically a strong contender for it has very low wind speed bias overall and across several stability regimes.

### 5.0.1.4 Hypotheses Testing

The hypotheses developed in Chapter 2 are addressed here and either the null hypotheses are accepted or an alternate hypotheses if possible is provided.

*The undisturbed model results (HRM) at the near LiDAR will will not account for wake effects unlike HRM-WF* ACCEPTED This is indeed demonstrated from results in Figures 16, 54, 55, 56- 57, Tables 6-8.

*In a no-wind farm or an undisturbed region, for e.g. Cabauw, the two runs will be nearly identical* ACCEPTED This is demonstrated by the results in Appendix B.

*In stable regimes, HRM-WF's power production (and/or wind speed) will be underestimated.* (Lee and Lundquist, 2017) REJECTED We observe an overestimation in power production (positive power production bias). However, it is true that HRM-WF does not perform its best particularly in stable regimes (Figure 56)

*The wind farm will have an effect on the TKE* ACCEPTED This is established by the 2-D cross-section plots of TKE provided in Figure 17

*The wind farm will cause a slowing down of wind speeds at hub height* ACCEPTED The weakening of wind speeds in the BWFZ is clearly depicted in the HRM vs. HRM-WF hub-averaged wind speed plots (Figure 16)

*Turbulence generation can cause mixing which in turn affects atmospheric variables and will have the strongest impact during the early hours of the day* (Roy, Pacala, and Walko, 2004) PARTIALLY ACCEPTED In the diurnal cycle figures, we see that the greatest mixing takes place between 5 AM and 10 AM (Figures 41 - 44) but the effect on other atmospheric variables (such as the surface fluxes) is not explored in this thesis.

*Wakes will recover faster in convective conditions compared to neutral and stable conditions* ACCEPTED Referring to Figure 56, for very unstable regimes at the far-lidar, HRM and HRM-WF have comparable biases compared to the biases for neutral and stable conditions.

Note: A very limited diurnal cycle was expected and that has been corroborated by Figures 29 - 30. Although, it is interesting that the diurnal cycle adopts certain temporal trends as noticed in the observational data which may be useful for further fine-tuning the models to represent real-world situations.

#### 5.0.1.5 Conditions with least and most bias

LEAST BIAS CONDITIONS	HRM	HRM-WF	GRASP LES
<i>Wind Speed Bias in m/s</i>	Far-Lidar, Very Unstable	Far-Lidar, Neutral	Near-Lidar, Stable
<i>Power Bias in MW</i>	-	Very Unstable	Very Unstable
MOST BIAS CONDITIONS	HRM	HRM-WF	GRASP LES
<i>Wind Speed Bias in m/s</i>	Near-Lidar, Stable	Near-Lidar , Stable	Near-Lidar, Neutral
<i>Power Bias in MW</i>	-	Stable	Neutral

Table 9: INTRA-MODEL PERFORMANCE INDICATING LEAST BIAS CONDITIONS AND MOST BIAS CONDITIONS. *This table illustrates a model's least and most bias conditions when compared with its bias values for all the stability regimes.*

From Table 9, some very simple inferences can be made. Firstly, HRM performs its best at the far-lidar during very unstable conditions since this is possibly the closest to an undisturbed wind flow condition. Both HRM and HRM-WF have quite large biases at the near-lidar during stable conditions and the exact cause needs further research. GRASP LES' near-lidar neutral results have reflected in its power performance as well but the LES model is able to capture near-lidar stable winds unlike HRM-WF.



# 6

---

## CONCLUSION AND RECOMMENDATIONS

---

### 6.1 RESEARCH OUTCOMES

- HOW DOES THE WIND FARM PARAMETRIZATION (WFP) IN HARMONIE-AROME PERFORM?

The wind farm parameterization is working as intended in HARMONIE-AROME and sufficiently represents the physical impact of a wind farm which includes an increased generation of TKE, a reduction in wind speed in the wake of a wind farm, wake signatures (to a limited extent), as well as closely matching observational wind speeds from the lidar (with an overall bias of 0.028 - 0.074 m/s (near and far lidar)) and consequently predicting power production (after curtailment) with a bias of 1.92 %.

- HOW CAN THE CURRENT WFP IN HARMONIE-AROME BE FURTHER IMPROVED?

It is worth looking into the performance of the model during stable conditions since the bias was the largest for both wind and power during this atmospheric regime (with HRM-WF having a larger bias than HRM specifically for undisturbed winds from the NE,E directions during stable regimes ). Furthermore, a better wake fingerprint that captures really long wakes as observed in SAR imagery would also improve in accurately assessing the impact of the Belgian wind turbines on the upcoming Borssele wind farm.

- WHAT ARE THE METEOROLOGICAL INSIGHTS ONE CAN GAIN FROM THE SIMULATION RESULTS?

From the far-lidar vs. HRM/HRM-WF comparisons, especially for stable regimes, it is established that long wakes up to and more than 17km are *possible* (determined by the difference between HRM and HRM-WF for the case for SW winds (since the far-lidar is around 17km from the wind farm). Furthermore, the reduction in wind speed and wake impacts are the largest in the early hours of the day. Additionally, the diurnal cycle of the wind speeds is limited as compared to onshore cycles. Also, in the observational wind speed data-set, during unstable

night-time (6 PM and 12 AM) and stable day-time (6 AM and 12 PM) conditions for the near-lidar, very little variation in wind shear profiles was observed (and this was duly captured only by the GRASP LES model). Finally, it appears that both wind speed and stability regime in tandem play a role in determining wake length. For very stable regimes with low wind speeds, only short wakes were observed but for an unstable regime with a relatively high wind speed, medium wakes were still present. This needs further exploration but these are the generic inferences that can be made from Figure 25.

## 6.2 RECOMMENDATIONS

The evaluation of a wind farm parameterization as well as using the models to detect patterns and trends (where observational data is absent) is a continuous process. In this thesis, while an effort to examine the most crucial model outputs was made, several potential areas of research were uncovered. Some of them are touched upon in this section.

Due to the limitation of the near-lidar data availability, seasonal trends and the reproducibility of the model was not explored but this is a potential area of study for another wind farm zone that has close proximity lidar data available for a longer time period. On that note, the hypotheses on the curtailment of power production needs to be looked into by contacting individual wind farm operators who may be able to confirm or deny the hypotheses regarding the same.

Among the assumptions that were made, blockage effects - a slowing down of wind just upstream of wind turbines (Bleeg et al., 2018) - were ignored and hence is a promising area that could perhaps be analysed by looking at the near-lidar for winds coming in from the North East. Additionally, wake meandering, which literature postulates is a phenomenon where winds far downstream that appear to undisturbed experience intense turbulence and reduced wind speeds ((Larsen, 2007), (Abkar and Porté-Agel, 2015b)), was not studied here and could be explored with respect to the Belgian wind farm. A spatial study on the relationship between wind speeds, atmospheric stability regimes and length of wakes seems to have potential for exploration (a succinct analysis was presented in this thesis in Chapter 4).

Finally, Baidya Roy (2011)'s work shows that wind farms have impacts not only on wind speed but on air temperature, humidity, surface fluxes which in turn affect the total water mixing ratio (and lapse rates, equivalent potential temperature). In another work, one of his experiments show, for onshore wind farms, that although impact on evapo-transpiration rate is insignificant, there is a large impact on the sensible heat flux (Roy, Pacala, and Walko, 2004) which in turn

needs to be explored for offshore wind farms. Furthermore, these effects are apparent downstream and not limited to the wind farm zone (Roy, Pacala, and Walko, 2004). His study, (Baidya Roy, 2011), also looks at dry and wet periods of the wind farm which would be intriguing to look at in offshore wind farms as well. Therefore, surface fluxes from the simulation data could be examined for wind farm impacts on fluxes offshore. Finally, precipitation patterns, cloud cover impacts, large-scale meteorological phenomenon impacted by local scale changes, could also be explored.

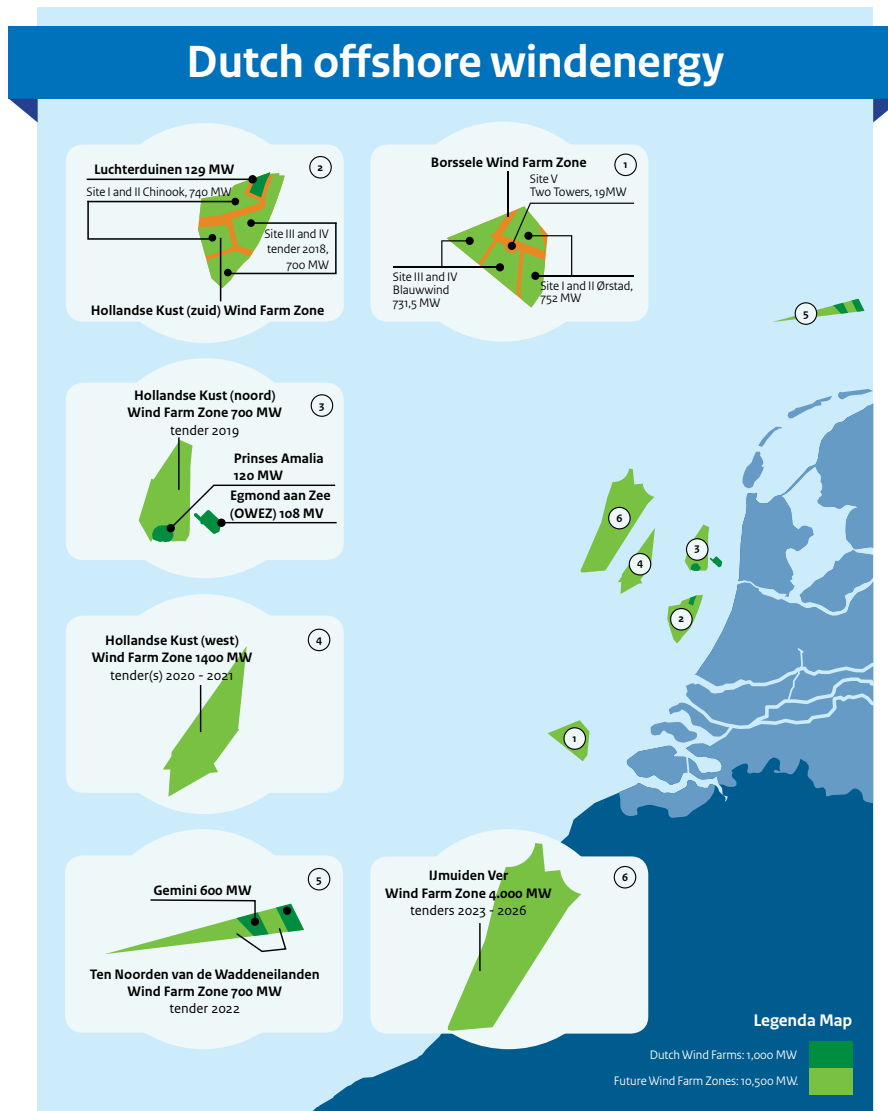


Figure 58: FUTURE WIND FARMS IN THE NORTH SEA. As the figure illustrates, there are 6 upcoming wind farm projects in the pipeline including the Borssele Wind Farm Zone which was the area of interest in this study.

It is worth mentioning that although these are relevant areas of study since they have the potential to reduce our knowledge gaps,

there is also a business interest regarding these kinds of studies. Currently, the Netherlands is planning several wind farm zones as depicted in Figure 58 (some of which even overlap existing wind farms) and the impact of which is yet to be fully understood. Therefore, there is not just a strong prospect for further research from a scientific point of view but from a commercial point of view as well.

---

## BIBLIOGRAPHY

---

- Abkar, Mahdi and Fernando Porté-Agel (2015a). "A New Wind-farm Parameterization for Large-scale Atmospheric Models." en. In: *Journal of Renewable and Sustainable Energy* 7.1, p. 013121. ISSN: 1941-7012.
- (2015b). "Influence of Atmospheric Stability on Wind-turbine Wakes: A Large-eddy Simulation Study." In: *Physics of Fluids* 27.3, p. 035104. ISSN: 1070-6631.
- Baidya Roy, Somnath (2011). "Simulating impacts of wind farms on local hydrometeorology." en. In: *Journal of Wind Engineering and Industrial Aerodynamics* 99.4, pp. 491–498. ISSN: 01676105.
- Bengtsson, Lisa et al. (2017). "The HARMONIE–AROME Model Configuration in the ALADIN–HIRLAM NWP System." en. In: *Monthly Weather Review* 145.5, pp. 1919–1935. ISSN: 0027-0644, 1520-0493.
- Blahak, Ulrich, Bernd Goretzki, and Jon Meis (2010). "A Simple Parameterization of Drag Forces Induced by Large Wind Farms for Numerical Weather Prediction Models." In: *Proceedings of European wind energy conference and exhibition*, pp. 186–189.
- Bleeg, James, Mark Purcell, Renzo Ruisi, and Elizabeth Traiger (2018). "Wind Farm Blockage and the Consequences of Neglecting Its Impact on Energy Production." en. In: *Energies* 11.6, p. 1609. ISSN: 1996-1073.
- Christiansen, Merete Bruun and Charlotte B. Hasager (2005). "Wake Effects of Large Offshore Wind Farms Identified from Satellite SAR." en. In: *Remote Sensing of Environment* 98.2-3, pp. 251–268. ISSN: 00344257.
- Ciaran, Gilbert, Jakob W. Messner, Pierre Pinson, Pierre-Julien Trombe, Remco Verzijlbergh, Pim van Dorp, and Harmen Jonker (2019). "Statistical Post-processing of Turbulence-resolving Weather Forecasts for Offshore Wind Power Forecasting." In: *Wind Energy*, 2019. doi: <https://doi.org/10.1002/we.2456>.
- DTU. *Methodology - Synthetic Aperture Radar (SAR)*. URL: <https://bit.ly/2Bx6boi> (visited on 04/11/2019).
- Dhirendra, Dhruv and Anthony Crockford (Aug. 2016). *Strategic Advice about Floating LiDAR Campaigns Borssele offshore wind farm*. English. Online. ECOFYS, p. 19. URL: <https://offshorewind.rvo.nl/file/download/44561812> (visited on 10/15/2019).
- Fitch, Anna C., Julie K. Lundquist, and Joseph B. Olson (2013). "Mesoscale Influences of Wind Farms throughout a Diurnal Cycle." en. In: *Monthly Weather Review* 141.7, pp. 2173–2198. ISSN: 0027-0644, 1520-0493.

- Fitch, Anna C., Joseph B. Olson, Julie K. Lundquist, Jimmy Dudhia, Alok K. Gupta, John Michalakes, and Idar Barstad (2012). "Local and Mesoscale Impacts of Wind Farms as Parameterized in a Mesoscale NWP Model." en. In: *Monthly Weather Review* 140.9, pp. 3017–3038. ISSN: 0027-0644, 1520-0493.
- Hansen, Martin O. L. (2008). *Aerodynamics of wind turbines*. 2nd. Earthscan. ISBN: 978-1-84407-438-9.
- Haupt, Sue Ellen, Pedro A. Jiménez, Jared A. Lee, and Branko Kosović (2017). "Principles of Meteorology and Numerical Weather Prediction." en. In: *Renewable Energy Forecasting*. Elsevier, pp. 3–28. ISBN: 978-0-08-100504-0.
- Holtslag, Bert (2015). "Boundary Layer (Atmospheric) and Air Pollution: Modeling and Parameterization." In: pp. 265–273. ISBN: 9780123822253.
- KNMI (Jan. 2019). *Difference between DOWA and KNW - DOWA project - Dutch Offshore Wind Atlas*. en-GB. Online. URL: <https://www.dutchoffshorewindatlas.nl/about-the-atlas/difference-dowa--knw>.
- Kamath, Chandrika (2010). "Understanding Wind Ramp Events through Analysis of Historical Data." In: *IEEE PES T&D 2010*. IEEE, pp. 1–6. ISBN: 978-1-4244-6546-0.
- Keith, D. W., J. F. DeCarolus, D. C. Denkenberger, D. H. Lenschow, S. L. Malyshev, S. Pacala, and P. J. Rasch (2004). "The Influence of Large-scale Wind Power on Global Climate." en. In: *Proceedings of the National Academy of Sciences* 101.46, pp. 16115–16120. ISSN: 0027-8424, 1091-6490.
- Larsen, Gunner C (2007). *Dynamic wake meandering modeling*. English. Risø National Laboratory. ISBN: 978-87-550-3602-4.
- Lee, Joseph C. Y. and Julie K. Lundquist (2017). "Evaluation of the Wind Farm Parameterization in the Weather Research and Forecasting Model (Version 3.8.1) with Meteorological and Turbine Power Data." en. In: *Geoscientific Model Development* 10.11, pp. 4229–4244. ISSN: 1991-9603.
- M. Motta, R. J. Barthelmie, and P. Vølund (2005). "The Influence of Non Logarithmic Wind Speed Profiles on Potential Power Output at Danish Offshore Sites." In: *Wind Energy* 8, pp. 219–236.
- Moene, Arnold F and J. C. van Dam (2014). *Transport in the atmosphere-vegetation-soil continuum*. Cambridge University Press. ISBN: 978-0-521-19568-3.
- NEA. *Borssele Wind Farm Site V, Innovation Site | RVO.nl*. en. URL: <https://bit.ly/2N1Tp6S> (visited on 10/14/2019).
- *Offshorewind.rvo.nl*. URL: <https://offshorewind.rvo.nl/generalborssele> (visited on 03/08/2019).
- Pondera, Whiffle, Deltares, and Old Baum (Oct. 2019). *Wind Resource Assessment Hollandse Kust (noord) Wind Farm Zone Version October 2019*. URL: <https://bit.ly/2qsTI2G>.

- Roy, Baidya, S. W. Pacala, and R.L Walko (2004). "Can Large Wind Farms Affect Local Meteorology?" en. In: *Journal of Geophysical Research* 109.D19. ISSN: 0148-0227.
- Schalkwijk, Jérôme, Harmen J. J. Jonker, A. Pier Siebesma, and Erik Van Meijgaard (May 2015). "Weather Forecasting Using GPU-Based Large-Eddy Simulations." en. In: *Bull. Amer. Meteor. Soc.* 96.5, pp. 715–723. ISSN: 0003-0007, 1520-0477.
- Simmons, A. J. and D. M. Burridge (1981). "An Energy and Angular-Momentum Conserving Vertical Finite-Difference Scheme and Hybrid Vertical Coordinates." In: *Monthly Weather Review* 109.4, pp. 758–766. ISSN: 0027-0644.
- Stratum, B.J.H. van, S. Basu, I.L. Wijnant, J. Barkmeijer, J. Onvlee, and A.P. Siebesma (2019). *Wind turbine parameterisation in HARMONIE-AROME*. en. Tech. rep. URL: <https://www.dutchoffshorewindatlas.nl/publications>.
- Untch, A. and M. Hortal (2004). "A finite-element scheme for the vertical discretization of the semi-Lagrangian version of the ECMWF forecast model." en. In: *Quarterly Journal of the Royal Meteorological Society* 130.599, pp. 1505–1530. ISSN: 1477-870X.
- User Guides - Sentinel-1 SAR - Overview - Sentinel Online*. URL: <https://sentinel.esa.int/web/sentinel/user-guides/sentinel-1-sar/overview> (visited on 03/08/2019).
- Vermeer, L. J., J. N. Sørensen, and A. Crespo (2003). "Wind Turbine Wake Aerodynamics." In: *Progress in Aerospace Sciences* 39.6, pp. 467–510. ISSN: 0376-0421.
- Warner, Thomas T. (2011). *Numerical weather and climate prediction*. Cambridge University Press. ISBN: 978-0-521-51389-0.





---

## DATA SOURCES

---

### A.1 ACCESS TO MODEL SIMULATIONS

KNMI's HARMONIE-AROME WITH WIND FARM PARAMETERIZATION (HRM-WF): Please contact KNMI

KNMI's HARMONIE-AROME WITHOUT WIND FARM PARAMETERIZATION (HRM): Instructions for downloading HARMONIE-AROME (w/o the wind farm parameterization) is provided on the website of the *Dutch Offshore Wind Atlas*. The data is located at KNMI's Data Centre (online: <https://data.knmi.nl/datasets>)

WHIFFLE'S GRASP LES: Please contact *Whiffle Weather Fine-casting* by emailing *info (at) whiffle.nl*

OBUKHOV LENGTH: Available online and to download from <https://map.neweuropeanwindatlas.eu>

### A.2 ACCESS TO OBSERVATIONAL DATA-SETS

SAR IMAGERY: Available online and to download from <https://satwinds.windenergy.dtu.dk/>

LIDAR OBSERVATIONS: Available online and to download from <https://www.windopzee.net/en/borssele-bwz/data/index.html>

POWER PRODUCTION MEASUREMENTS FOR THE BELGIAN WIND FARM ZONE: Available online and to download from <https://www.elia.be/en/grid-data/power-generation/wind-power-generation>



# B

---

## SUPPLEMENTARY RESULTS

---

### B.1 DESCRIPTIVE STATISTICS: A TABULAR COMPOSITE VIEW

#### B.1.0.1 *Wind Speed - Far LiDAR*

Table 10: Very Unstable

IN M/S	HRM-WF	GRASP LES	HRM	FAR-LIDAR
MEAN	6.96	6.972	7.088	7.123
MIN	0.0338	0.415	0.187	1.03
MAX	18.85	20.08	17.882	18.122
BIAS	-0.158	-0.1502	-0.0344	-
RMSE	1.22	1.105	1.198	-

Table 11: Unstable

IN M/S	HRM-WF	GRASP LES	HRM	FAR-LIDAR
MEAN	10.93	11.055	11.0/2	10.854
MIN	1.507	1.377	1.1704	2.243
MAX	20.72	20.77	19.491	18.733
BIAS	0.0766	0.201	0.227	-
RMSE	1.471	1.66	1.566	-

Table 12: Stable

IN M/s	HRM-WF	GRASP LES	HRM	FAR-LIDAR
MEAN	11.61	11.14	11.975	11.204
MIN	3.536	3.441	2.536	3.005
MAX	28.56	28.815	29.052	26.15
BIAS	0.405	-0.066	0.771	-
RMSE	1.34	1.83	1.612	-

Table 13: Very Stable

IN M/s	HRM-WF	GRASP LES	HRM	FAR-LIDAR
MEAN	8.398	8.56	8.773	8.673
MIN	0.785	1.48	0.46	1.046
MAX	19.6	19.552	19.783	20.05
BIAS	-0.274	-0.113	0.1002	-
RMSE	1.76	1.7501	1.899	-

Table 14: Neutral

IN M/s	HRM-WF	GRASP LES	HRM	FAR-LIDAR
MEAN	11.989	12.375	12.245	12.03
MIN	2.968	2.394	2.457	1.86
MAX	24.82	28.82	25.154	25.882
BIAS	-0.039	0.347	0.217	-
RMSE	1.135	1.409	1.177	-

B.1.0.2 *Wind Speed - Near LiDAR*

Table 15: Very Unstable

IN M/S	HRM-WF	GRASP LES	HRM	NEAR-LIDAR
MEAN	6.7204	6.815	7.063	6.84
MIN	0.243	0.377	0.145	0.954
MAX	18.496	19.751	18.298	17.704
BIAS	-0.12	-0.0232	0.224	-
RMSE	1.1	1.055	1.23	-

Table 16: Unstable

IN M/S	HRM-WF	GRASP LES	HRM	NEAR-LIDAR
MEAN	10.745	10.89	11.314	10.686
MIN	1.622	1.45	1.64	2.252
MAX	20.969	20.46	21.66	18.959
BIAS	0.06	0.211	0.627	-
RMSE	1.533	1.605	1.787	-

Table 17: Stable

IN M/s	HRM-WF	GRASP LES	HRM	NEAR-LIDAR
MEAN	10.641	9.993	11.756	10.0034
MIN	2.593	2.85	0.668	2.3102
MAX	27.84	28.76	28.904	26.183
BIAS	0.637	-0.0104	1.753	-
RMSE	1.529	1.648	2.623	-

Table 18: Very Stable

IN M/s	HRM-WF	GRASP LES	HRM	NEAR-LIDAR
MEAN	7.714	8.172	8.76	8.115
MIN	0.7103	1.38	0.237	1.063
MAX	18.25	19.302	19.513	19.905
BIAS	-0.4006	0.056	0.652	-
RMSE	1.828	1.601	2.191	-

Table 19: Neutral

IN M/s	HRM-WF	GRASP LES	HRM	NEAR-LIDAR
MEAN	11.704	12.01	12.44	11.442
MIN	2.32	1.474	4.414	2.301
MAX	24.32	28.36	25.082	25.34
BIAS	0.261	0.568	0.997	-
RMSE	1.543	1.647	2.025	-

B.1.0.3 *Power Production*

Table 20: Very Unstable

IN MW	HRM-WF	GRASP LES	ELIA
MEAN	166.18	177.11	166.99
MIN	0	0	0.104
MAX	684.59	684.59	682.48
BIAS	-0.809	10.12	-
RMSE	56.006	58.8	-

Table 21: Unstable

IN MW	HRM-WF	GRASP LES	ELIA
MEAN	403.115	409.48	381.41
MIN	0	0	1.142
MAX	684.59	684.59	678.874
BIAS	21.71	28.07	-
RMSE	87.762	100.712	-

Table 22: Stable

IN MW	HRM-WF	GRASP LES	ELIA
MEAN	409.703	361.053	354.31
MIN	0	0.982	1.76
MAX	684.59	684.59	671.802
BIAS	55.391	6.74	-
RMSE	112.902	106.81	-

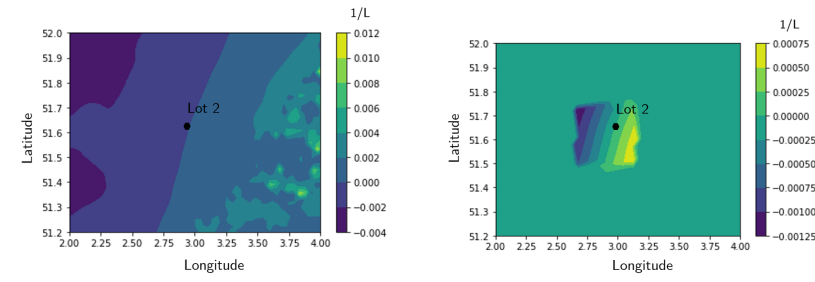
Table 23: Very Stable

IN MW	HRM-WF	GRASP LES	ELIA
MEAN	212.84	220.002	208.65
MIN	0	7.75	0.28
MAX	684.59	676.298	670.85
BIAS	4.188	11.35	-
RMSE	102.265	86.58	-

Table 24: Neutral

IN MW	HRM-WF	GRASP LES	ELIA
MEAN	439.83	442.543	406.11
MIN	0.898	6.67	2.4
MAX	684.59	684.59	678.12
BIAS	33.72	36.44	-
RMSE	86.46	95.21	-

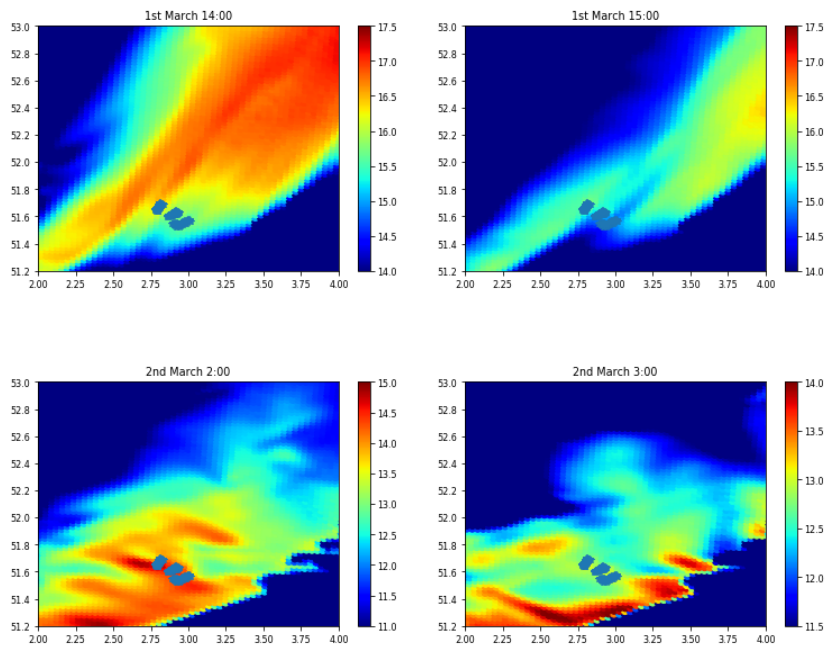
B.2 INVERSE OBUKHOV LENGTH FROM THE NEW EUROPEAN WIND ATLAS

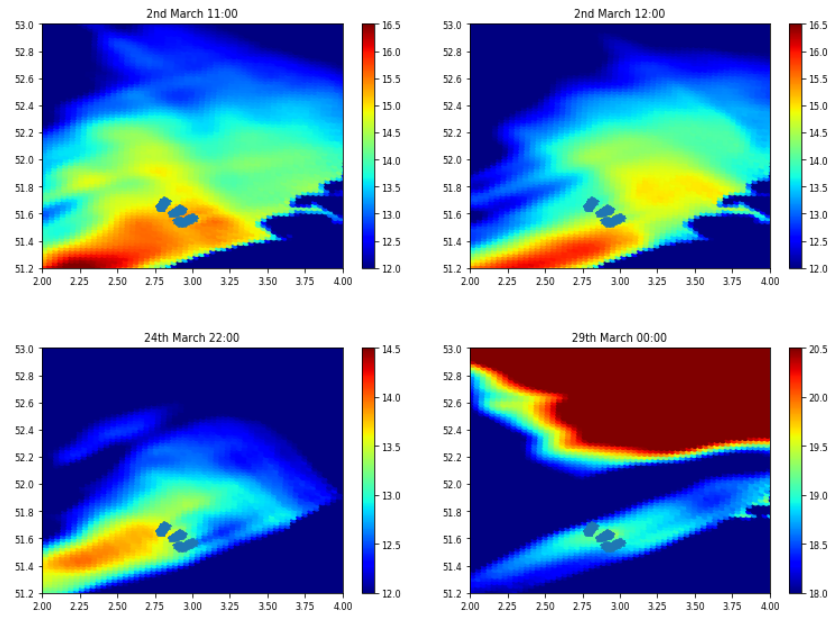


Right panel is the Belgian wind farm with other regions masked

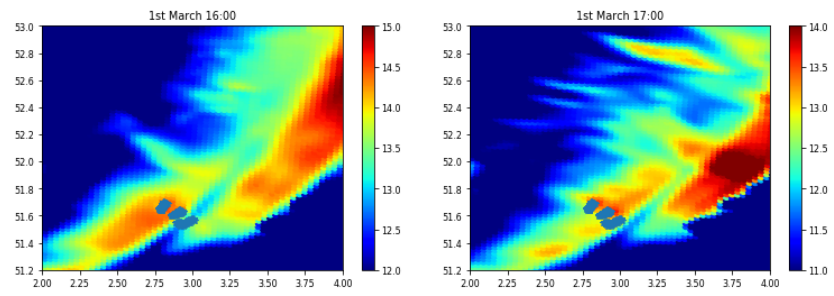
B.3 SPATIAL PLOTS FOR WAKE PHASE DIAGRAM CONSTRUCTION

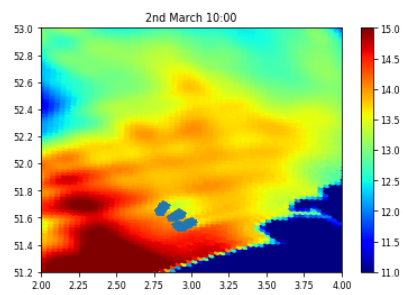
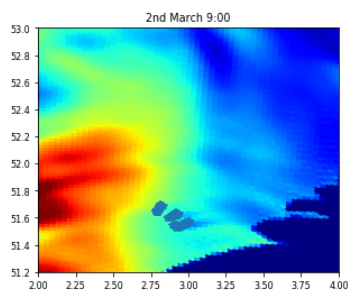
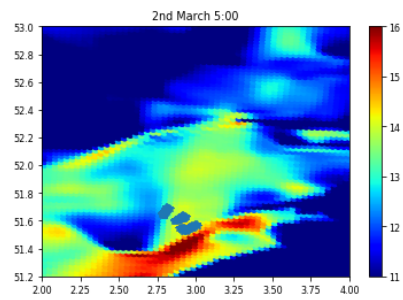
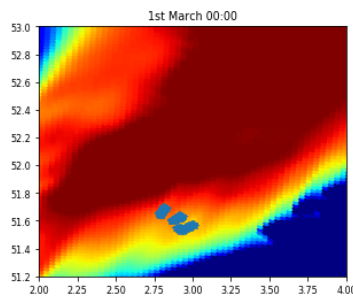
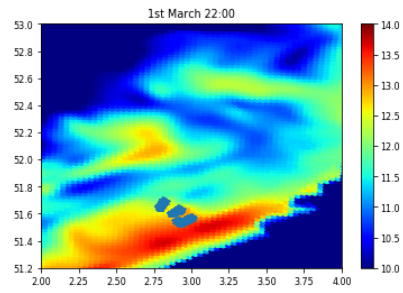
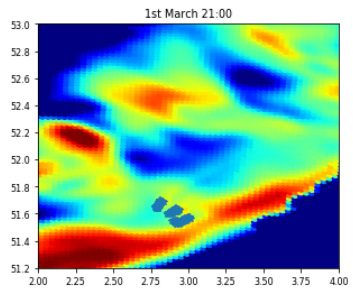
Neutral



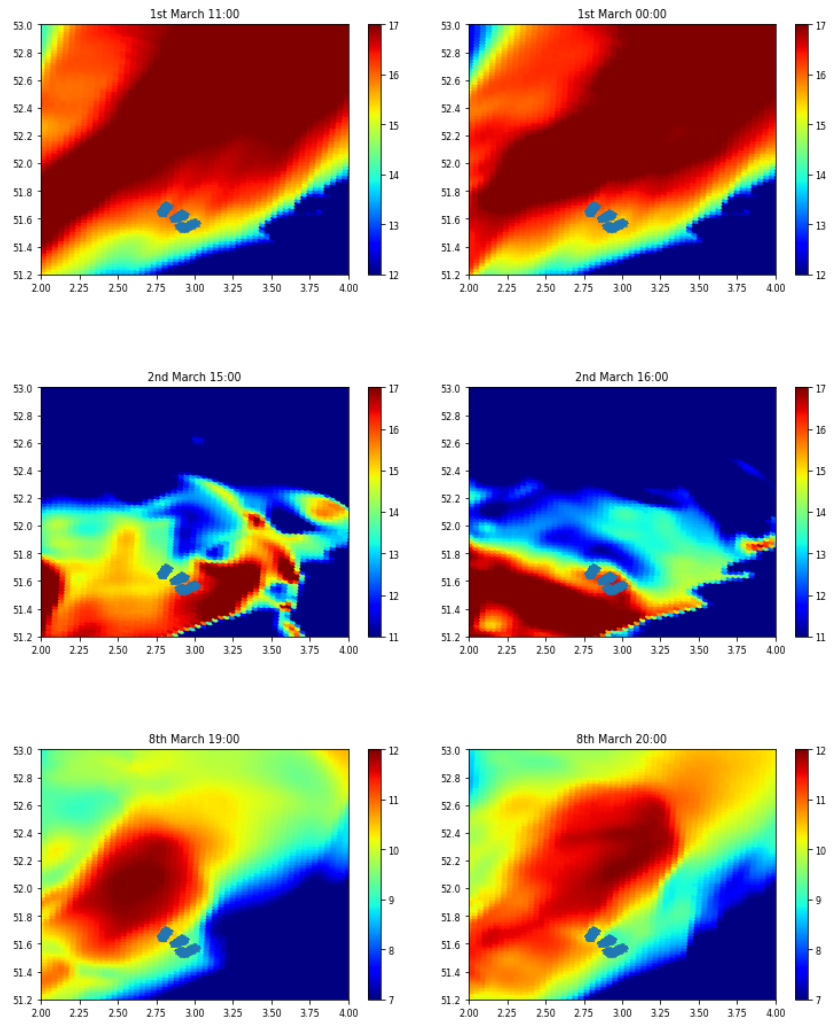


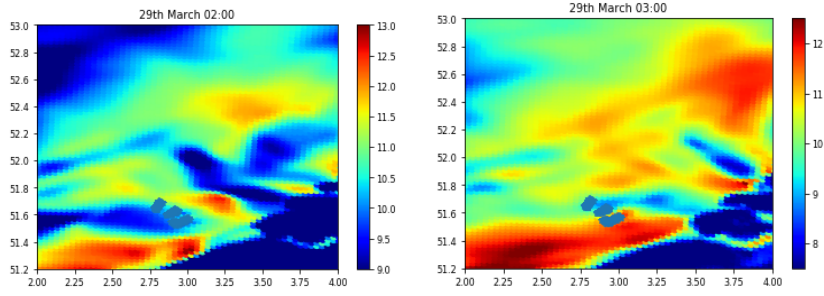
Stable



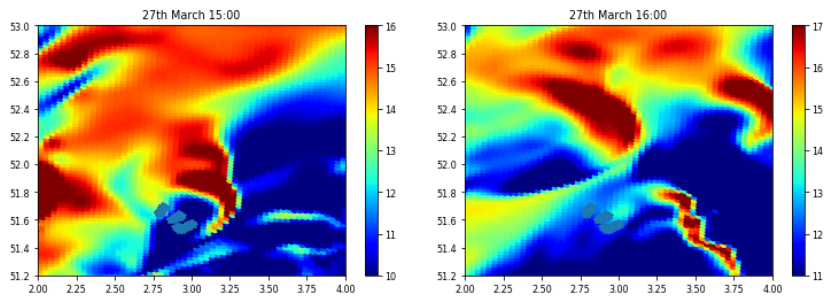
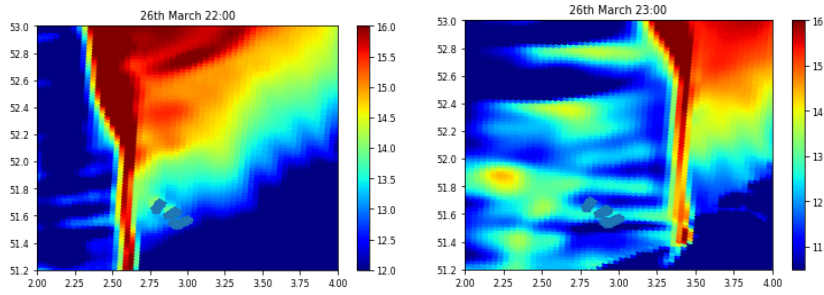


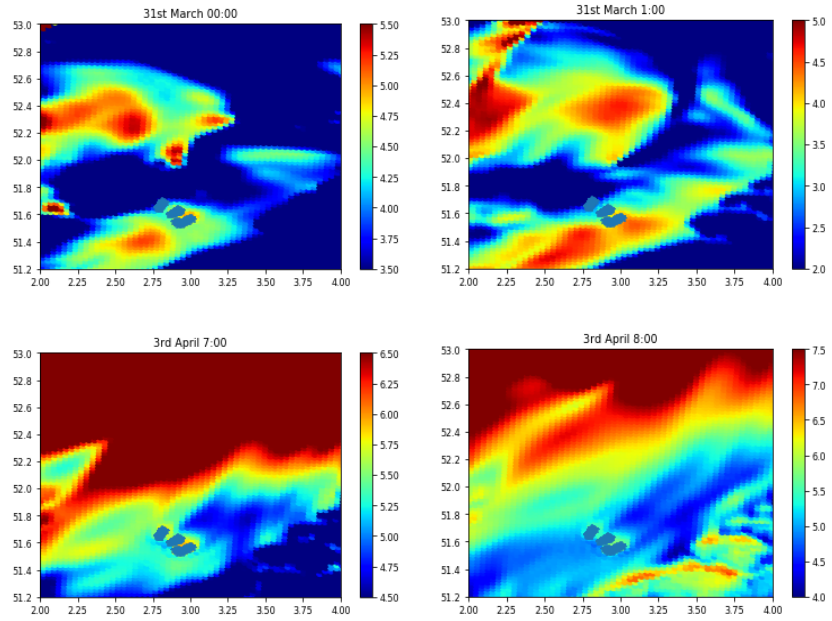
## Unstable



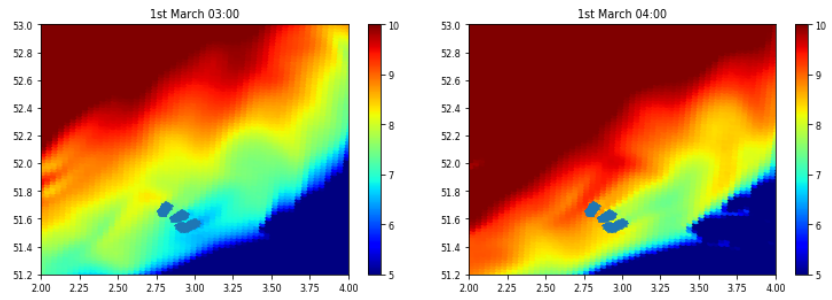


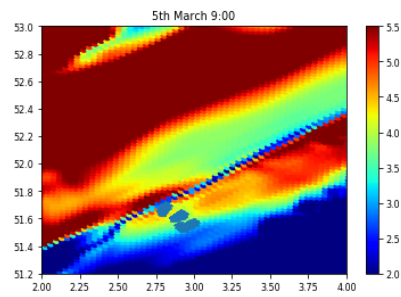
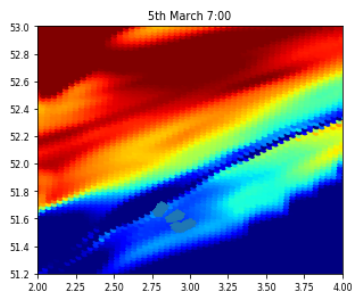
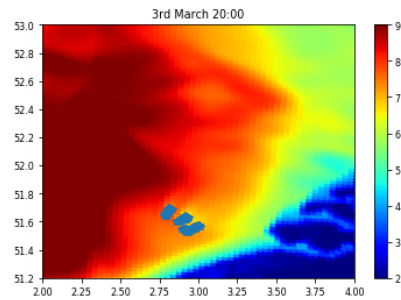
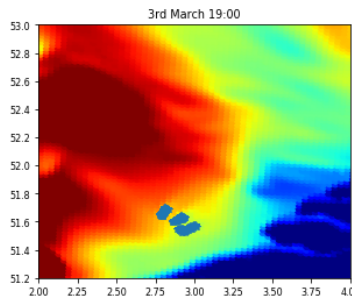
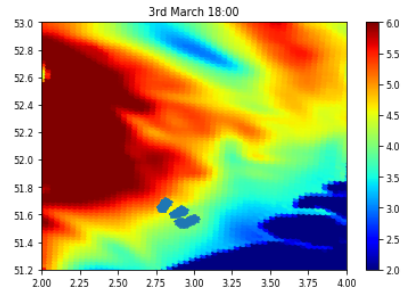
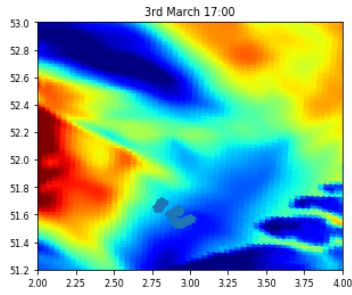
Very Stable





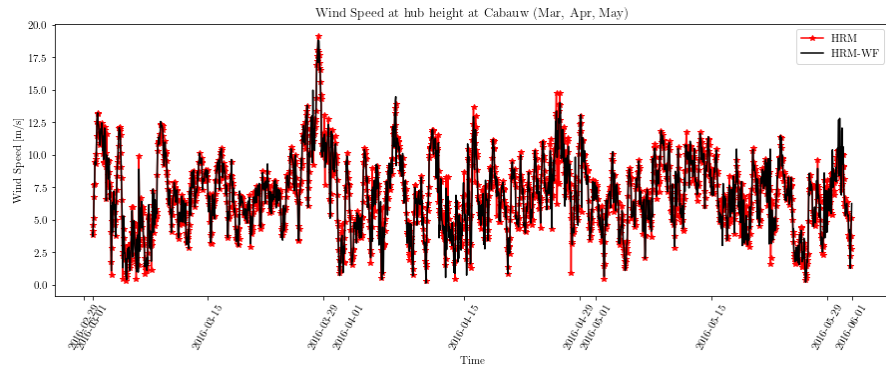
Very Unstable



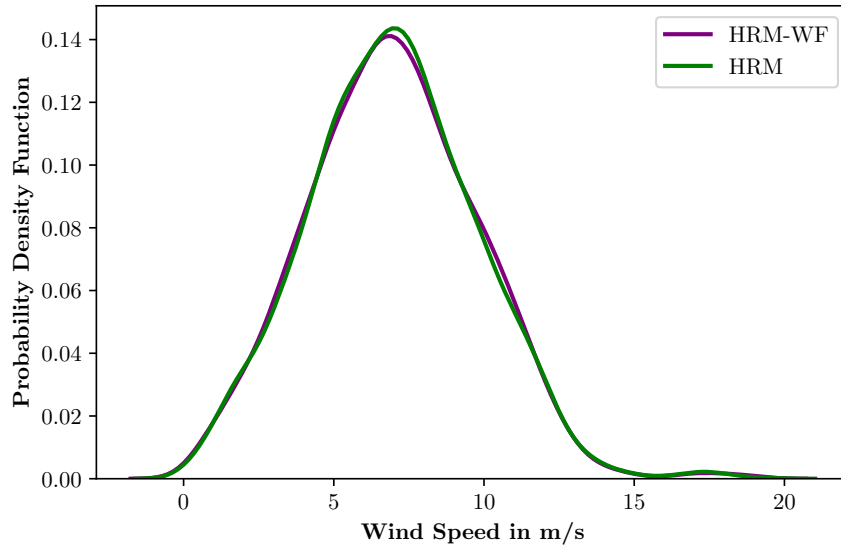


B.4 ADDITIONAL FIGURES

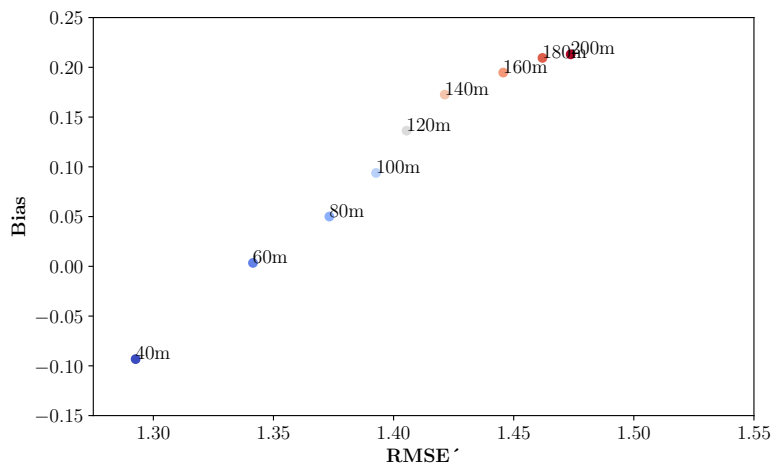
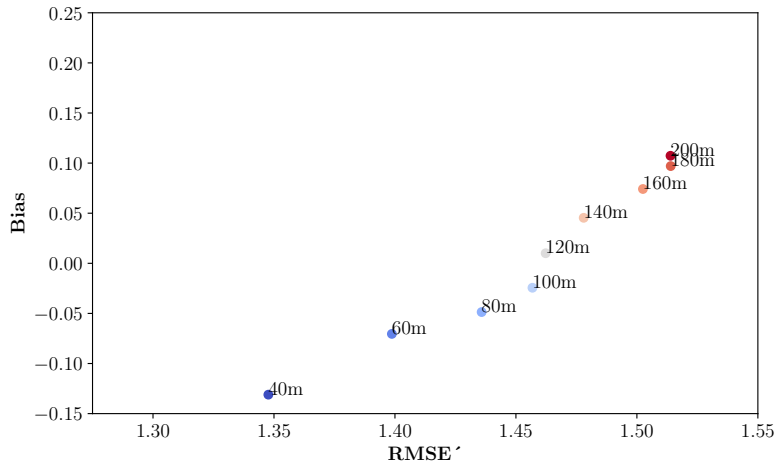
HRM and HRM-WF at Cabauw



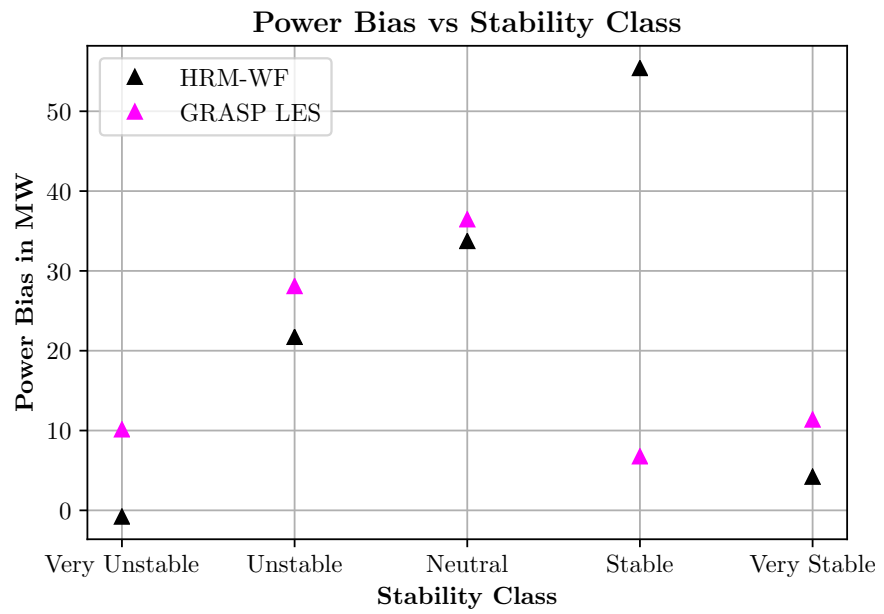
WIND SPEEDS AT 100M HUB HEIGHT FOR CABAUW

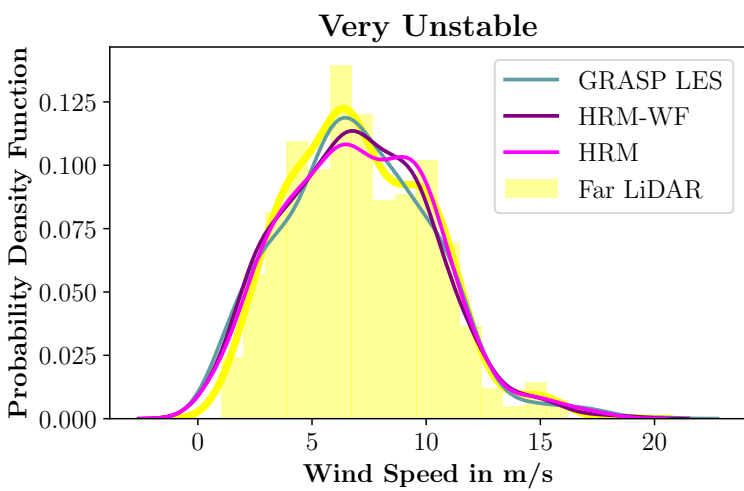
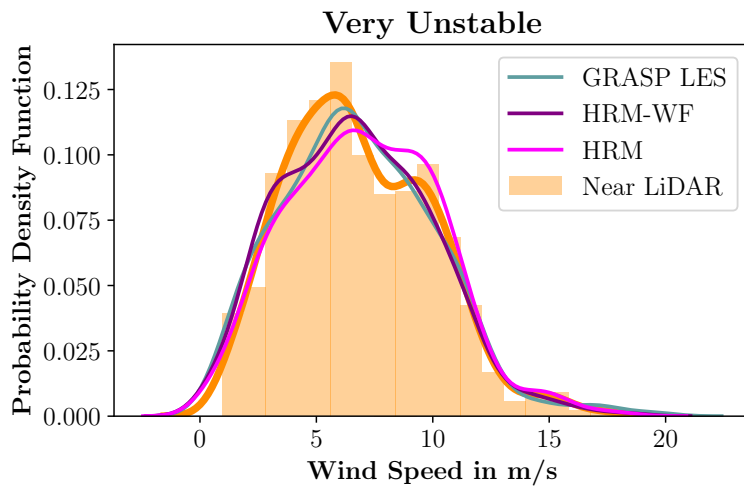
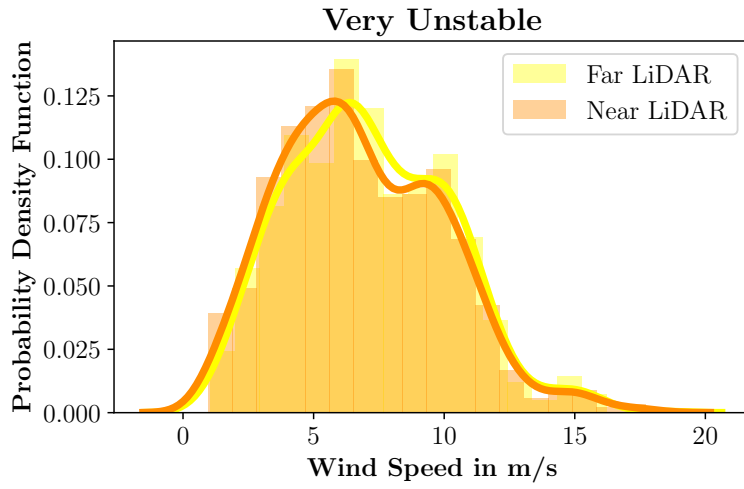


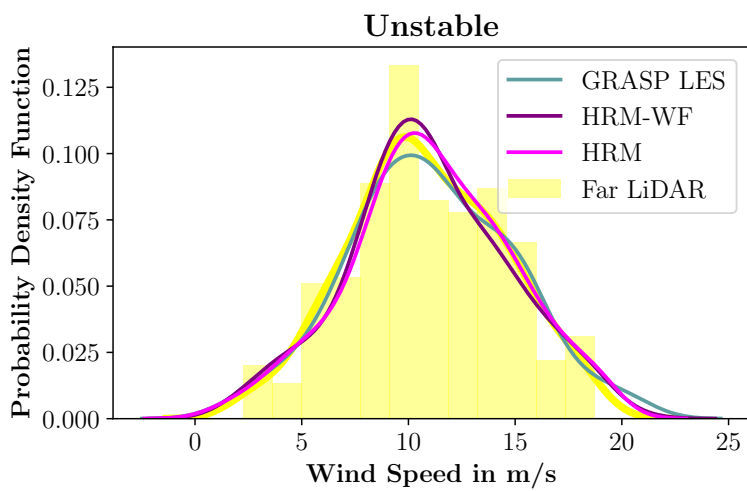
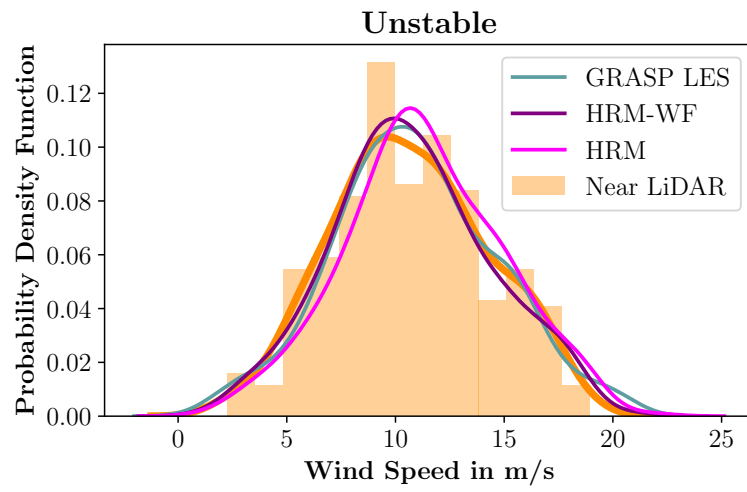
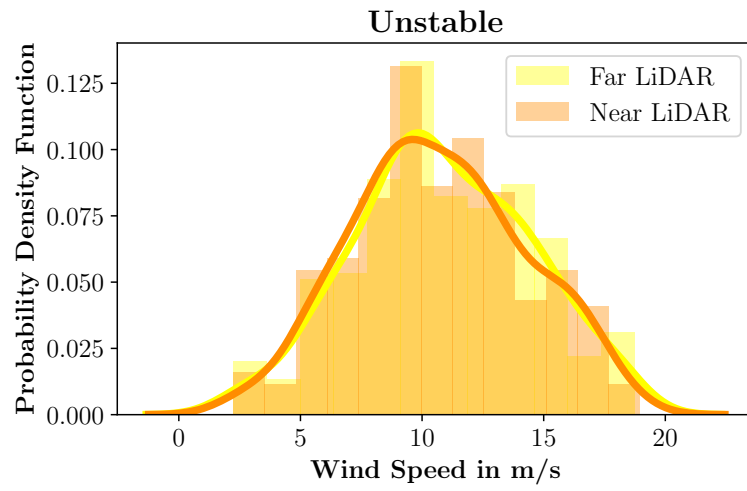
PDF FOR WIND SPEEDS AT 100M HUB HEIGHT FOR CABAUW

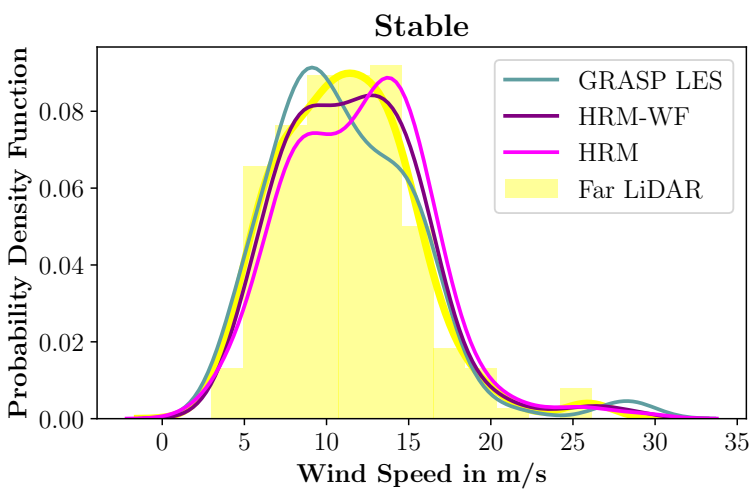
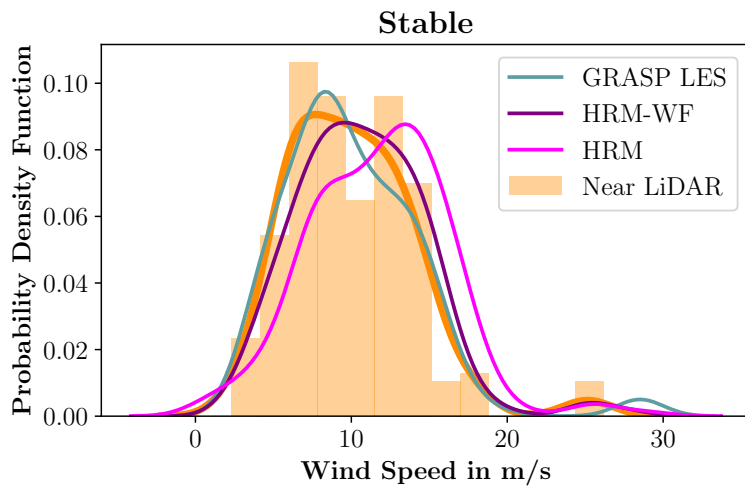
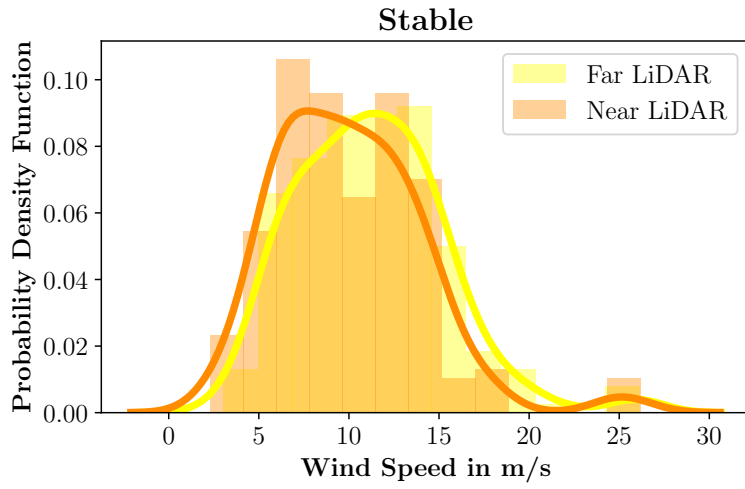


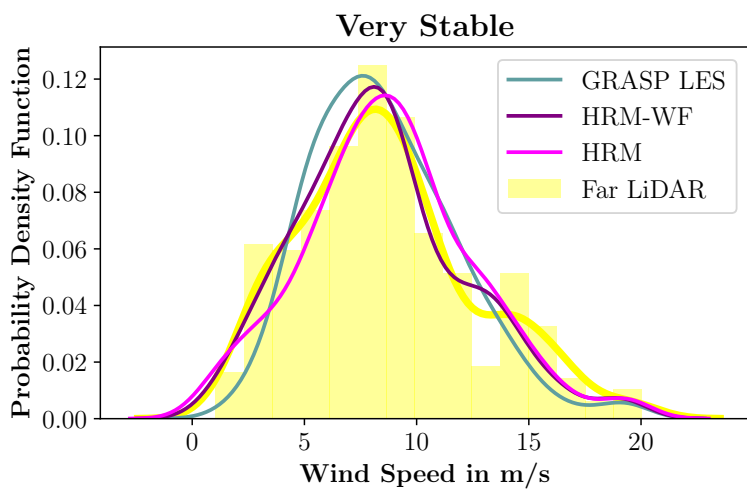
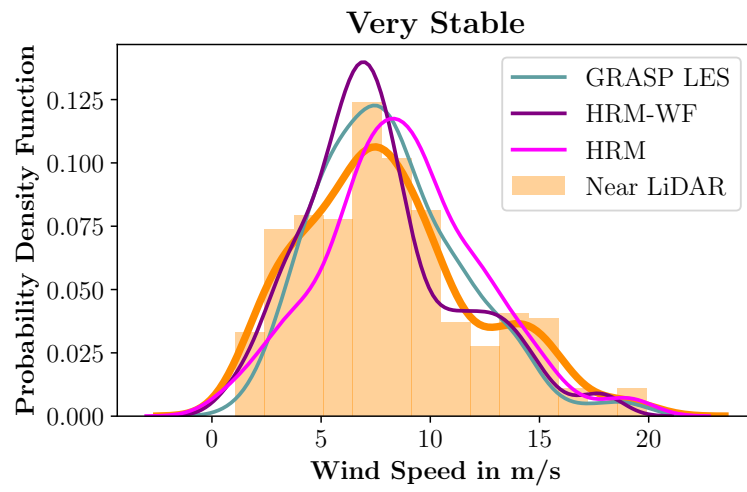
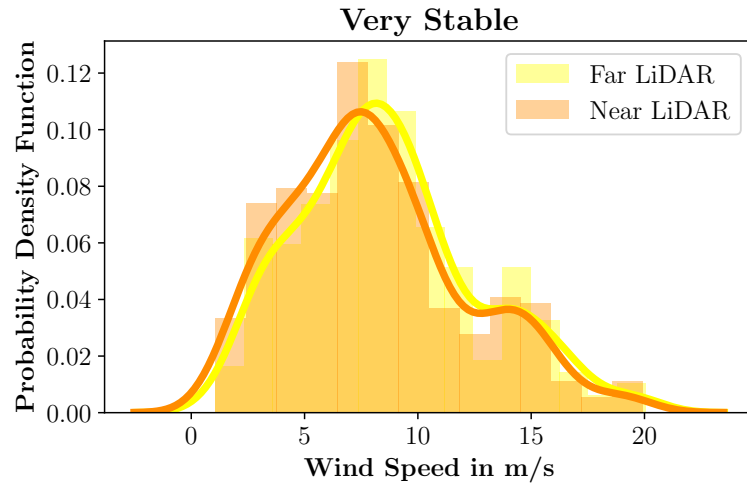
GRASP LES TARGET DIAGRAM

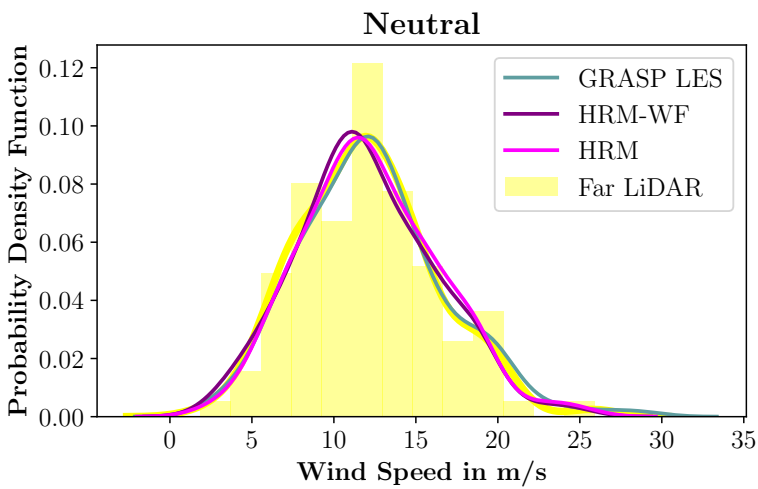
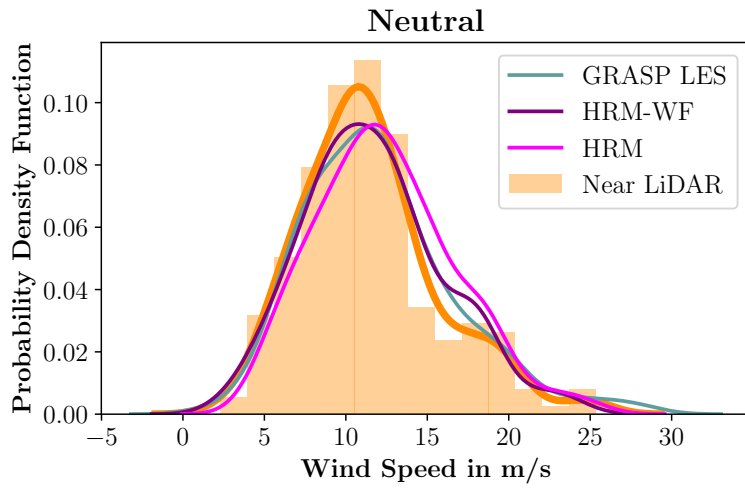
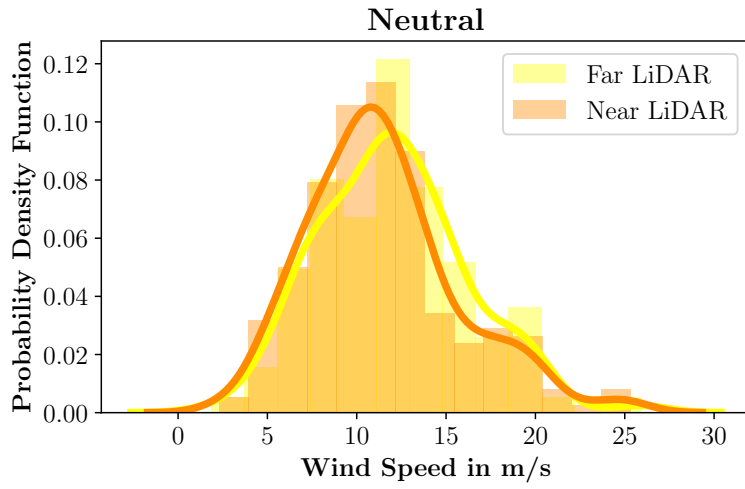




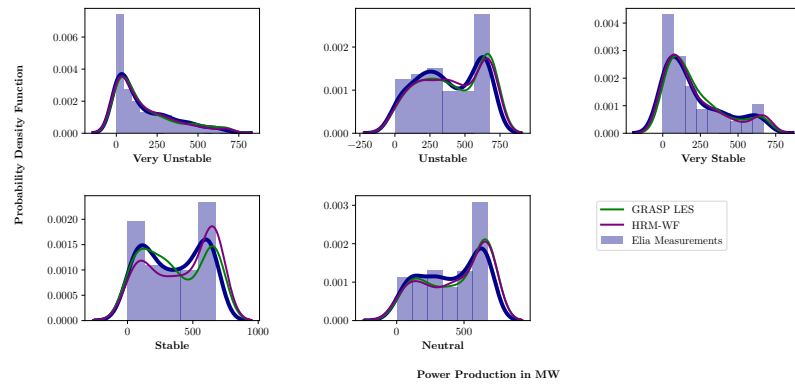
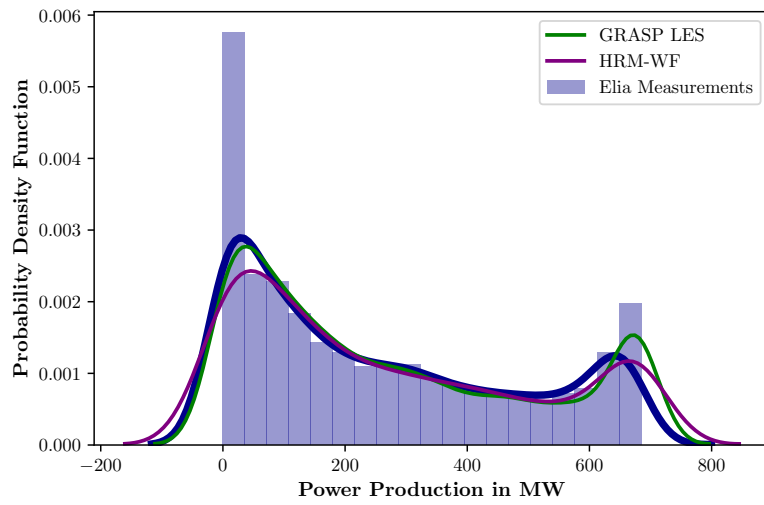




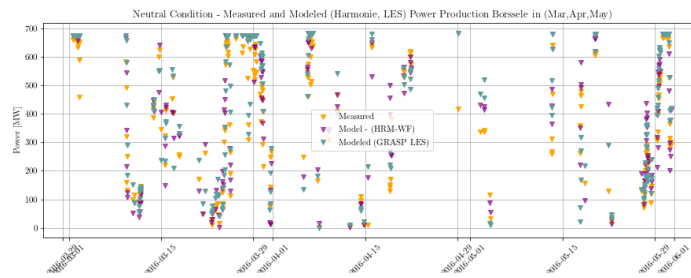


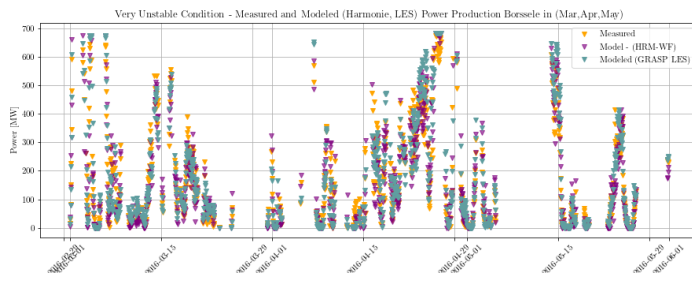
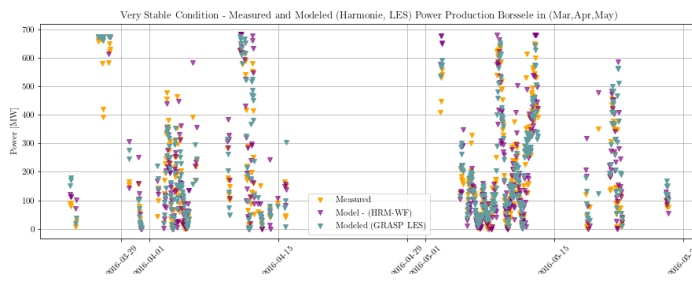
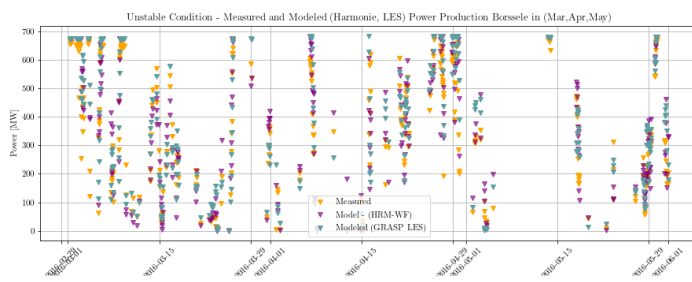
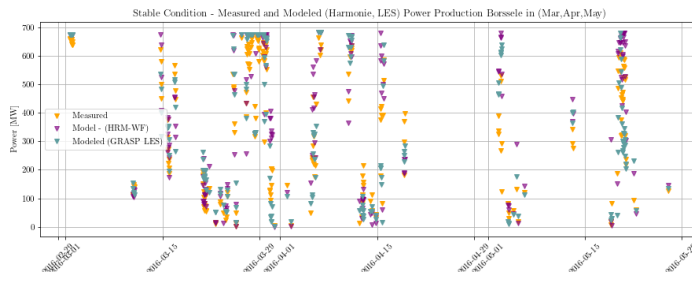


### Power Production Probability Density Functions



### Power Production Time Series (Stability Composites)







#### COLOPHON

This document was typeset using the typographical look-and-feel classicthesis developed by André Miede. The style was inspired by Robert Bringhurst's seminal book on typography "*The Elements of Typographic Style*". classicthesis is available for both L<sup>A</sup>T<sub>E</sub>X and L<sup>Y</sup>X:

<https://bitbucket.org/amiede/classicthesis/>

*Final Version* as of November 20, 2019 (classicthesis Master Thesis).